



1 **Arctic spring and summertime aerosol optical depth baseline from**  
2 **long-term observations and model reanalyses, with implications for**  
3 **the impact of regional biomass burning processes**

4

5

6 Peng Xian<sup>1</sup>, Jianglong Zhang<sup>2</sup>, Travis D. Toth<sup>3</sup>, Blake Sorenson<sup>2</sup>, Peter R. Colarco<sup>4</sup>,  
7 Zak Kipling<sup>5</sup>, Norm T. O'Neill<sup>6</sup>, Edward J. Hyer<sup>1</sup>, James R. Campbell<sup>1</sup>, Jeffrey S. Reid<sup>1</sup>  
8 and Keyvan Ranjbar<sup>6</sup>

9

10 <sup>1</sup>Naval Research Laboratory, Monterey, CA, USA.

11 <sup>2</sup>Department of Atmospheric Sciences, University of North Dakota, Grand Forks, ND

12 <sup>3</sup>NASA Langley Research Center, Hampton, Virginia, USA.

13 <sup>4</sup>NASA Goddard Space Flight Center, Greenbelt, MD, USA.

14 <sup>5</sup>European Centre for Medium-Range Weather Forecasts, Reading, UK.

15 <sup>6</sup>Département de géomatique appliqué, Université de Sherbrooke, Sherbrooke, Québec,  
16 Canada

17

18 Correspondence: Peng Xian ([peng.xian@nrlmry.navy.mil](mailto:peng.xian@nrlmry.navy.mil))



19 **Abstract**

20

21 We present an Arctic aerosol optical depth (AOD) climatology and trend analysis for  
22 2003-2019 spring and summertime periods derived from a combination of multi-agency  
23 aerosol reanalyses, remote sensing retrievals, and ground observations. This includes  
24 the U.S. Navy Aerosol Analysis and Prediction System ReAnalysis version 1 (NAAPS-  
25 RA v1), the NASA Modern-Era Retrospective Analysis for Research and Applications,  
26 version 2 (MERRA-2), and the Copernicus Atmosphere Monitoring Service ReAnalysis  
27 (CAMSRA). Space-borne remote sensing retrievals of AOD are considered from the  
28 Moderate Resolution Imaging Spectroradiometer (MODIS), the Multi-angle Imaging  
29 SpectroRadiometer (MISR), and Cloud-Aerosol Lidar with Orthogonal Polarization  
30 (CALIOP). Ground-based data include sun photometer data from Aerosol Robotic  
31 Network (AERONET) sites and oceanic Maritime Aerosol Network (MAN)  
32 measurements. Aerosol reanalysis AODs and space-borne retrievals show consistent  
33 climatological spatial patterns and trends for both spring and summer seasons over the  
34 sub-Arctic (60-70°N). Consistent signs in the AOD trend are also found for the high  
35 Arctic (north of 70°N) from reanalyses. The aerosol reanalyses yield more consistent  
36 AOD results than climate models, verify well with AERONET, and corroborate  
37 complementary climatological and trend analysis. Speciated AODs are more variable  
38 than total AOD among the three reanalyses, and a little more so for March-May (MAM)  
39 than for June-August (JJA). Black Carbon (BC) AOD in the Arctic comes predominantly  
40 from biomass burning sources in both MAM and JJA, and biomass burning overwhelms  
41 anthropogenic sources in JJA for the study period.

42 AOD exhibits a negative trend in the Arctic in MAM, and a positive trend in JJA during  
43 2003-2019, due to an overall decrease in sulfate/anthropogenic pollutions, and a  
44 significant increase in biomass burning smoke in JJA. Interannual Arctic AOD variability  
45 is significantly large, driven by fine-mode, and specifically, biomass burning (BB)  
46 smoke, though more so in JJA than in MAM. Extreme AOD events during spring and  
47 summer in the Arctic, defined as AOD greater than the 95th percentile value, are mainly  
48 attributed to BB smoke transport events. Extreme AOD cases tend to occur later in the  
49 season (i.e., July and August, in the latter decade rather than spreading over April-  
50 August in the early decade during 2003-2019) corresponding to a shift to a later time in  
51 extreme boreal BB activities.

52



53 **1. Introduction**

54

55 The Arctic is warming faster than the overall global climate, a phenomenon widely  
56 known as Arctic amplification (Serreze and Francis 2006; Serreze and Barry 2011). This  
57 has led to rapid changes in regional sea ice properties. September sea ice coverage is  
58 shrinking at an unprecedented rate (Comiso 2012; Meier et al., 2014). Younger and  
59 thinner ice is replacing thick multi-year sea ice (Kwok and Rothrock 2009; Hansen et al,  
60 2013; Rosel et al. 2018). Mechanisms contributing to sea ice changes include increased  
61 anthropogenic greenhouse gases (Notz and Stroeve 2016; Dai et al., 2019), sea ice-  
62 albedo feedback (Perovich and Polashenski 2012), increased warm and moist air  
63 intrusion into the Arctic (Boisvert et al. 2016; Woods et al., 2016; Graham et al. 2017),  
64 radiative feedbacks associated with cloudiness and humidity (Kapsch et al. 2013;  
65 Morrison et al. 2018), and increased ocean heat transport (Nummelin et al., 2017;  
66 Taylor et al. 2018). However, one of the least understood factors of Arctic change is the  
67 impact of aerosols on sea ice albedo and concentration (IPCC 2013).

68

69 Atmospheric aerosol particles from anthropogenic and natural sources reach the Arctic  
70 region through both long-range transport and local emissions, affecting regional energy  
71 balance through both direct and indirect radiative processes (Quinn et al., 2008; Engvall  
72 et al., 2009; Flanner, 2013; Sand et al., 2013; Markowicz et al., 2018; Yang et al.,  
73 2018). Aerosol particles influence cloud microphysical properties as cloud condensation  
74 nuclei (CCN) and/or ice nuclei (IN), affecting cloud albedo, lifetime, phase, and  
75 probability of precipitation (e.g. Lubin and Vogelmann, 2006; Lance et al., 2011; Zamora  
76 et al, 2016; Zhao and Garrett 2015; Bossioli et al., 2021). Additionally, deposition of  
77 light-absorbing aerosol species such as dust and black/brown carbon on the surface of  
78 snow and ice can trigger albedo feedbacks and facilitate melting and prolong melting  
79 seasons (Hansen & Nazarenko, 2004; Jacobson, 2004; Flanner et al., 2007; Skiles et  
80 al., 2018; Dang et al., 2017; Kang et al., 2020). However, the impact of aerosol particles  
81 on polar climate change is still not well characterized, and their relative importance  
82 compared to other warming factors is difficult to isolate and quantify.

83 Climate modeling studies show that due to stronger feedback processes between the  
84 atmosphere-ocean-sea-ice-land the Arctic region is more sensitive to local changes in  
85 radiative forcing than tropical and mid-latitude regions (Shindell and Faluvegi 2009;  
86 Sand et al., 2013). On the other hand, there seems to be an emerging agreement on a  
87 higher sensitivity of Arctic clouds by aerosol particles than lower-latitude regions due to  
88 the very low aerosol amounts compared to lower latitudes (Prenni et al., 2007;  
89 Mauritsen et al. 2011; Birch et al., 2012; Coopman et al., 2018; Wex et al., 2019). Both  
90 suggest the important role aerosol particles may play in the Arctic weather and climate,  
91 and the urgency to better quantify the amount of aerosols in the Arctic.



92 A variety of atmospheric aerosol species exist in the Arctic region. Anthropogenic  
93 pollution contributes significantly to the formation of the Arctic haze, which often occurs  
94 in later winter and spring due to wintertime build-up in the shallow boundary layer with  
95 effective transport and reduced removal (e.g., Law and Stohl, 2007; Quinn et al., 2008).  
96 Biomass burning (BB) smoke, originating from wildfires in boreal North America and  
97 Eurasia, are often observed and/or modeled being transported into the Arctic (Eck et al.  
98 2009; Eckhardt et al. 2015; Stohl et al. 2007; Warneke et al. 2009; Iziomon et al., 2006;  
99 Evangeliou et al. 2016; Kondo et al., 2011; Brieder et al., 2014; Markowicz et al. 2016;  
100 Khan et al., 2017; Engelmann et al., 2021). Airborne dust, emitted from exposed sand  
101 or soils due to glacier retreat (Bullard et al., 2016; Groot Zwaafink et al., 2016), are  
102 likely on the rise as the Arctic warms. Dust can also originate from lower latitude  
103 deserts, e.g. Sahara and Asia, and arrive in the Arctic through long-range transport  
104 (Stone et al, 2007; Breider et al., 2014). As the Arctic sea-ice melts and opens up the  
105 ocean surface, emissions of sea salt and biogenic aerosols (e.g., from dimethylsulfide;  
106 Dall et al., 2017; Gabric et al., 2018) are expected to increase. There are also ultrafine  
107 particles nucleated from gaseous precursors, though in small amounts (Baccarini et al.,  
108 2021; Abbatt et al., 2019).

109 Because of the harsh surface environment endemic to the Arctic, aerosol field  
110 measurements are limited compared with the mid-latitude and tropical environments.  
111 Despite an increasing number of field campaigns carried out in the past two decades  
112 (e.g. review by Wendisch et al., 2019; and more recently the MOSAiC, [https://mosaic-](https://mosaic-expedition.org)  
113 [expedition.org](https://mosaic-expedition.org)) and their usefulness in improving process-level understanding, field  
114 measurement periods tend to be short and limited to certain areas and thus are not  
115 necessarily representative spatially and temporally of the whole Arctic. There are many  
116 studies on aerosol optical properties that are based on long-term site measurements  
117 (e.g. Herber et al., 2002; Tomasi et al., 2007; Eck et al., 2009; Saha et al., 2010; Glantz  
118 et al., 2014; Ranjbar et al., 2019; AboEl-Fetouh et al., 2020), however, the number of  
119 the sites is limited, and the sites are mostly located on the northern edge of the North  
120 American, Eurasian continents, and the Svalbard region, not yielding a continuous  
121 spatial distribution.

122 Climate models without constraint from observations exhibit large variations in basic  
123 aerosol optical properties, with an order of magnitude difference in simulated regional  
124 aerosol optical depth (AOD) and large differences in the simulated seasonal cycle of  
125 AOD over the Arctic (e.g. Glantz et al., 2014; Sand et al., 2017). These results do not  
126 reduce the uncertainty in the radiative impact of aerosols through direct (including  
127 surface albedo effect) and indirect forcings in the Arctic climate. Impacts of aerosols and  
128 clouds, overall, constitute one of the largest sources of uncertainty in climate models  
129 (IPCC 2013). This is apparently exacerbated in a warming Arctic (Goosse et al., 2018).  
130 A modeling study by DeRepentigny et al. (2021) shows that the inclusion of



131 interannually varying BB emissions, compared with using climatological ones alone,  
132 introduces a large Arctic climate variability and enhances sea ice loss. This finding  
133 suggests the sensitivity of climate relevant processes to aerosol interannual variability in  
134 the Arctic.

135 In this paper, we present an AOD climatology, trend analysis and extreme events  
136 statistics for the 2003-2019 Arctic spring and summertime, based on a combination of  
137 multi-national interagency aerosol reanalyses, satellite remote sensing retrievals, and  
138 ground observations. We define the Arctic/high-Arctic as regions north of 60°N/70°N,  
139 and sub-Arctic as regions between 60°N-70°N. To reference lower-latitude source  
140 influences, the area of 50°N-90°N is included for context.

141 There are clear advantages of using aerosol reanalyses from chemical transport models  
142 in comparison with climate models for Arctic aerosol studies. Smoke emissions are  
143 frequently updated (e.g., hourly rather than monthly BB smoke emission) and satellite  
144 observations of both meteorological and aerosol data are incorporated into those  
145 aerosol reanalyses through data assimilation. High-latitude fires are strongly influenced  
146 by weather patterns including large-scale transport patterns (e.g. Flannigan and  
147 Harrington 1998; Skinner et al. 1999). Thus, BB smoke in particular, is more realistically  
148 accounted for in aerosol reanalyses.

149 To our knowledge, this is the first time aerosol reanalysis products are evaluated and  
150 compared over the Arctic. The goal of the study is to provide a baseline of AOD  
151 distribution, magnitude, speciation, and interannual variability over the Arctic during sea  
152 ice melting season, which can be used for evaluating aerosol models and further  
153 calculating aerosol radiative forcing, and providing background information for field  
154 campaign data analysis and future field campaign planning in a larger climate context.  
155 The paper is organized as follows: Sect. 2 and 3 introduce the data sets and methods  
156 respectively. Sect. 4 verifies the reanalyses. Results are reported in Sect. 5.  
157 Discussions and conclusions are provided in Sect. 6 and 7.

158

## 159 **2. Data**

160 A combination of aerosol reanalyses, remote sensing aerosol data, and ground-based  
161 aerosol measurements are used to describe source dependent AOD and its trend over  
162 the Arctic during spring (March-May, ie., MAM) and summertime (June-August, ie.,  
163 JJA). The aerosol reanalyses include the Navy Aerosol Analysis and Prediction System  
164 reanalysis (NAAPS-RA; Lynch et al., 2016) developed at the Naval Research  
165 Laboratory, the NASA Modern-Era Retrospective Analysis for Research and  
166 Applications, version 2 (MERRA-2; Randles et al., 2017), and the Copernicus  
167 Atmosphere Monitoring Service ReAnalysis (CAMSR; Inness et al., 2019) produced at  
168 ECMWF. The remote sensing data include retrievals of AOD from the Moderate



169 Resolution Imaging Spectroradiometer (MODIS; Levy et al., 2013), the Multi-angle  
170 Imaging SpectroRadiometer (MISR; Kahn et al., 2010), and Cloud-Aerosol Lidar with  
171 Orthogonal Polarization (CALIOP). Sun photometer data from the Aerosol Robotic  
172 Network (AERONET; Holben et al., 1998) sites and oceanic Maritime Aerosol Network  
173 (MAN, Smirnov et al., 2009) measurements are also used. Overviews of remote sensing  
174 techniques for Arctic aerosols can be found in Tomasi et al. (2015) and Kokhanovsky et  
175 al. (2020). The analysis period is focused on 2003-2019, when all three aerosol  
176 reanalyses are available. Also, both Terra and Aqua Moderate Resolution Imaging  
177 Spectroradiometer (MODIS) AOD retrievals were ingested into those aerosol  
178 reanalyses through data assimilation. It is notable that MODIS AOD retrievals are very  
179 limited over the Arctic region due to snow and ice coverage as well as challenges in  
180 cloud-clearing over cold and bright surfaces. Still, we expect the assimilation of MODIS  
181 AOD over lower latitudes to provide certain constraints in AOD for those aerosol  
182 reanalyses over the Arctic region.

183

#### 184 2.1 MODIS AOD

185 AOD data from MODIS on Terra and Aqua was based on Collection 6.1 Dark Target  
186 and Deep Blue retrievals (Levy et al., 2013). Additional quality control and some  
187 corrections were applied as described in Zhang and Reid 2006, Hyer et al. 2011, Shi et  
188 al. 2011, and Shi et al. 2013, and were updated for the Collection 6.1 inputs. The  
189 quality-assured and quality-controlled MODIS C6 AOD data (550 nm) are a level 3  
190 product that is produced at  $1^\circ \times 1^\circ$  latitude/longitude spatial and 6-hrly resolution. To  
191 study long-term aerosol climatology and trends, the MODIS AOD data are further  
192 binned into monthly from those 6-hrly averages. Seasonal means and trends are  
193 derived only when the total count of  $1^\circ \times 1^\circ$  degree and 6-hrly data is greater than 10 for  
194 a season.

195

#### 196 2.2 MISR AOD

197 Onboard the Terra satellite platform, the MISR instrument provides observations at nine  
198 different viewing zenith angles at four different spectral bands ranging from 446 to 866  
199 nm, allowing for AOD retrievals over bright surfaces, such as desert regions (Kahn et  
200 al., 2010). MISR Version 23 AOD data at 558 nm (Garay et al., 2020) were analyzed  
201 between Jan 2003 and December 2019. No MISR AOD is available over Greenland due  
202 to snow and ice coverage. Monthly gridded MISR AOD data were created by averaging  
203 only MISR data with 100% clear pixels, as defined by each pixel's 'cloud screening  
204 parameter', at a spatial resolution of  $1^\circ \times 1^\circ$  latitude/longitude. Further only data points  
205 with number of seasonal gridded data greater than 20 is used to derive the climatology  
206 and trend.

207



## 208 2.3 CALIOP AOD

209 CALIOP, the primary instrument on the Cloud-Aerosol Lidar and Infrared Pathfinder  
210 Satellite Observations (CALIPSO) satellite, is a polarization-sensitive lidar that operates  
211 at two wavelengths (532 and 1064 nm; Winker et al. 2003). Since its launch in 2006, it  
212 has collected vertical observations of atmospheric aerosols and clouds for over fifteen  
213 years. The CALIPSO analyses for this study primarily utilize daytime and nighttime 532  
214 nm aerosol extinction coefficient data from the Version 4.2 (V4.2) Level 2 (L2) aerosol  
215 profile product (5 km horizontal/60 m vertical resolution) (Kim et al., 2018), with the V4.2  
216 L2 aerosol layer product used for quality assurance (QA) procedures. The CALIOP  
217 aerosol profiles are rigorously QAed before analysis, as implemented and described in  
218 detail in past studies (Campbell et al. 2012; Toth et al. 2016; 2018). Only cloud-free  
219 CALIOP profiles are used, as determined through the atmospheric volume description  
220 (AVD) parameter included in the aerosol profile product (i.e., we implement a strict  
221 cloud screening procedure for which we exclude CALIOP profiles with any range bin  
222 classified as cloud by the AVD parameter). Additionally, we note that a significant  
223 portion of CALIOP aerosol profile data consists of retrieval fill values (-9999s, or RFVs),  
224 due in part to the minimum detection limits of the lidar. In fact, for some areas in the  
225 Arctic region, over 80% of CALIOP profiles consist entirely of RFVs (Toth et al. 2018).  
226 These result in column AODs equal to zero, and as such including them in the  
227 composites would artificially lower the mean AOD. Thus, they are excluded from our  
228 analysis. Lastly, the cloud-free QAed profiles without AOD equal to zero profiles are  
229 used to compute mean CALIOP AOD at  $2^\circ \times 5^\circ$  latitude/longitude resolution. To ensure  
230 spatial and temporal representation, seasonal means and trends are derived only when  
231 the total count of gridded data is greater than 20 for a season.

## 232 2.4 AERONET

233 The AErosol RObotic NETwork (AERONET) is a ground-based global scale sun  
234 photometer network. AERONET instruments measure sun and sky radiance at several  
235 wavelengths, ranging from the near-ultraviolet to the near-infrared. This network has  
236 been providing high-accuracy daytime measurements of aerosol properties since the  
237 1990s (Holben et al., 1998; Holben et al., 2001). Only cloud-screened, quality-assured  
238 version 3 Level 2 AERONET data (Giles et al., 2019) are used in this study.  
239 The 500 nm fine mode (FM) and coarse mode (CM) AODs from the Spectral  
240 Deconvolution Method (SDA) of O'Neill et al. (2003), along with the FM spectral  
241 derivative at 500 nm are used to extrapolate FM AOD to 550 nm. It is assumed the CM  
242 AOD at 500 nm and 550 nm are equal. Total AOD at 550 nm is simply the sum of FM  
243 and CM AODs at 550 nm. The SDA product is an AERONET product that has been  
244 verified using in situ measurements (see for example Kaku et al., 2014) and a variety of  
245 co-located lidar experiments (see, for example, Saha et al., 2010 and Baibakov et al.,  
246 2015). The FM and CM separation is effected spectrally: this amounts to a separation of



247 the FM and CM optical properties associated with their complete FM and CM particle  
248 size distributions. This optical separation, characterized by the ratio of FM AOD to total  
249 AOD at 550 nm is referred to as the fine mode fraction (FMF). An analogous FM and  
250 CM AOD separation in terms of a cutoff radius applied to the retrieved or measured  
251 particle size distribution is referred to as the sub-micron fraction (SMF; where the  
252 numerator of the SMF is the FM AOD associated with the AOD contribution of particles  
253 below the cutoff radius). The SMF is the basis of the comprehensive AERONET (AOD &  
254 sky radiance) inversion. The SDA algorithm and the AERONET inversion generate FM  
255 and CM AODs that are moderately different (see Sect. 4 Kleidman et al., 2005): the  
256 advantage of the SDA is its significantly higher retrieval resolution (~ a few minutes  
257 versus ~ an hour for the AERONET inversion) and thus retrieval numbers, its  
258 independence from a variable cut off radius and its greater operational generality (being  
259 applicable to other networks such as the MAN sunphotometer network).

260

261 AERONET data are binned into 6-hr intervals centered at normal synoptic output times  
262 of the reanalyses (0, 6, 12, and 18 UTC) and then averaged within the bins. Monthly  
263 mean AERONET AOD is derived only when the count of 6-hr AERONET data exceeds  
264 18 to ensure temporal representativeness. Ten AERONET sites were selected (Table 1,  
265 Fig. 1) based on regional representativeness (coupled with the reality of the sparsity of  
266 AERONET sites in the Arctic), the availability of data records between Jan 2003 and  
267 Dec 2019 (the main study period), and for easier comparison with other Arctic studies  
268 (e.g. Sand et al., 2017).

269

270 We found that thin clouds could occasionally be identified and retrieved as CM aerosols  
271 in level 2, version 3 AERONET data. These retrievals were manually removed by  
272 identifying such thin clouds using Terra and Aqua visible-wavelength imagery from  
273 [NASA Worldview](#) and comparing 6-hrly NAAPS-RA with AERONET AODs. CM AOD  
274 greater than 3-sigma level was then also removed (as per AboEl-Fetouh et al., 2020).

275

## 276 2.5 MAN AOD

277 The Marine Aerosol Network (MAN) is a hand-held Microtops sun photometer  
278 counterpart to AERONET, available for over ocean measurements where a standard  
279 Cimel sun photometer is not feasible (Smirnov et al., 2009, 2011). The products share  
280 AERONET nomenclature, and data processing is similar to that of AERONET. For this  
281 study, Level2 data above 60°N for the period of 2003-2019 are used. FM and CM AOD  
282 at 550 nm are derived based on SDA (O'Neill et al., 2003) and averaged over 6-hr time  
283 bins.

284

## 285 2.6 NAAPS AOD reanalysis v1



286 The Navy Aerosol Analysis and Prediction System (NAAPS) AOD reanalysis (NAAPS-  
287 RA) v1 provides 550 nm speciated AOD at a global scale with  $1^{\circ}\times 1^{\circ}$  degree spatial and  
288 6-hrly temporal resolution for the years 2003-2019 (Lynch et al., 2016). This reanalysis  
289 is based on NAAPS with assimilation of quality-controlled retrievals of AOD from  
290 MODIS and MISR (Zhang et al., 2006; Hyer et al., 2011; Shi et al., 2011). AODs from  
291 anthropogenic and biogenic fine aerosol species (ABF, a mixture of sulfate, BC, organic  
292 aerosols and secondary organic aerosols from non-BB sources), dust, biomass-burning  
293 smoke, and sea salt aerosols are available. The aerosol source functions were tuned to  
294 obtain the best match between the model FM and CM AODs and the AERONET AODs  
295 for 16 regions globally. Wet deposition processes were constrained with satellite-  
296 derived precipitation (Xian et al., 2009). The reanalysis reproduces the decadal AOD  
297 trends found using standalone satellite products over the globe (except the polar  
298 regions due to lack of verification data) in other studies (e.g., Zhang et al., 2010; 2017).  
299 Note that although a first-of-its-kind Ozone Monitoring Instrument (OMI) data  
300 assimilation method has been developed for directly assimilation OMI Aerosol Index (AI)  
301 over bright surfaces such as snow and ice covered regions (Zhang et al., 2021),  
302 research progress is on-going for developing data-assimilation quality OMI AI data over  
303 the Arctic region and thus, the OMI AI data assimilation is not included in this study.

#### 304 2.7 MERRA-2 AOD reanalysis

305 NASA Modern-Era Retrospective Analysis for Research and Applications, version 2  
306 (MERRA-2) includes aerosol reanalysis, which incorporates assimilation of AOD from a  
307 variety of remote sensing sources, including MODIS and MISR after 2000. The aerosol  
308 module used for MERRA-2 is the Goddard Chemistry, Aerosol Radiation and Transport  
309 model (GOCART; Chin et al. 2000; Colarco et al., 2010), which provides simulations of  
310 sulfate, black and organic carbon, dust and sea salt aerosols. A detailed description and  
311 global validation of the AOD reanalysis product can be found in Randles et al. (2017)  
312 and Buchard et al. (2017). For this study, monthly mean speciated AODs and total AOD  
313 at 550 nm with  $0.5^{\circ}$  latitude and  $0.625^{\circ}$  longitude spatial resolution are used.

#### 314 2.8 CAMSRA AOD reanalysis

315 The Copernicus Atmosphere Monitoring Service (CAMS) Reanalysis (CAMSRA, Inness  
316 et al., 2019) is a new global reanalysis of atmospheric composition produced at the  
317 ECMWF, after the MACC reanalysis (Inness et al., 2013) and CAMS interim reanalysis  
318 (Flemming et al., 2017). The dataset covers the period of 2003–2020 and is being  
319 continued for subsequent years. The model is driven by the Integrated Forecasting  
320 System (IFS) used at ECMWF for weather forecasting and meteorological reanalysis,  
321 but at a coarser resolution and with additional modules activated for prognostic aerosol  
322 species (dust, sea salt, organic matter, black carbon and sulfate) and trace gases.



323 Radiative impact of aerosol particles and ozone on meteorology is included. Satellite  
324 retrievals of total AOD at 550 nm are assimilated from MODIS for the whole period, and  
325 from the Advanced Along-Track Scanning Radiometer for 2003–2012, using a 4D  
326 variational data assimilation system with a 12-hour data assimilation window along with  
327 meteorological and trace gas observations. The speciated AOD products are available  
328 at a 3-hourly temporal resolution and a  $\sim 0.7^\circ$  spatial resolution, and monthly mean  
329 AODs at 550 nm are used in this study. Model development has generally improved the  
330 speciation of aerosols compared with earlier reanalyses, and evaluation against  
331 AERONET globally is largely consistent over the period of the reanalysis.

### 332 2.9 Multi-reanalysis-consensus (MRC) AOD

333 All three of the individual reanalyses are largely independent in their underlying  
334 meteorology and in their aerosol sources, sinks, microphysics, and chemistry. They  
335 were also generated through data assimilation (DA) of satellite and/or ground-based  
336 observations of AOD. The assimilation methods, and the assimilated AOD observations,  
337 including the treatments of the observations prior to assimilation (quality control, bias  
338 correction, aggregation, and sampling, etc.), are often different too, despite consistent  
339 use of data from the MODIS with its daily global spatial coverage.

340 Based on the three aerosol reanalysis products described above, we made an MRC  
341 product following the multi-model-ensemble method of the International Cooperative for  
342 Aerosol Prediction (ICAP, Sessions et al., 2015; Xian et al., 2019). The MRC is a  
343 consensus mean of the three individual reanalyses, with a  $1^\circ \times 1^\circ$  degree spatial and  
344 monthly temporal resolution. Speciated AODs and total AOD at 550 nm for 2003–2019  
345 are available. This new product is validated here with ground-based AERONET  
346 observations for the Arctic along with three component reanalysis members. Validation  
347 results in terms of bias, RMSE, and coefficient of determination ( $r^2$ ) for monthly-mean  
348 total, FM and CM AODs are presented in Tables 2, 3, 4. The MRC, in accordance with  
349 the ICAP multi-model-consensus evaluation result, is found to generally be the top  
350 performer among all of the reanalyses for the study region.

351

### 352 2.10 Fire Locating and Modeling of Burning Emissions (FLAMBE) v1.0

353

354 FLAMBE is a biomass-burning emission inventory based on satellite active fire hotspot  
355 approach (Reid et al., 2009; Hyer et al., 2013). FLAMBE can take satellite fire products  
356 from either geostationary sensors, which offer faster refresh rates and observation of  
357 the full diurnal cycle, or polar orbiters, which have a greater sensitivity. There are  
358 significant daily sampling biases and additional artifacts from day to day shifts in the  
359 orbital pattern for polar-orbiting satellites (e.g., Heald et al., 2003, Hyer et al., 2013).  
360 However, the polar-only version of FLAMBE, which takes MODIS-based fire data, is



361 more appropriate for reanalysis and trend analysis, as over the study period, multiple  
362 changes in the geostationary constellation posed a challenge for consistency of the  
363 smoke source function. Because of the same requirement for temporal consistency, the  
364 FLAMBE MODIS-only smoke source was also used in the NAAPS-RA v1. Inferring from  
365 the time series of yearly BB emission for the Arctic region based on other inventories,  
366 including the Global Fire Assimilation System (GFAS; Kaiser et al., 2012), and the  
367 Global Fire Emission Dataset (GFED; Randerson et al., 2006; van derWerf et al., 2006),  
368 FLAMBE has the same sign of trend of BB emissions for the similar study period (using  
369 BC emission of Fig. 2 in McCarty et al., 2021).

370

### 371 **3. Method**

372 The Arctic AOD climatology and trends are analyzed in this study using remote sensing  
373 products derived from MODIS, MISR, CALIOP, and AERONET (each sensor typically  
374 generating aerosol products of different native wavelengths). The 550 nm AOD was  
375 employed as the benchmark parameter for this study since the three aerosol reanalyses  
376 AODs and the MODIS AOD are all available at 550 nm while the 558nm and 532nm  
377 AODs of MISR and CALIOP are appreciably close to 550 nm. AERONET and MAN  
378 modal AODs at 550 nm were derived using the SDA method as described in Sect. 2.4  
379 and 2.5. Arithmetic means were employed for all the data processing in order to be  
380 consistent with the arithmetic statistics that are usually reported in the literature and with  
381 the arithmetic statistics of the monthly data from the aerosol reanalyses. Various studies  
382 have shown that geometric statistics are more representative of AOD histograms (see,  
383 for example, Hesaraki et al., 2017 and Sayer et al., 2019). However, Hesaraki et al.  
384 (2017) showed that arithmetic statistics could be employed to readily estimate  
385 geometric statistics<sup>1</sup>. This option effectively renders the reporting of arithmetic or  
386 geometric statistics less critical.

387 The species of interest are biomass burning (BB) smoke, anthropogenic and biogenic  
388 fine aerosols (ABF) in NAAPS, and its equivalent of sulfate for MERRA-2 and CAMSRA,  
389 dust and sea salt aerosols. Anthropogenic aerosol particles, as an external climate  
390 forcer, normally draw noticeable attention in climate studies (e.g. Wang et al., 2018;  
391 Ren et al., 2020; Yang et al., 2018; Sand et al., 2016; Eckhardt et al., 2015; Brieder et  
392 al., 2017). However, BB smoke, which can be both natural and anthropogenic in origin,  
393 are often shown to be the largest contributor to AOD and concentration during the Arctic  
394 summer over the last two decades, in both modeling (Evangelidou et al. 2016; Sand et al.  
395 2017) and observational-based studies (Eck et al. 2009; Eckhardt et al. 2015; Stohl et  
396 al. 2007; Warneke et al. 2009). Recent measurements of BC in Arctic snow also show a  
397 strong association with BB based on tracer correlations and optical properties (Hegg et

---

<sup>1</sup> with an erratum: the equation (2) transformation to geometric mean should be  $\tau_{g,x} = \frac{\langle \tau_x \rangle}{\exp\left(\frac{\ln^2 \mu_x}{2}\right)}$



398 al., 2009; Doherty et al., 2010; Hegg et al., 2010; Khan et al., 2017). A climate modeling  
399 study recently found that a much larger Arctic climate variability and enhanced sea ice  
400 melting are introduced by using BB emissions with interannual variability compared to  
401 using a climatological monthly mean BB emission (DeRepentigny et al., 2021),  
402 indicating the importance of quantifying the magnitude and interannual variability of BB  
403 smoke in Arctic climate forcing estimates. Thus BB smoke AOD is separated out from  
404 the total AOD as a single species in this study.

405 The separation of species in this analysis is a bit arbitrary as the representation of  
406 different aerosol types and sources in each reanalysis is slightly different. The NAAPS  
407 model is unique compared to other reanalyses and operational models in that it carries  
408 aerosol species by source rather than chemical speciation. For example, biomass  
409 burning and a combined ABF are carried as separate species and permit explicit  
410 hypothesis testing about the sources, sinks, and optical properties. Conversely,  
411 MERRA-2 and CAMSRA carry organic carbon (OC)/organic matter (OM), black carbon  
412 (BC) and various inorganic species combining a multitude of anthropogenic, biogenic  
413 and open biomass burning source pathways. In this study the sum of OC/OM and BC  
414 AOD is used to approximate BB smoke AOD from CAMSRA and MERRA-2. The ratio of  
415 BC to the sum of BC and OC/OM is about 10% for areas north of 60°N on average for  
416 both MERRA-2 and CAMSRA for both MAM and JJA, except about 20% in MERRA-2  
417 for MAM.

418 It is worth noting that all the three reanalyses use hourly/daily BB smoke emission  
419 inventories that use dynamic smoke sources detected by polar-orbiting satellites, e.g.,  
420 FLAMBE (Reid et al., 2009) for NAAPS-RA, Quick Fire Emissions Dataset (QFED) for  
421 MERRA-2 after 2010 (GFED with monthly BB emission before 2010, Randerson et al.,  
422 2006; van derWerf et al., 2006), and Global Fire Assimilation System (GFAS, Kaiser et  
423 al., 2012) for CAMSRA. This is expected to yield a better spatial and temporal  
424 representation of BB smoke emissions compared to the climate models in which  
425 monthly mean BB inventories are often applied (e.g. Sand et al., 2017).

426 We also assume all dust and sea salt are CM, while other model aerosol species,  
427 including ABF in NAAPS-RA, sulfate in MERRA-2 and CAMSRA, BB smoke in NAAPS-  
428 RA, black carbon and organic carbon in MERRA-2 and CAMSRA are FM aerosol  
429 particles. This approximation (the sequestering of dust and sea salt to the coarse mode  
430 regime) is based on the fact that FM dust and sea salt only contribute to a small portion  
431 of the total dust or sea salt AOD at 550 nm (for example, FM mode dust contributes to  
432 about 30% and 39% of total dust AOD globally in MERRA-2 and CAMSRA respectively.  
433 The numbers are 17% and 10% for sea salt), while NAAPS-RA has a simple  
434 microphysics that assumes all dust and sea salt are CM. This usage renders the bulk-  
435 aerosol analysis more convenient.



436 The significance test for trend analysis applies the same calculation method as in Zhang  
437 et al. (2010; 2017), following the method of Weatherhead et al. (1998). This trend  
438 analysis method requires a continuous time series of data.

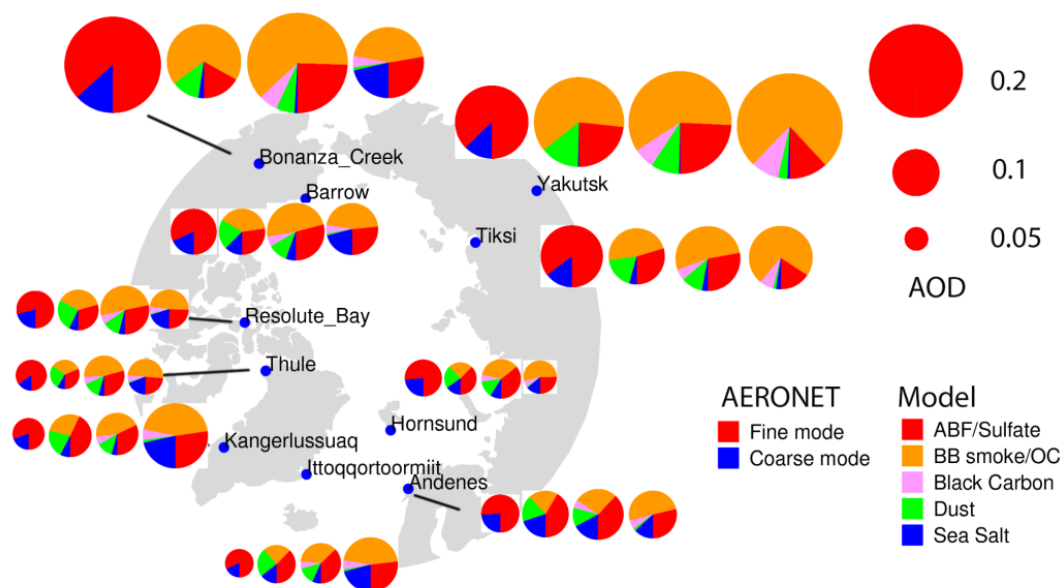
#### 439 **4. Comparison of AODs from aerosol reanalyses and AERONET**

440 AERONET observations are typically more frequent during the summer than in the  
441 spring and are therefore more temporally representative in JJA. As a consequence, we  
442 preferentially used a JJA climatology to illustrate reanalyses vs AERONET  
443 comparisons. Figure 1 shows the 2003-2019 JJA mean fine mode (FM) and coarse  
444 mode (CM) AODs at 550 nm from AERONET and the speciated AODs at 550 nm from  
445 NAAPS-RA, MERRA-2, and CAMSRA. All three aerosol reanalyses appear to capture  
446 the total AOD magnitudes to varying extents. The AERONET retrievals show that total  
447 AOD during the Arctic JJA season is dominated by contributions from FM aerosols.  
448 High FM AOD values (indicative of strong BB smoke influence) are found in Yakutsk  
449 and Tiksi in Siberia, and Bonanza Creek in Alaska. CM aerosols also contribute a  
450 substantial fraction, varying from a minimum of 15% in regions close to BB smoke  
451 sources to a maximum of ~25% at the Norwegian Sea and Greenland Sea coastal sites  
452 (Hornsund, Andenes, and Ittoqqortoormitt): these sites are likely impacted by sea salt  
453 aerosols lifted by North Atlantic cyclonic events. NAAPS-RA produces comparable FM  
454 and total AODs in general while showing a tendency to overestimate CM AODs (see  
455 Table 2 for explicit biases). The other two reanalyses (MERRA-2 and CAMSRA)  
456 produce higher FM AOD and total AOD and lower CM AOD compared to AERONET  
457 (see also Table 2).

458 Differences exist between the three reanalyses with respect to the FM and CM  
459 partitioning of aerosol species. For example, sea salt aerosols always dominate in the  
460 CAMSRA CM: this is a comment that even applies to some inland sites (e.g. Bonanza-  
461 Creek) and implies a modeling issue. Dust is the dominant CM species in NAAPS-RA  
462 and MERRA-2. This latter result was found for all AERONET sites: it is attributable to  
463 elevated dust layers transported from lower latitudes (Stone et al., 2007; Jacob et al.,  
464 2010; Breider et al., 2014; Aboele-Fetouh et al., 2020). The proportional contribution of  
465 dust to total AOD is the largest in NAAPS-RA: a result that could have contributed to its  
466 high bias in CM AOD (Table 2). The contribution of organic matter to FM AOD is  
467 generally larger in CAMSRA than in the other two reanalyses. On the whole, BB smoke  
468 is the largest contributing species to total JJA AOD over the Arctic. This is consistent  
469 across all the reanalyses except for some sites in NAAPS-RA (e.g. Andenes, Hornsund,  
470 and Kangerlussuaq where ABF AOD is slightly larger than BB smoke AOD). This can  
471 be partially due to the different types of speciation employed in NAAPS-RA: ABF  
472 includes anthropogenic and biogenic pollution aerosols, including sulfate, BC and  
473 organic aerosols of all origins except for biomass burning. It is also worth noting that



474 mean AODs over these Arctic sites are, in general, higher (0.01-0.02, and can be ~0.1  
475 higher for the sites close to BB sources) than their median counterparts (Table 1) as  
476 well as their geometric means because AOD histograms are typically more lognormal  
477 than normal in form (asymmetric linear-AOD histograms with positively skewed tails as  
478 per, for example, Hesaraki et al., 2017): arithmetic means are, accordingly, often driven  
479 by extreme (>95% percentile for example) AOD events. Because these extreme events  
480 constitute an important part of the Arctic aerosol environment, the AOD means are  
481 presented here.



482  
483 **Figure 1.** Polar projection map showing the locations of the AERONET Arctic sites (blue  
484 dots) used in this study. Long-term (2003-2019) JJA-mean FM and CM AODs at 550  
485 nm from AERONET (leftmost circle of each group of four circles) and respectively, the  
486 speciated pie-charts of 550 nm AODs from NAAPS-RA, MERRA2, and CAMSRA for  
487 each site. Warm colors represent fine mode and cool colors represent coarse mode.  
488

489 **Table 1.** Geographical properties of AERONET sites used in this study, and seasonal  
490 mean total, FM and CM AOD at 550nm derived with SDA for MAM and JJA based on  
491 2003-2019 data when available. “n” represents the number of 6-hrly AERONET data.



sites	latitude	longitude	elevation (m)	region	MAM (mean median std)				MAM FMF		JJA (mean median std)				JJA FMF	
					total AOD	FM AOD	CM AOD	n	mean median	total AOD	FM AOD	CM AOD	n	mean median		
Hornsund	77.0N	15.6E	12	Svalbard	0.10 0.09 0.06	0.07 0.06 0.04	0.03 0.02 0.04	877	0.70	0.74	0.08 0.06 0.07	0.06 0.04 0.06	0.02 0.01 0.03	977	0.76	0.82
Thule	76.5N	68.8W	225	Greenland	0.09 0.07 0.05	0.06 0.05 0.03	0.03 0.01 0.04	1,233	0.76	0.81	0.07 0.05 0.07	0.06 0.04 0.06	0.01 0.01 0.02	1,555	0.85	0.88
Kangerlussuaq	67.0N	50.6W	320	Greenland	0.07 0.06 0.04	0.05 0.04 0.02	0.02 0.02 0.03	964	0.69	0.73	0.07 0.05 0.05	0.05 0.04 0.05	0.01 0.01 0.02	1,769	0.78	0.84
Ittoqqortoormit	70.5N	21.0W	68	Greenland	0.07 0.06 0.05	0.04 0.04 0.02	0.03 0.01 0.04	635	0.72	0.78	0.06 0.04 0.05	0.05 0.03 0.05	0.01 0.01 0.02	1,280	0.81	0.86
Andenes	69.3N	16.0E	379	Norway	0.08 0.07 0.05	0.05 0.04 0.03	0.03 0.02 0.04	828	0.66	0.70	0.08 0.07 0.05	0.06 0.05 0.05	0.02 0.01 0.02	1,008	0.75	0.78
Resolute Bay	74.7N	94.9W	35	Canada	0.10 0.08 0.06	0.07 0.06 0.04	0.03 0.02 0.04	515	0.73	0.78	0.08 0.05 0.11	0.06 0.04 0.10	0.02 0.01 0.03	1,146	0.78	0.83
Barrow	71.3N	156.7W	8	Alaska	0.11 0.09 0.08	0.08 0.06 0.05	0.04 0.02 0.05	619	0.72	0.77	0.10 0.07 0.15	0.08 0.05 0.15	0.02 0.01 0.03	1,157	0.79	0.82
Bonanza Creek	64.7N	148.3W	353	Alaska	0.11 0.08 0.10	0.06 0.04 0.08	0.04 0.03 0.05	975	0.61	0.60	0.21 0.09 0.36	0.18 0.06 0.35	0.03 0.02 0.03	1,718	0.74	0.76
Tiksi	71.6N	129.0E	17	Siberia	0.10 0.10 0.03	0.08 0.08 0.03	0.02 0.01 0.02	39	0.80	0.82	0.13 0.08 0.18	0.11 0.07 0.17	0.02 0.01 0.02	449	0.80	0.85
Yakutsk	61.7N	129.4E	119	Siberia	0.15 0.11 0.15	0.11 0.08 0.13	0.04 0.02 0.05	1,454	0.74	0.78	0.16 0.09 0.25	0.14 0.07 0.25	0.02 0.01 0.02	2,414	0.80	0.84

492

493 Table 1 provides detailed geographical properties of the ten AERONET sites and the  
 494 (arithmetic) mean, median and standard deviation of total, FM and CM AODs at 550 nm  
 495 for both MAM and JJA based on available 2003-2019 data (the availability of AERONET  
 496 data can be inferred from the monthly time series in Figure 2). The seasonal mean total  
 497 AOD for Resolute Bay, the Greenland sites and Hornsund sites are  $< \sim 0.1$  (0.06-0.10)  
 498 while the Alaskan and Siberian sites values are  $> \sim 0.1$  (0.10 to 0.15 with Bonanza  
 499 Creek displaying a substantially larger value of 0.21 in JJA). All sites, except Bonanza  
 500 Creek, tend to have moderately higher median AOD in MAM: this is consistent with  
 501 other Arctic sunphotometer studies (Tomasi et al., 2015; Xie et al., 2018). The decrease  
 502 in JJA, according to the reanalyses (Fig 4 and 5), is related to higher FM ABF/sulfate  
 503 and/or CM dust and sea salt in MAM. It is also noted that this AOD seasonal difference  
 504 may have evolved in the past two decades with a decreasing trend in ABF/sulfate as  
 505 discussed in Sect. 5.3. The seasonal mean AOD is greater in JJA than in MAM for  
 506 Yakutsk, Tiksi and Bonanza Creek: this is likely due to strong FM AOD variations  
 507 associated with BB smoke events (see, for example, the discussions concerning the  
 508 seasonal competition between FM AOD smoke and FM AOD Arctic haze, in AboEI-  
 509 Fetouh et al., 2020). The standard deviations of the total and FM AODs are also high for  
 510 those three sites.

511 The Table 1 median and mean of the FMF vary, respectively, between 0.60 to 0.88 and  
 512 0.66 to 0.85 with higher FMF in JJA than in MAM. The MAM to JJA increase is coherent  
 513 with the month-to-month increase of AboEI-Fetouh et al., (2020) although their 550 nm  
 514 arithmetic means tend to be larger (monthly-binned extremes of 0.81 to 0.98). Most of  
 515 this difference is likely attributable to differences between our FMF (SDA) separation of  
 516 the product and the SMF (AERONET-inversion) separation of AboEI-Fetouh et al.'s  
 517 climatology: the SMF is generally larger than the FMF because it tends to attribute a  
 518 fraction of the CM particle size distribution and thus a fraction of the CM AOD to the FM  
 519 AOD (see, for example, the 550 nm SMF vs FMF comparisons of Kleidman et al.,  
 520 2005). More discussions about the differences in terms of FMF vs. SMF and arithmetic  
 521 vs. geometric statistics are available in the supplement material.

522 **Table 2.** Total, FM and CM AOD bias of CAMSRA, MERRA-2, NAAPS-RA and their  
 523 consensus mean MRC compared to AERONET monthly data.



524

sites	Bias-total AOD				Bias-FM AOD				Bias-CM AOD			
	CAMSRA	MERRA2	NAAPS-RA	MRC	CAMSRA	MERRA2	NAAPS-RA	MRC	CAMSRA	MERRA2	NAAPS-RA	MRC
Hornsund	-0.02	0.01	0.00	0.00	-0.01	0.01	-0.01	0.00	-0.01	0.01	0.02	0.00
Thule	0.00	0.02	0.00	0.01	0.01	0.02	-0.01	0.01	-0.01	0.00	0.01	0.00
Kangerlussuaq	0.02	0.02	0.02	0.02	0.03	0.02	0.02	0.02	-0.01	0.00	0.02	0.00
Ittoqqortoormiit	0.04	0.03	0.02	0.03	0.04	0.02	0.00	0.02	0.00	0.01	0.02	0.01
Andenes	0.03	0.04	0.02	0.03	0.03	0.02	0.00	0.02	0.00	0.02	0.02	0.01
Resolute_Bay	0.01	0.02	0.01	0.01	0.03	0.02	0.00	0.02	-0.02	0.00	0.01	0.00
Barrow	0.02	0.03	0.00	0.02	0.04	0.03	-0.01	0.02	-0.02	0.00	0.02	0.00
Bonanza_Creek	0.06	0.04	0.00	0.03	0.09	0.00	0.05	0.05	-0.02	-0.01	0.00	-0.01
Tiksi	0.02	0.02	-0.01	0.01	0.04	0.02	-0.01	0.02	-0.02	0.00	0.01	0.00
Yakutsk	0.03	0.04	0.01	0.03	0.05	0.05	0.00	0.03	-0.02	0.00	0.01	-0.01
mean	0.02	0.03	0.01	0.02	0.04	0.03	0.00	0.02	-0.01	0.00	0.01	0.00
median	0.02	0.03	0.01	0.02	0.04	0.02	0.00	0.02	-0.02	0.00	0.02	0.00

525

526 **Table 3.** Same as Table 2, except for RMSE.

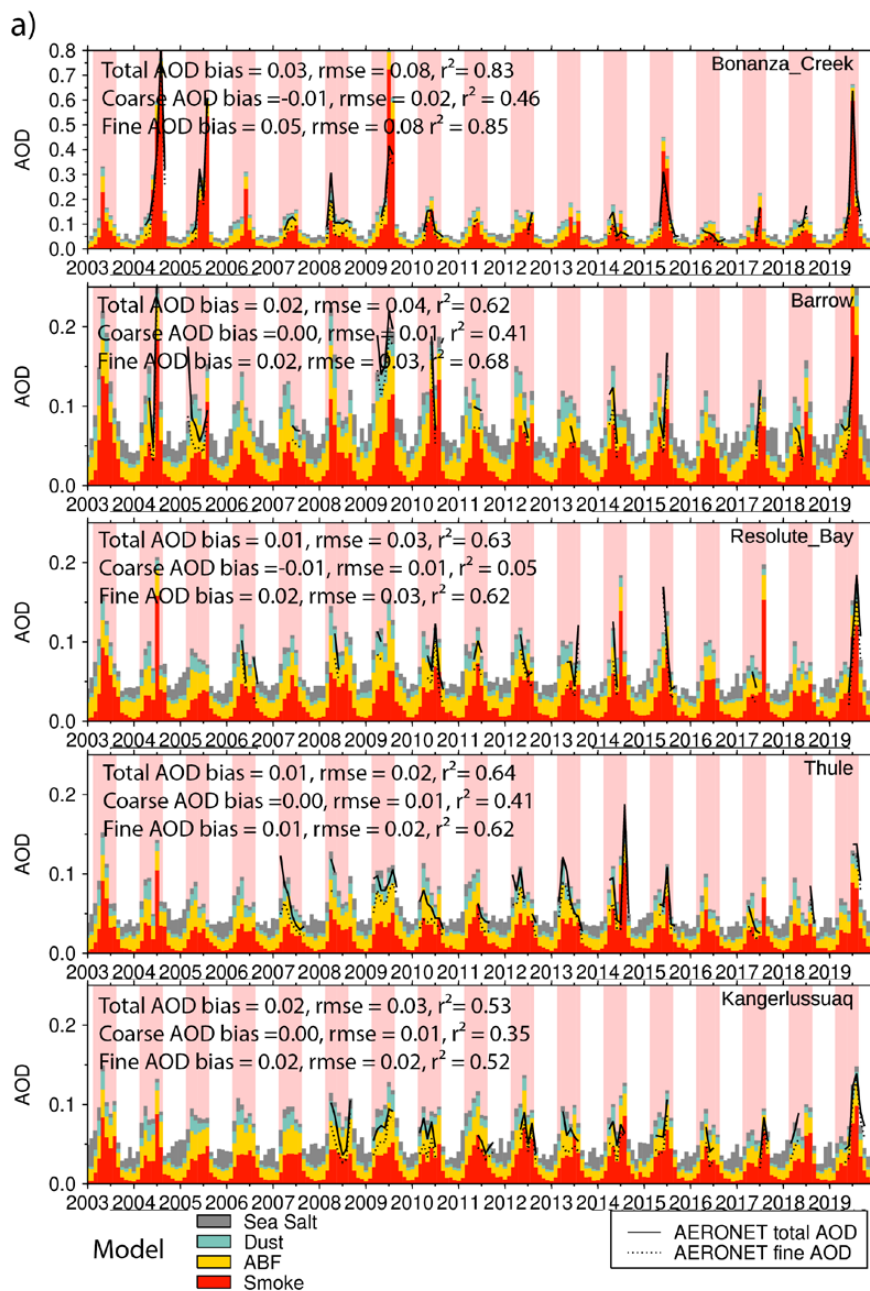
527

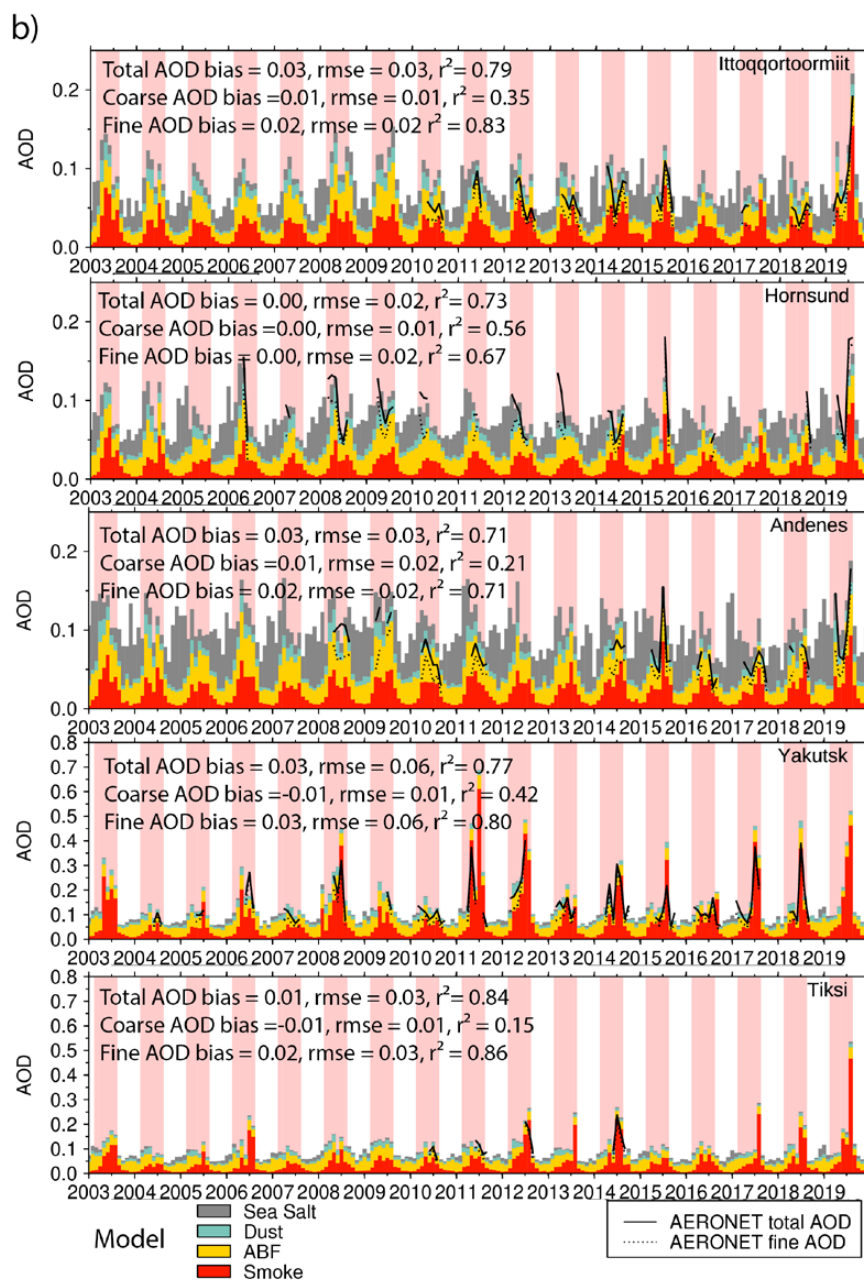
sites	RMSE-total AOD				RMSE-FM AOD				RMSE-CM AOD			
	CAMSRA	MERRA2	NAAPS-RA	MRC	CAMSRA	MERRA2	NAAPS-RA	MRC	CAMSRA	MERRA2	NAAPS-RA	MRC
Hornsund	0.04	0.02	0.02	0.02	0.03	0.02	0.02	0.02	0.02	0.01	0.02	0.01
Thule	0.02	0.03	0.02	0.02	0.03	0.03	0.02	0.02	0.02	0.01	0.02	0.01
Kangerlussuaq	0.03	0.03	0.03	0.03	0.04	0.02	0.02	0.02	0.01	0.01	0.02	0.01
Ittoqqortoormiit	0.04	0.03	0.02	0.03	0.05	0.03	0.01	0.02	0.01	0.01	0.02	0.01
Andenes	0.03	0.04	0.03	0.03	0.03	0.03	0.02	0.02	0.01	0.02	0.03	0.02
Resolute_Bay	0.03	0.04	0.02	0.03	0.04	0.04	0.02	0.03	0.02	0.01	0.02	0.01
Barrow	0.05	0.05	0.03	0.04	0.06	0.04	0.03	0.03	0.02	0.01	0.02	0.01
Bonanza_Creek	0.11	0.10	0.07	0.08	0.12	0.10	0.06	0.08	0.03	0.02	0.01	0.02
Tiksi	0.05	0.04	0.02	0.03	0.06	0.04	0.02	0.03	0.02	0.01	0.01	0.01
Yakutsk	0.07	0.07	0.04	0.06	0.08	0.07	0.04	0.06	0.03	0.01	0.01	0.01
mean	0.05	0.05	0.03	0.04	0.05	0.04	0.03	0.03	0.02	0.01	0.02	0.01
median	0.04	0.04	0.03	0.03	0.05	0.04	0.02	0.03	0.02	0.01	0.02	0.01

528 **Table 4.** Same as Table 2, except for  $r^2$ .

529

sites	$r^2$ -total AOD				$r^2$ -FM AOD				$r^2$ -CM AOD			
	CAMSRA	MERRA2	NAAPS-RA	MRC	CAMSRA	MERRA2	NAAPS-RA	MRC	CAMSRA	MERRA2	NAAPS-RA	MRC
Hornsund	0.23	0.78	0.75	0.73	0.35	0.73	0.71	0.67	0.27	0.45	0.55	0.56
Thule	0.50	0.47	0.73	0.64	0.52	0.45	0.70	0.62	0.01	0.26	0.44	0.41
Kangerlussuaq	0.48	0.54	0.42	0.53	0.52	0.52	0.35	0.52	0.00	0.57	0.16	0.35
Ittoqqortoormiit	0.68	0.75	0.67	0.79	0.63	0.81	0.76	0.83	0.24	0.36	0.14	0.35
Andenes	0.67	0.63	0.68	0.71	0.68	0.66	0.64	0.71	0.10	0.23	0.21	0.21
Resolute_Bay	0.52	0.51	0.67	0.63	0.53	0.49	0.73	0.62	0.02	0.06	0.03	0.05
Barrow	0.33	0.68	0.70	0.62	0.45	0.76	0.69	0.68	0.05	0.27	0.41	0.41
Bonanza_Creek	0.81	0.78	0.80	0.83	0.83	0.79	0.82	0.85	0.06	0.43	0.45	0.46
Tiksi	0.77	0.80	0.87	0.84	0.82	0.82	0.90	0.86	0.02	0.20	0.10	0.15
Yakutsk	0.70	0.70	0.80	0.77	0.78	0.71	0.80	0.80	0.01	0.41	0.42	0.42
mean	0.57	0.66	0.71	0.71	0.61	0.67	0.71	0.72	0.08	0.32	0.29	0.34
median	0.60	0.69	0.72	0.72	0.58	0.72	0.72	0.70	0.04	0.32	0.31	0.38





531  
532  
533  
534  
535  
536

**Figure 2.** Monthly time series of fine, coarse, and total AODs from AERONET and MRC speciated AOD at a) Bonanza Creek, Barrow, Resolute\_Bay, Thule, Kangerlussuq, and b) Ittoqqortoormiit, Hornsund, Andenes, Yakutsk, and Tiksi sites. The JJA periods are highlighted with pink shading for easy reading. Annotations for each time series show bias, RMSE and  $r^2$  calculated from the MRC. Monthly mean AERONET AOD is obtained



537 only when the total number of 6-hr AERONET data exceeds 18 to ensure temporal  
538 representativeness.

539 Figure 2 shows the time series of monthly mean modal AODs and total AODs from the  
540 10 AERONET stations (CM AOD can be inferred from the difference between total AOD  
541 and FM AOD) and the speciated AODs from MRC (recall the approximation of dust and  
542 sea salt as CM, and ABF/sulfate and smoke as FM). The MRC verification statistics at  
543 the ten AERONET sites based on monthly data are given in the legends of Figure 2.  
544 Verification statistics of individual aerosol reanalysis members and the MRC based on  
545 monthly data are presented in Tables 2, 3, and 4 for bias, RMSE, and  $r^2$  respectively.  
546 The MRC is consistently biased slightly high for FM AOD across all sites and about  
547 neutral for CM AOD for most. As a result, total AOD tends to bias slightly high, with  
548 biases ranging from 0.00 to 0.03. RMSE values range from 0.02 to 0.03 for most sites,  
549 except for Bonanza Creek, Yakutsk and Barrow with RMSE values of 0.06, 0.05 and  
550 0.04, driven mainly by FM variations. The  $r^2$  value ranges from 0.53 to 0.84, with FM  
551 AOD correlation ranging from much higher to marginally higher than that of CM AOD.  
552 This is understandable as FM AOD displays large variabilities (which models are more  
553 capable of capturing) while CM AOD displays relatively low values and smaller absolute  
554 variabilities on seasonal and interannual time scales. Also, emissions of CM aerosols  
555 like dust and sea salt, are driven dynamically by model or reanalysis surface winds  
556 where the surface wind dependency increases exponentially in amplitude: the  
557 simulation of this dependency has been a challenge to all global aerosol models  
558 (Sessions et al., 2015; Xian et al., 2019).

559 Our previous experience with multi-reanalysis and multi-model ensembles indicates, in  
560 general, that the consensus of multi-reanalyses or multi-models show better verification  
561 scores than individual component members (Sessions et al., 2015; Xian et al., 2019;  
562 Xian et al., 2020). However, these studies are based on more global analyses for which  
563 the Arctic impact is relatively weak because of the sparsity of observational Arctic data.  
564 Tables 2, 3 and 4 indicate that the Arctic is rather unique inasmuch as the MRC is not  
565 necessarily the top AOD-estimation performer. NAAPS-RA generally has moderately  
566 better bias, RMSE and  $r^2$  verification scores for the total and FM AODs compared to  
567 MERRA-2 and CAMSRA while CM AOD does not perform as well. In previous MRC and  
568 multi-model consensus evaluations, all component members either performed  
569 comparably in terms of AOD RMSE, bias and  $r^2$  or the number of multi models was  
570 relatively larger (e.g. 5 to 6 for the International Cooperative for Aerosol Prediction multi-  
571 model consensus). This study is the first time that all three developing centers have  
572 systematically evaluated their AOD reanalysis performance on an Arctic-wide climate  
573 scale.

## 574 **5. Results of Arctic AOD climatology, trend and extreme event statistics**

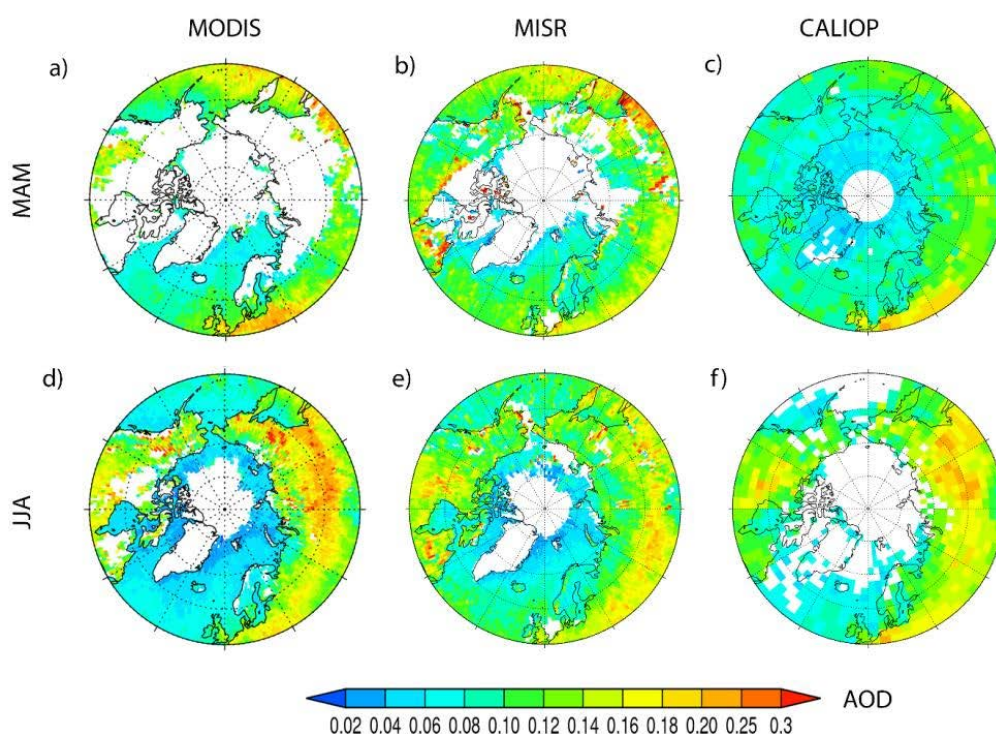


575 In this section we present spring and summertime Arctic AOD climatologies derived  
576 from space-borne remote sensing retrievals and aerosol reanalyses. We then present  
577 the seasonal cycle, interannual variability and trends of total and speciated AODs.  
578 Statistics of extreme AOD events in the Arctic are provided in the end.

579

## 580 5.1 Spring and Summertime AOD Climatology for the Arctic

### 581 5.1.1 Space-based remote sensing AOD climatology



582

583 **Figure 3.** Satellite-derived, mean climatological MAM (upper) and JJA (lower) MODIS  
584 AOD at 550 nm (left), MISR AOD at 558 nm (middle), and CALIOP AOD at 532 nm  
585 (2006-2019, right). These are based on MODIS C6 DT+DB and MISR AOD v23 over  
586 2003-2019, and CALIOP AOD over 2006-2019. White area means lack of data.

587 Bright, snow- and ice-covered surfaces, large solar zenith angles (to the extreme of sub-  
588 horizon SZAs during the polar night), and extensive cloud coverage result in limited  
589 (quality assured) Arctic aerosol retrievals by passive-based sensors like MODIS and  
590 MISR. The latitude limit of an active, downward-looking, polar-orbiting sensor like CALIOP  
591 on CALIPSO results in a polar region profile gap above 82°N. Known issues of CALIOP  
592 with retrieval filled values (RFVs) (Toth et al., 2018) and high noise to signal ratio over  
593 the Arctic also limit its aerosol retrievals near the Arctic. These challenges are reflected



594 as no data coverage (Fig. 3) in the high Arctic and Greenland, and over large regions of  
595 North America and Siberia in both March-April-May (MAM) and June-July-August (JJA)  
596 in the AOD climatology maps based on MODIS, MISR, and CALIOP. Compared to MAM,  
597 JJA has larger data coverage from MODIS and MISR over higher latitudes as aerosol  
598 retrievals from MODIS and MISR are based on reflected sunlight. Also, when snow and  
599 sea ice melt in summer, darker ocean and land surfaces that are suitable for applying  
600 passive-based aerosol retrieval methods are exposed. MAM data coverage for CALIOP  
601 is more than that of JJA due to less solar contamination during the night than during  
602 daytime for lidars. Nevertheless, the long operation time of these sensors (about two  
603 decades) provides sufficient data to construct a climatology for the near Arctic and the  
604 midlatitude where most sources of Arctic aerosols reside.

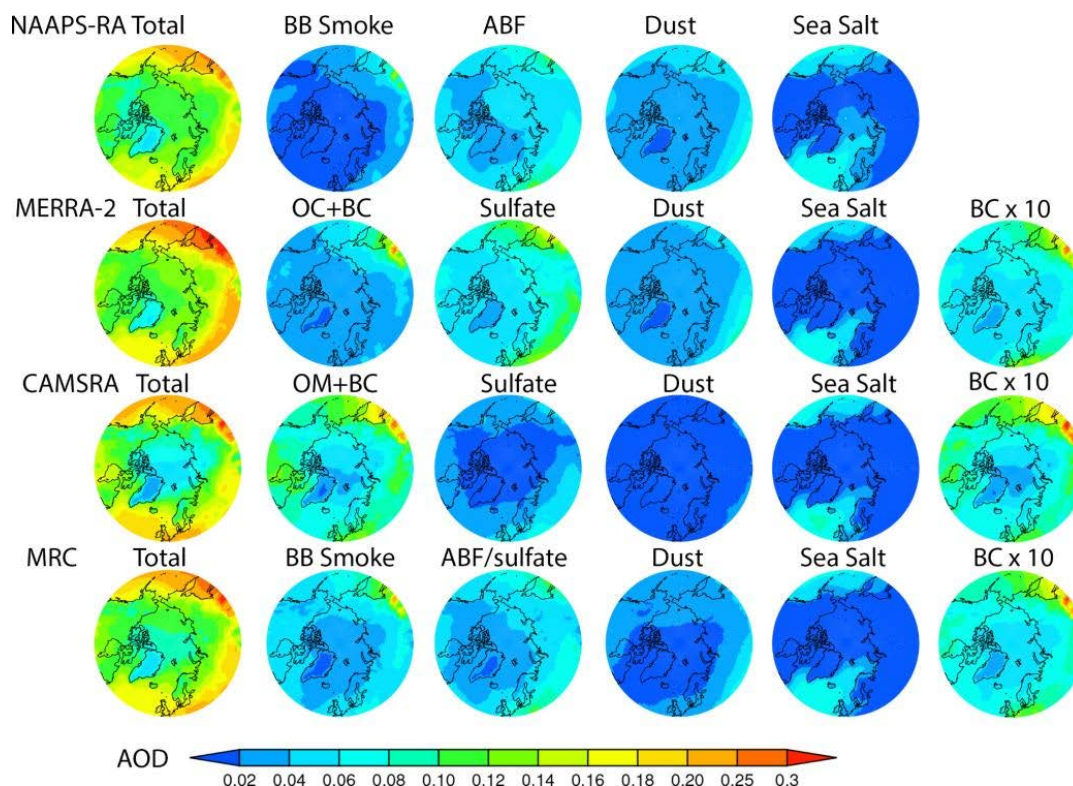
605 In general, the AOD patterns from the three sensors are similar. High AODs of 0.15-0.25  
606 appear in the 50°N-65°N latitude belt over land, i.e., large areas of boreal and subarctic  
607 Siberia, east and central Europe and North America sector in both spring and summer,  
608 with AOD mostly higher than 0.2 over Siberia in JJA, associated with biomass burning  
609 events (Fig. 12). The average AOD over water is considerably lower, ranging from 0.02  
610 to 0.12, with relatively high AOD in the northeast Pacific influenced by outflows from the  
611 Eurasian Continent, and lower AOD over the north Atlantic, and the lowest (0.02-0.06)  
612 over the Arctic Ocean. It is also visible that AOD over water is slightly higher in MAM than  
613 in JJA, which is consistent with other observation-based studies within the Arctic circle  
614 (e.g. Tomasa et al., 2015), possibly related to higher pollution levels from the upstream  
615 continents in MAM. CALIOP AOD exhibits a similar spatial pattern as MODIS and MISR.  
616 Additionally, AOD over Greenland is on the order of 0.02-0.06, and is a minimum  
617 compared to other regions due to its high elevations (nearly 2km on average). AOD over  
618 Siberia and North America is distinctively higher in JJA than in MAM based on CALIOP.  
619 This seasonal difference can also be seen with MISR and can be explained by seasonal  
620 boreal fire activities, i.e., boreal fire is generally more active in JJA than in MAM (Giglio  
621 et al., 2013). The seemingly larger seasonal difference in CALIOP than in MODIS and  
622 MISR over Siberia and North American could also be associated with different averaging  
623 times (2006-2019 vs. 2003-2019, and figure 2) as well as data sampling rate, as the swath  
624 for MODIS and MISR is on the order of a few hundred to a few thousand kilometers, while  
625 the swath for CALIPSO is on the order of 70m (see e.g., Colarco et al., 2014).

#### 626 5.1.2 Arctic AOD climatology derived from aerosol reanalyses

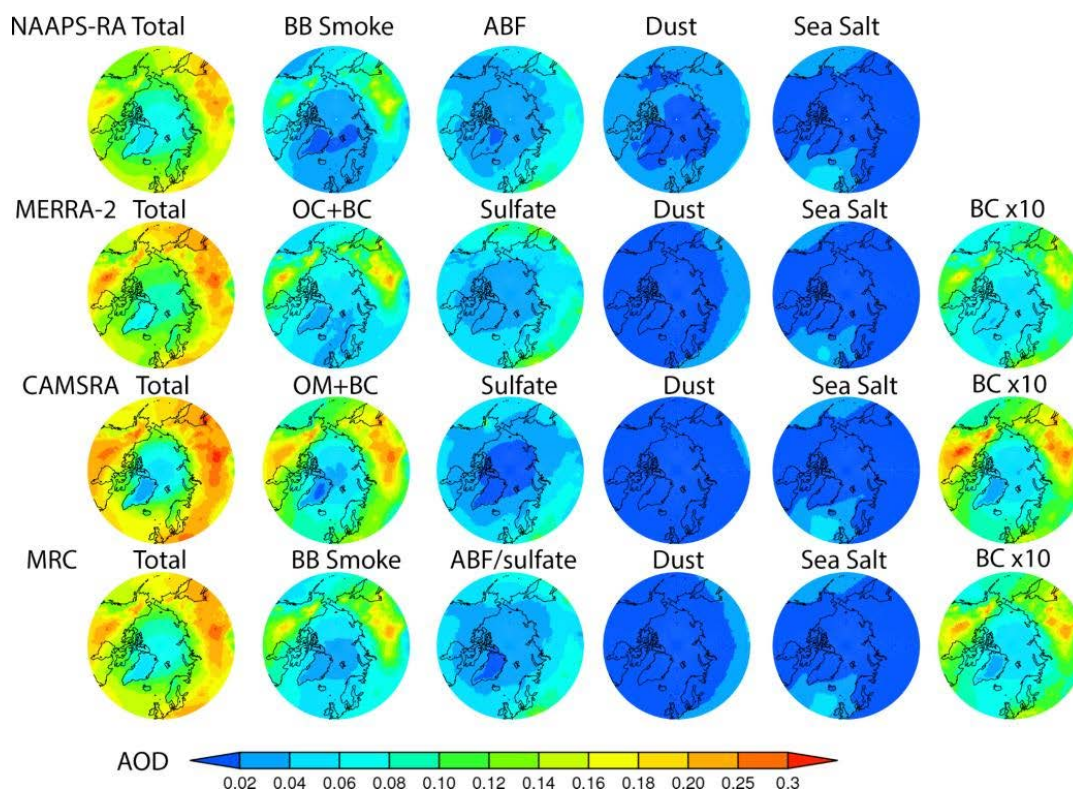
627 Figure 4 and 5 show spatial distributions of 2003-2019 mean total and speciated AOD  
628 from the three aerosol reanalyses and their consensus mean for spring and summer  
629 respectively. Although there is limited AOD data available for DA in the Arctic, lower  
630 latitude aerosols, whose AOD is constrained with DA, can affect Arctic AOD through  
631 transport and thus exert an indirect AOD constraint there. Additionally, all the



632 reanalyses use satellite-fire-hotspot-based BB emissions with fine temporal resolution  
633 (hourly to daily), which exert a source constraint, especially temporally (emission  
634 magnitude differs more than timing among the different models). As a result, there are  
635 good similarities in spatial distributions of total AODs among the three reanalyses. For  
636 example, AOD values are high in the 50°N-65°N belt over the Eurasia continent and its  
637 downwind Pacific region (0.16-0.30), low and on the order of 0.1 or less for regions  
638 north of 70°N, and at a minimum over Greenland for MAM. The high AODs over boreal  
639 North America and Siberia BB regions are more prominent in JJA compared to MAM. In  
640 general, the distribution patterns and magnitude of total AOD are comparable to those  
641 derived from MODIS, MISR, and CALIOP where available to a large extent.



642 **Figure 4.** 2003-2019 Climatological MAM-mean total and speciated AOD at 550 nm  
643 from NAAPS-RA, MERRA-2 and CAMSRA over the Arctic. As MERRA2 and CAMSRA  
644 do not have a biomass-burning-induced single aerosol species, the sum of the organic  
645 carbon (OC)/organic matter (OM) and black carbon (BC) AODs is used to approximate  
646 biomass-burning smoke AOD. The ratio of BC to the sum of BC and OC/OM in MAM for  
647 area >60°N is about 18% for MERRA-2 and 10% for CAMSRA. The ratios change little  
648 for area >70°N and area >80°N.  
649  
650



651  
 652 **Figure 5.** Same as Figure 4, except for JJA. The ratio of BC to the sum of BC and  
 653 OC/OM in JJA is between 10%-11% for area >60°N for both MERRA2 and CAMSRA.  
 654 This ratio changes little for area >70°N and area >80°N.

655 Speciated AODs have more variability than total AOD among the three reanalyses, and  
 656 a little more so for MAM than for JJA (Fig. 4, 5, 6). This is understandable because  
 657 passive retrievals of AOD are more available in summer than in spring near the Arctic,  
 658 and therefore reanalyses have more observational constraints in summer. While total  
 659 AOD is constrained through data assimilation, however, speciated AOD is not and  
 660 models must rely on their physics and boundary conditions. The MRC shows that BB  
 661 smoke and ABF/sulfate are similar in magnitude for the Arctic in MAM. However, by  
 662 model, NAAPS-RA and MERRA-2 suggest the dominance of ABF/sulfate over BB  
 663 smoke, and the reverse for CAMSRA. Based on the high bias of FM AOD verified with  
 664 AERONET (Sect. 4, Table 2), CAMSRA possibly overestimates OC and BC, and hence  
 665 BB smoke. BB smoke becomes the dominant species in JJA as boreal BB activity  
 666 increases in summer on average and ABF/sulfate turns to the 2nd place overall. The  
 667 strengthening of smoke AOD from spring to summer is a consistent feature across all  
 668 the reanalyses despite that CAMSRA tends to have higher BB smoke AOD and lower  
 669 sulfate AOD compared to the other two reanalyses in both seasons. ABF/sulfate AOD

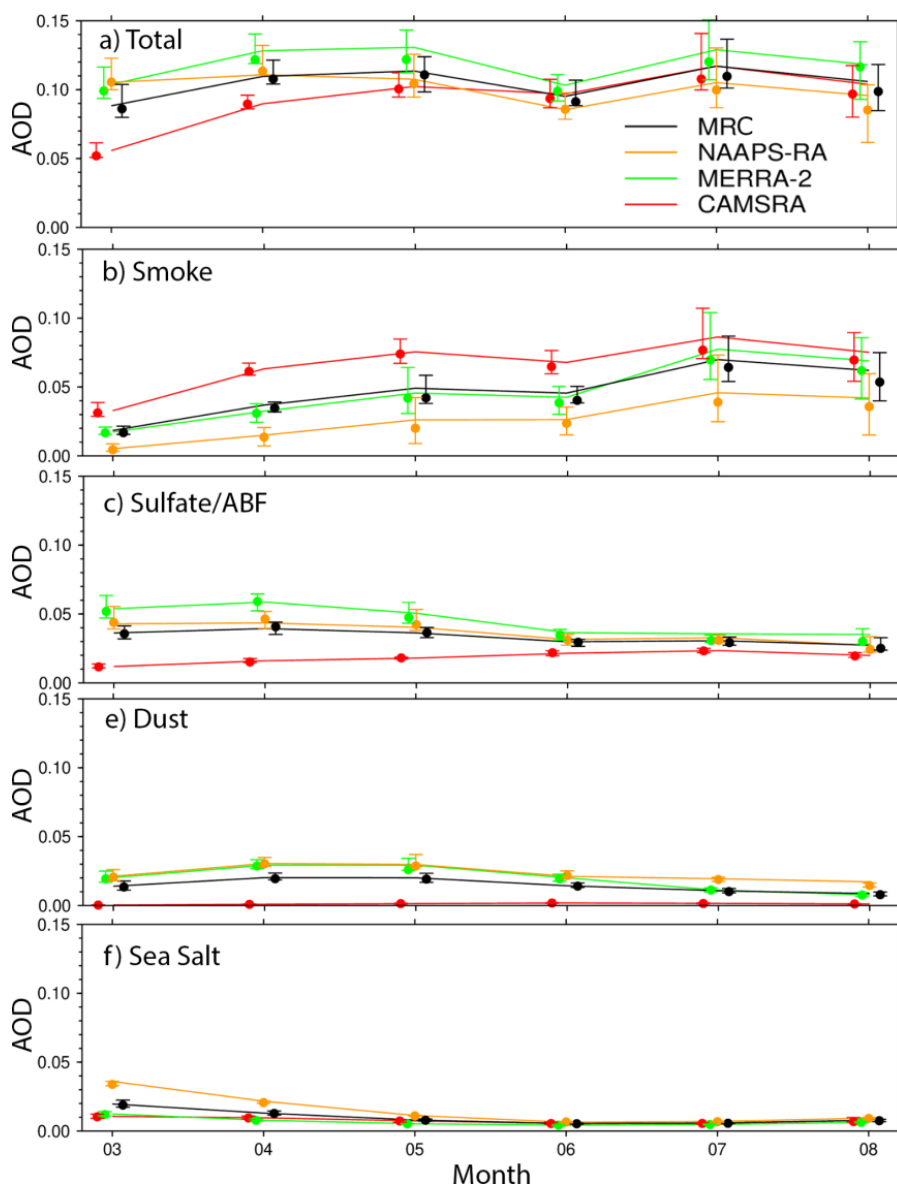


670 level is slightly higher in MAM than in JJA for MRC (from slightly less than 0.04 to about  
671 0.03 for 60-90°N regional average). A June minimum in total AOD is apparent from all  
672 reanalyses, associated with a general decrease in ABF/sulfate, dust and sea salt AODs  
673 after springtime and before severe BB activities in July and August. The spatial  
674 distributions of seasonal mean BC AOD from MERRA-2 and CAMSRA greatly resemble  
675 those of smoke AOD, and more so for JJA than MAM, except over Europe. This  
676 suggests a dominant role of the BB source over the anthropogenic sources of BC AOD  
677 over the Arctic for spring and summer seasons. This also supports McCarty et al.  
678 (2021)'s BC emission estimate that wildfire emissions account for more than half of all  
679 BC emissions north of 60N yearly (noting much lower BB emissions during wintertime  
680 when anthropogenic BC emission is at its maximum).

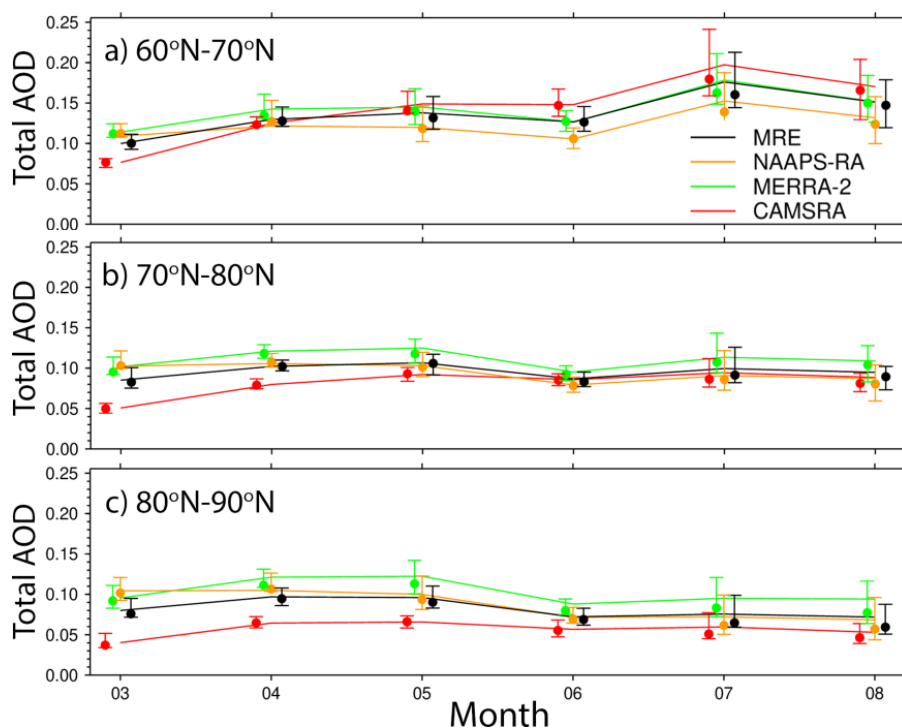
681 For both seasons, dust and sea salt are secondary contributors to the total AOD in the  
682 Arctic, except for the noticeable influences of Saharan and Asian dust in spring (Stone  
683 et al., 2007; Brieder et al., 2014) and of sea salt in the North Atlantic, Greenland Sea,  
684 Norwegian Sea, and North Pacific associated with cyclonic activities, especially in  
685 spring. It is also noteworthy that dust AOD in CAMSRA is much lower than the other two  
686 models (<0.02) in the spring.

687 From the 10-degree zonal average, it is also seen that monthly and regional mean AOD  
688 gradually decreases from lower latitudinal belts to higher latitudinal belts (Fig. 7). Total  
689 AOD for the 60°-70°N belt, on average, increases from MAM to JJA due to the  
690 seasonality of BB activities. However, the total AOD for the 80-90°N belt decreases  
691 slightly from MAM to JJA. This means the latitudinal gradient of total AOD is larger in  
692 JJA than in MAM, which is most likely due to more wet removal of aerosols during  
693 transport from source regions to the high Arctic in summer (Garrett et al., 2010, 2011). It  
694 is also noted that the latitudinal gradient of AOD from CAMSRA is larger than those  
695 from the two other reanalyses, suggesting stronger aerosol removal in the Arctic in  
696 CAMSRA compared to MERRA-2 and NAAPS-RA.

697  
698  
699



700  
701 **Figure 6.** Climatological (2003-2019) seasonal cycle of Arctic (60°-90°N) average total  
702 and speciated AODs at 550 nm from the three aerosol reanalyses and the MRC. The  
703 top and bottom whiskers represent the 25% and 75% percentiles of monthly AODs, and  
704 dots represent the median of monthly AODs.



705  
706  
707  
708

**Figure 7.** Similar to Figure 6, but for different latitudinal belts and total AOD.

709 5.2 Interannual variability of AOD in the Arctic  
710 5.2.1 Interannual variability of AOD

711 There are, as can be seen in Figure 2 (and supported by the MAM/JJA discussion in  
712 Sect. 4), significant interannual AOD variabilities, especially for sites close to boreal fire  
713 sources. For example, the summertime peak of the total AERONET AOD at Bonanza  
714 Creek, Alaska, is around 0.6 - 0.8 in 2004, 2005, and 2019, while it is  $< \sim 0.1-0.2$  for  
715 other years between 2003-2019. The year to year difference between high- and low-  
716 amplitude summertime peak AOD values at Yakutsk, Siberia, can be 6 fold. The MRC  
717 shows that these large interannual variabilities consistent with AERONET FM AOD  
718 variabilities, are very likely attributable to interannual variabilities in BB smoke.

719

720 For sites far from smoke sources, like Ittoqqortoormiit on the east coast of Greenland,  
721 Hornsund in Svalbard, and Thule on the northwest coast of Greenland, the high-  
722 amplitude peak AODs are about 2-3 times the low-amplitude peak AODs. This  
723 interannual spring to summer variability is also largely associated with BB smoke as  
724 suggested by the MRC and the coherent variation of the AERONET FM AOD. Some of  
725 the strongest AOD events reported in previous studies have been shown to be  
726 associated with the long-range transport of BB smoke. For instance, the strong AOD

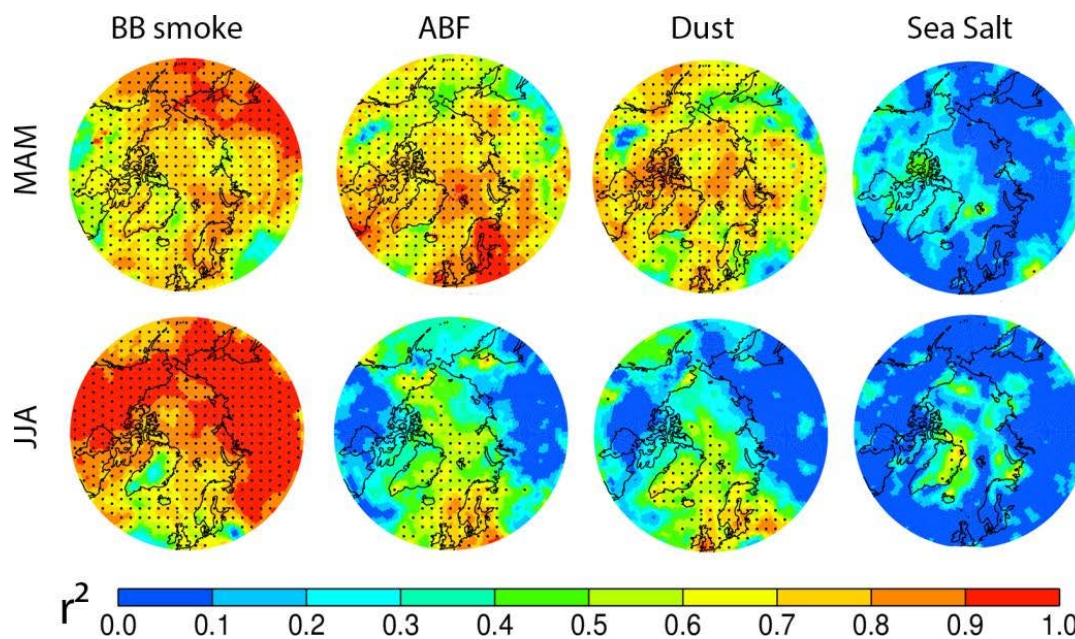


727 peak in the summer of 2015 over Hornsund and Andenes was shown to be associated  
728 with a series of intense fires that originated in North America (Markowicz et al., 2016).  
729 The strong peak AODs in August 2017 over Resolute Bay, Eureka and Thule were most  
730 probably related to intense, fire-induced pyroCB events in North America and the long-  
731 range transport of high-altitude smoke (Ranjbar et al., 2019; Das et al., 2021). The high  
732 amplitude AOD peak in the spring of 2006 over Hornsund was traced to agricultural fires  
733 in Eastern Europe (Stohl et al., 2007). The boreal fires in North America in the summer  
734 2004 led to the maximum-amplitude AOD peaks (over the 2003-2019 period of Figure  
735 2) for the two Alaskan sites and enhanced AOD on the pan-Arctic scale (Stohl et al.,  
736 2004). Some of the high-amplitude AOD peak events were recorded during intensive  
737 field campaigns. These included the ARCTAS/ARCPAC multi-platform campaign in the  
738 summer of 2008 (Matsui et al., 2011; Saha et al., 2010; McNaughton et al., 2011) and  
739 the NETCARE research vessel (Canadian Arctic) campaign in the spring of 2015  
740 (Abbatt et al., 2019).

741

742 The AERONET sites adjacent to the North Atlantic, the Greenland Sea, and the  
743 Norwegian Sea, notably Ittoqqortoormiit, Hornsund, and Andenes have higher CM  
744 AODs and higher CM to total AOD ratio compared to other sites: this is due to  
745 contributions from sea salt aerosols. Sea salt AOD, indicated by the MRC, is normally  
746 higher in MAM than in JJA.

747



748

749

750

**Figure 8.** Interannual variability of MRC MAM (upper panel) and JJA-mean (lower panel) total AOD at 550 nm explained by biomass-burning smoke AOD, ABF, dust, and



751 sea salt aerosols (i.e., the square of the correlation coefficient between speciated AOD  
752 and total AOD) respectively.  $r^2$  in dotted area is statistically significant at the 95% level  
753 using a two-tailed Student  $t$  test.

754

#### 755 5.2.2 Attribution of AOD interannual variability

756

757 It can be observed in Figure 6 that the simulated interannual (60-90°N) AOD variability  
758 (represented by the Figure 6 whisker bars) is mostly attributable to the large interannual  
759 variability of smoke AOD (especially from May to August). This is consistent across all  
760 the reanalysis products. For March and April, the contribution from sulfate/ABF is as  
761 important as BB smoke, if not larger. The interannual variation of dust AODs, as  
762 indicated with MERRA-2 and NAAPS-RA data, is non-negligible in MAM.

763

764 Regarding spatial distribution, Figure 8 shows the interannual variabilities of spring and  
765 summer Arctic AOD explained by different aerosol species (i.e. the square of the  
766 correlation coefficient between speciated AOD and total AOD) suggested by MRC for  
767 2003-2019. Consistent with the variability of monthly AOD time series shown in Figures  
768 2 and 6, both MAM and JJA interannual variabilities are explained mostly by BB smoke,  
769 with a higher degree of explanation for JJA than for MAM, and a lower degree of  
770 explanation for over the North Atlantic, Norwegian Sea and Greenland than over North  
771 American and Eurasian sectors overall. For north of 70°N, smoke explains 60%-80% of  
772 MAM and about 80% (except Greenland) of JJA AOD interannual variabilities. Over  
773 North American and Eurasian sectors (>60°N), the number is about 100% for JJA. The  
774 second-largest contributor is ABF/sulfate and dust for MAM and to a lesser extent for  
775 JJA. Contribution from sea salt is the least and is only statistically significant east of  
776 Greenland in JJA.

777

778 The contribution from ABF/sulfate is above 80% over the industry- and -population-  
779 concentrated European and northeast North American sectors and their outflow regions  
780 of the North Atlantic, Greenland Sea, Norwegian Sea, and the Arctic Ocean in MAM,  
781 while this number decreases to above 60% over Europe and the European Arctic  
782 (including water) and is insignificant over North America. Dust, possibly from Asian and  
783 high-latitude sources, could explain some of the interannual AOD variabilities over some  
784 regions, e.g. Greenland and Greenland Sea in JJA and additionally North Pacific and  
785 the Arctic ocean in MAM, however there exist large uncertainties in this evaluation  
786 based on the worse verification score of CM compared to FM AOD (Tables 2,3,4). And  
787 only CAMSRA among the three reanalyses considers high-latitude dust. Co-variability of  
788 species, e.g., BB smoke, ABF/sulfate, and dust, is discernible due to the same transport  
789 pathways from the midlatitudes to the Arctic. It is also possible that these species  
790 covary because of artifacts introduced by intrinsic treatment in AOD data assimilation  
791 for low AOD situations (Zhang et al., 2008).



792

793 5.3 Total and speciated AOD trends over 2003-2019

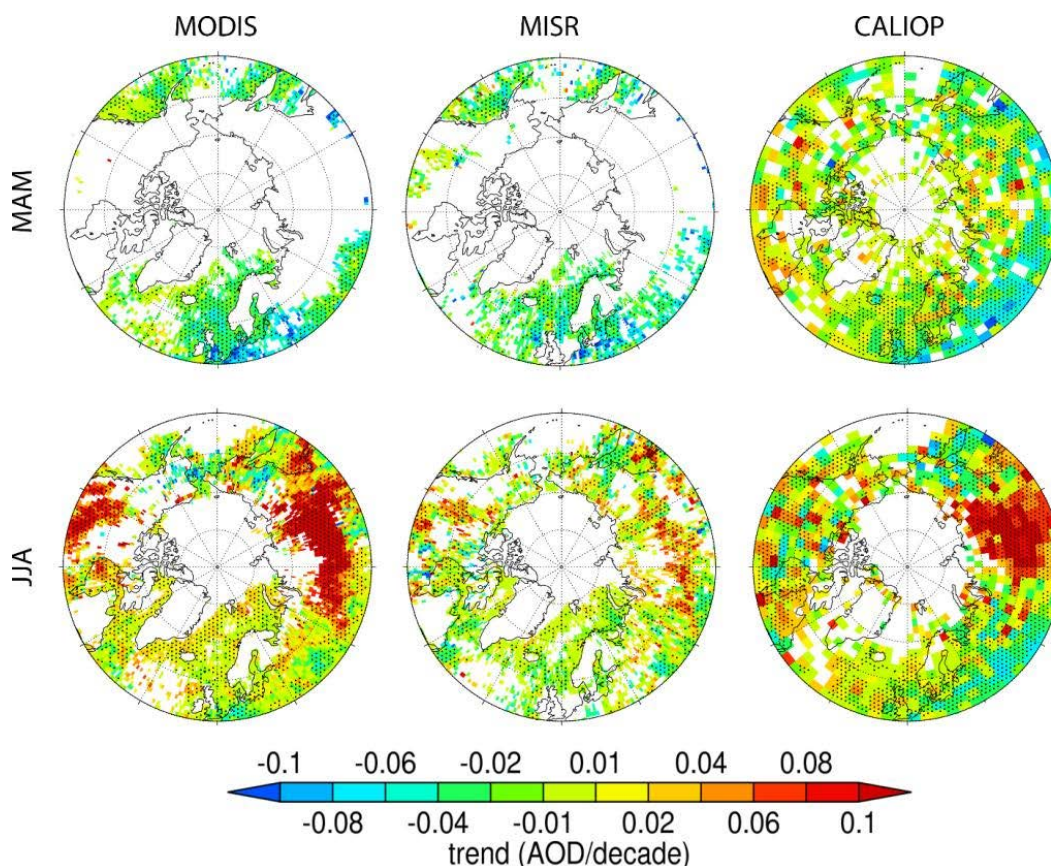
794

795 The total AOD trend for spring and summer over 2003-2019 derived from MODIS,  
796 MISR, and CALIOP are presented in Figure 9. Because of the scarcity of valid retrievals  
797 over the Arctic, the valid trend analysis is mostly limited to south of 70°N, and the north  
798 Atlantic region, and with less coverage in MAM than in JJA from MODIS and MISR and  
799 less coverage in JJA than MAM from CALIOP for reasons mentioned in Sect. 5.1.1.

800

801 5.3.1 AOD trends for springtime

802 For MAM, there is a general negative trend in total AOD over the 50-60°N belt and the  
803 North Atlantic, with the largest negative trend of -0.06 to -0.10 AOD/decade being over  
804 Europe, most probably due to a decrease in ABF/sulfate from decreased anthropogenic  
805 emissions as indicated by the reanalyses (Figure 10). The negative trend from CALIOP  
806 is slightly smaller than those from MODIS and MISR, again possibly attributed to a  
807 shorter length of the data record, where earlier and more polluted years for Europe and  
808 North America (2003-2006) is not included. All the reanalyses also show a negative  
809 trend in total AOD pan-Arctic (-0.01 to -0.02 AOD/decade), except for a close-to-neutral  
810 trend over the Arctic ocean and a very slight positive trend over boreal North America  
811 from CAMSRA. All the reanalyses suggest that the negative trend over the southeast  
812 Siberia and East Asian outflow region is associated with a decrease in BB smoke, and a  
813 decrease in ABF/sulfate from NAAPS-RA and MERRA-2 in tandem. Other consistent  
814 features found across the reanalyses include the negative trend over Europe associated  
815 with decreasing ABF/sulfate, which is possibly related to anthropogenic emission  
816 decrease over the past two decades (Breider et al., 2017), as well as a weak positive  
817 trend of sea salt over the North Atlantic, which is possibly due to the observed increase  
818 in cyclonic activities there (Rinke et al., 2017; Waseda et al., 2021; Valkonen et al.,  
819 2021). It is worth noting that NAAPS-RA does not include emission trend for ABF, and  
820 MERRA-2 doesn't either after 2008, which means the ABF/sulfate trends seen from  
821 these two reanalyses are mostly driven by a negative AOD correction applied by the  
822 data assimilation systems. This corroborates the negative trend in ABF/sulfate.



823

824

**Figure 9.** MAM and JJA AOD trends from MODIS, MISR, and CALIOP for the corresponding time periods and AOD wavelengths shown in Figure 3. The trend in the dotted area is statistically significant.

826

827

828

### 5.3.2 AOD trends for summertime

829

For JJA, the most prominent feature across all three space-borne sensors is the strong positive trend of total AOD over vast regions of Siberia and North America with a magnitude of around or greater than 0.10 AOD/decade. All the reanalyses capture this positive trend and indicate it is attributed to a significant increase in BB smoke AOD in these regions over 2003-2019 (Figure 11). This is in accordance with strong positive regional trends in BB emissions north of 50°N and north of 60°N derived from FLAMBE, a MODIS-fire hotspot-based emission inventory (Figure 12), and from other BB emission inventories, e.g., GFED and GFAS (Fig. 2 in McMarty et al., 2021). At the same time, there are negative trends in total AOD over Alaska, northeast of Russia, and North Pacific from the reanalyses, which is seemingly consistent with the trend in remote sensing AODs (though for some satellite datasets the coverage is spotty in these regions). These trends are driven by BB smoke and smoke emission trends as

830

831

832

833

834

835

836

837

838

839

840



841 suggested by all the reanalyses and FLAMBE. In addition, there is a continued negative  
842 trend from MAM to JJA in ABF/sulfate over Europe, which is also reflected in total AOD  
843 trend, as shown in the reanalyses. This is consistent with the discernible negative  
844 though weak trend from the three sensors. JJA AOD trends in dust and sea salt are  
845 neutral from the reanalyses.

846

847 Besides rising surface temperature, climate phenomena such as the El Niño–Southern  
848 Oscillation (ENSO), Arctic Oscillation (AO), and Pacific Decadal Oscillation (PDO) have  
849 been reported as affecting fire activity in several key boreal fire source regions (Balzter  
850 et al., 2007; Macias Fauria and Johnson, 2007; Kim et al., 2020). However rising  
851 surface temperature probably contributes more to the observed trend in BB emission in  
852 the high latitudes. In addition, agricultural fire activity in Eastern Europe and European  
853 Russia (peaking at April to May) and central Asia and Asiatic Russian (peaking in  
854 August) (Korontzi et al., 2006; Hall et al., 2016) also affects the seasonality of total BB  
855 emissions. The MAM negative trend in BB smoke may be relevant to a strengthening of  
856 agriculture burning regulations in the later part of the 2003-2019 time period. For  
857 example, the MAM BB emission maxima in 2003, 2006 and 2008 are all associated with  
858 wide-spread springtime agriculture burnings in high latitudes (Korontzi et al., 2006; Stohl  
859 et al., 2007; Saha et al., 2010). The aforementioned climate oscillations also modulate  
860 interannual variations of the transport of pollutants from the mid latitudes to the Arctic  
861 (e.g., Eckhardt et al., 2003; Fisher et al., 2010).

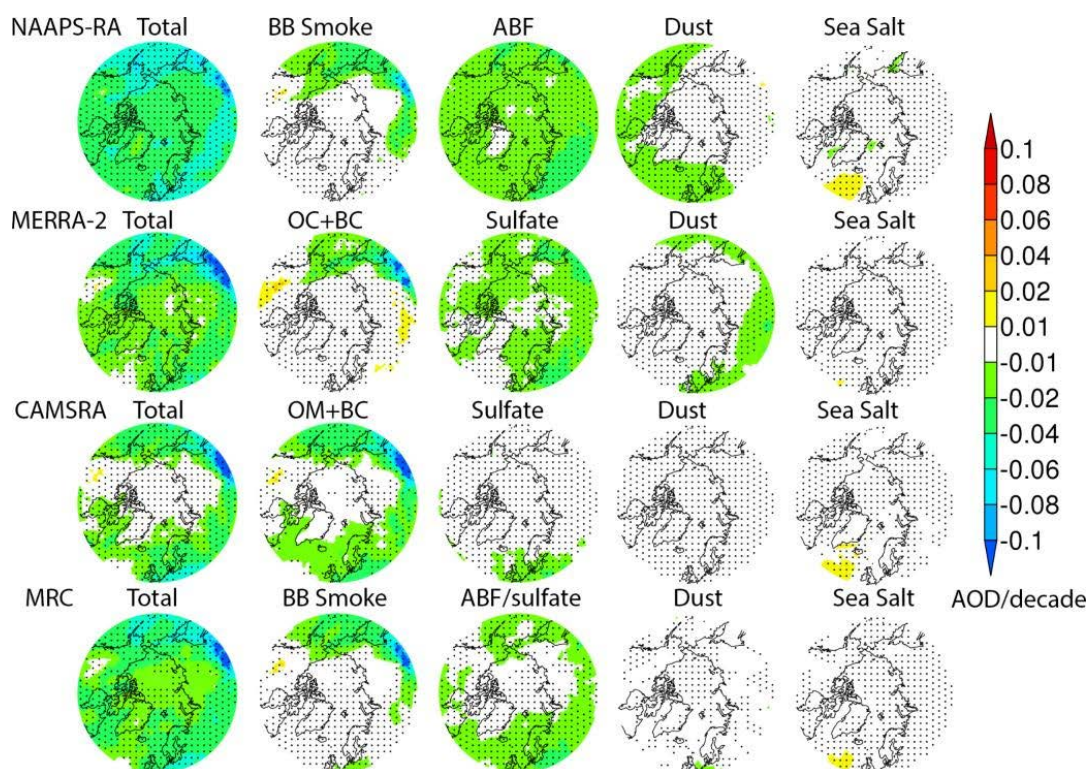
862

### 863 5.3.3 High Arctic AOD trends

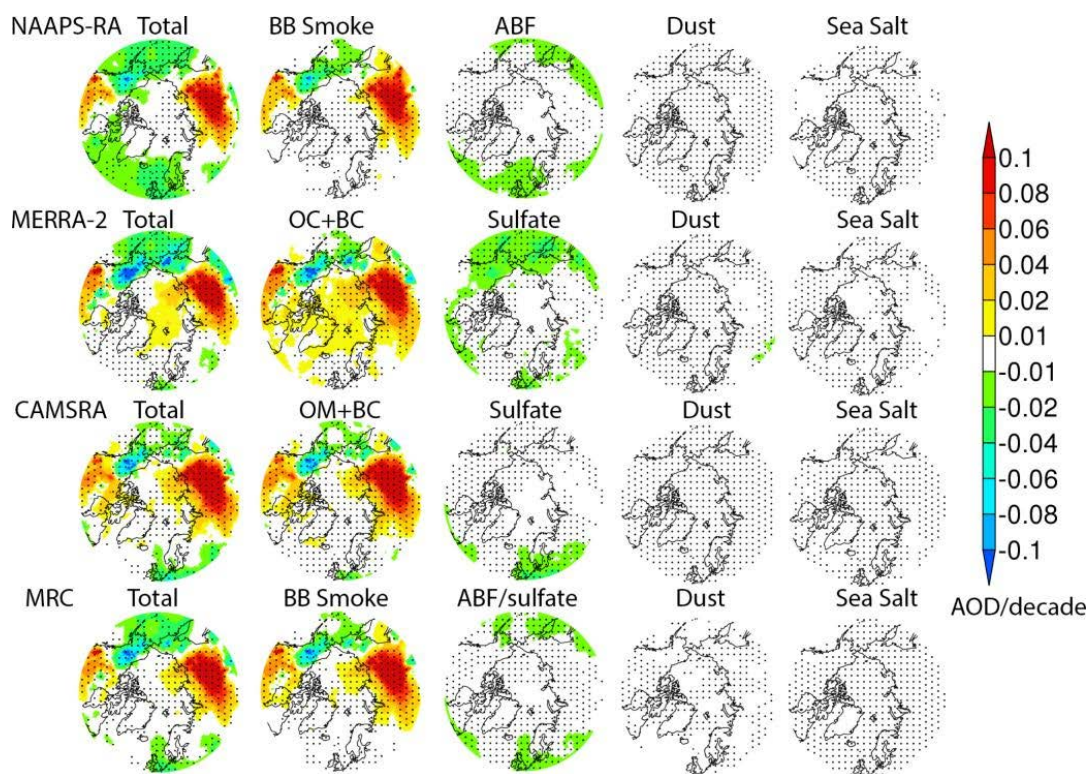
864 For the high Arctic ( $>70^{\circ}\text{N}$ ), AOD trends are hardly seen with the same color scale as  
865 those for the lower latitudes because of lower AOD. Thus, they are shown separately in  
866 Figure 13, where time series of MAM and JJA area-mean total, smoke, and ABF/sulfate  
867 AODs are shown individually and for all the reanalyses and the MRC over the 2003-  
868 2019 time period. There is a negative trend across models in MAM total AOD with -  
869 0.017 AOD/decade (-18%/decade), and a positive trend in JJA total AOD with 0.007  
870 AOD/decade (8%/decade) based on the MRC. The largest contributor to the MAM  
871 negative trend is ABF/sulfate, and the smoke AOD trend is also negative. In the  
872 summertime, ABF/sulfate trend continues to be negative; however, the smoke AOD  
873 trend turns positive, with a high positive trend of 0.010 AOD/decade (22%/decade). BC  
874 AOD trends from MERRA-2 and CAMSRA are dominantly driven by smoke AOD, and  
875 have similar trends with smoke AOD in percentage per decade. The negative trend in  
876 ABF/sulfate AOD is in line with the decreasing trend in surface sulfate mass  
877 concentrations measured over Arctic observational sites (e.g., Breider et al., 2017). The  
878 negative trend in MAM and positive trend in JJA for smoke AOD are consistent with the  
879 seasonal-and-area-mean BB emission trends shown in Figure 12 (e,f). The magnitudes  
880 of the trends among the three aerosol reanalyses are different, but the signs are the



881 same, corroborating the trend analysis results based on the MRC. These results are  
882 consistent with the trend analysis for lower latitude source regions as shown in Figures  
883 9-11. All these results also demonstrate that the Arctic aerosol baseline is changing  
884 quickly (Schmale et al., 2021), and the estimation here could contribute to the  
885 understanding and quantification of this new baseline.  
886  
887

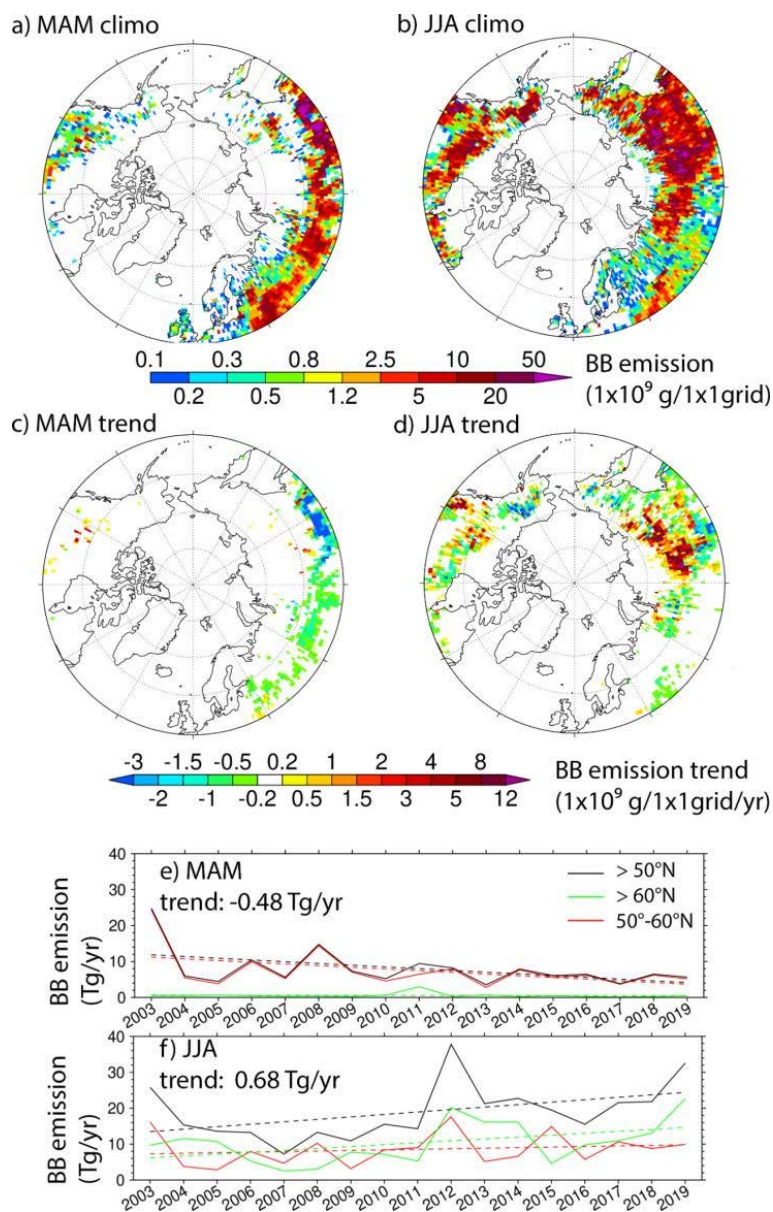


888  
889 **Figure 10.** Trends of MAM 550 nm total AOD and contributions from biomass-burning  
890 smoke  $/(BC+OC)/(BC+OM)$ , ABF/Sulfate, dust and sea salt from NAAPS-RA, MERRA-2  
891 and CAMSRA and the MRC.



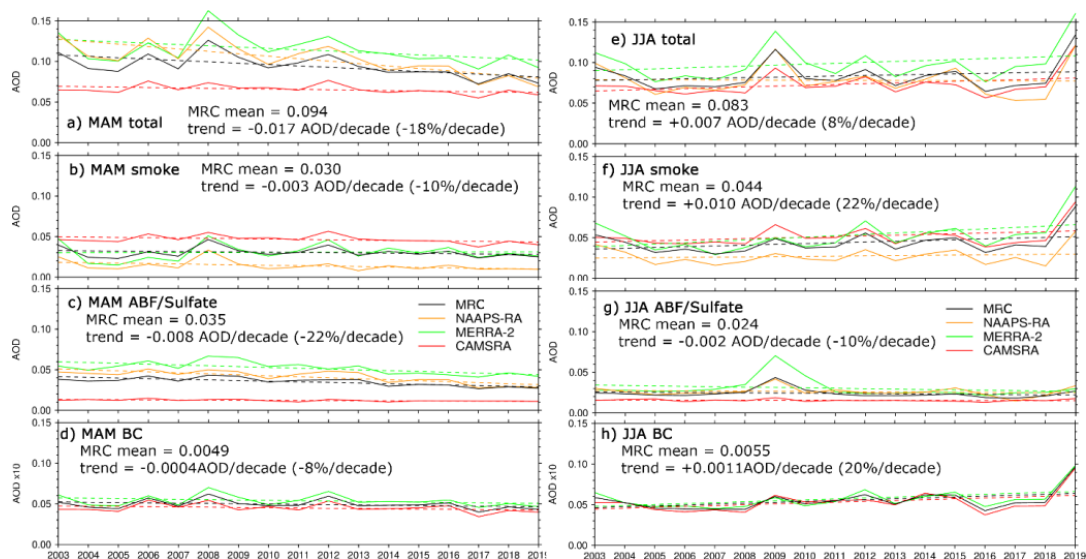
892  
893  
894  
895  
896

**Figure 11.** Same as Fig. 10, except for JJA.



897  
 898  
 899  
 900  
 901  
 902  
 903

**Figure 12.** MAM/JJA seasonal total BB smoke particle emission climatology and trend for 2003-2019 derived from FLAMBE (a-d). e) and f) Time series of seasonal-total and area-mean (>50°N, >60°N and 50-60°N) BB smoke emissions for MAM and JJA respectively. Dashed lines represent linear trends, which are statistically significant with a confidence level of 95%. The trend for north of 50°N is also displayed in texts.



904  
905  
906

**Figure 13.** Time series of MAM and JJA 70°-90°N area mean total, BB smoke, ABF/sulfate and BC AODs from the reanalyses and the MRC for 2003-2019 time period. Solid lines are AODs, and dashed lines are linear regressions indicating trends. For easier visualization, BC AOD is multiplied by 10.

911

#### 5.4. Extreme AOD events in the Arctic

912

The interannual AOD variability in the Arctic is, as discussed in the previous section, substantial and mostly driven by FM aerosol events (especially biomass burning transport events). We employed resampled, 6hrly AERONET AODs as well as speciated daily/6hrly NAAPS-RA AOD to better demonstrate the frequency and magnitude of the large FM AOD events. We chose NAAPS-RA reanalysis given its slightly better (monthly-mean) FM and total AOD bias, RMSE, and  $r^2$  scores referenced to AERONET data over the Arctic as well as its source-orientated capability of separating BB smoke from other aerosol species.

920

921

##### 5.4.1 General statistics of extreme events

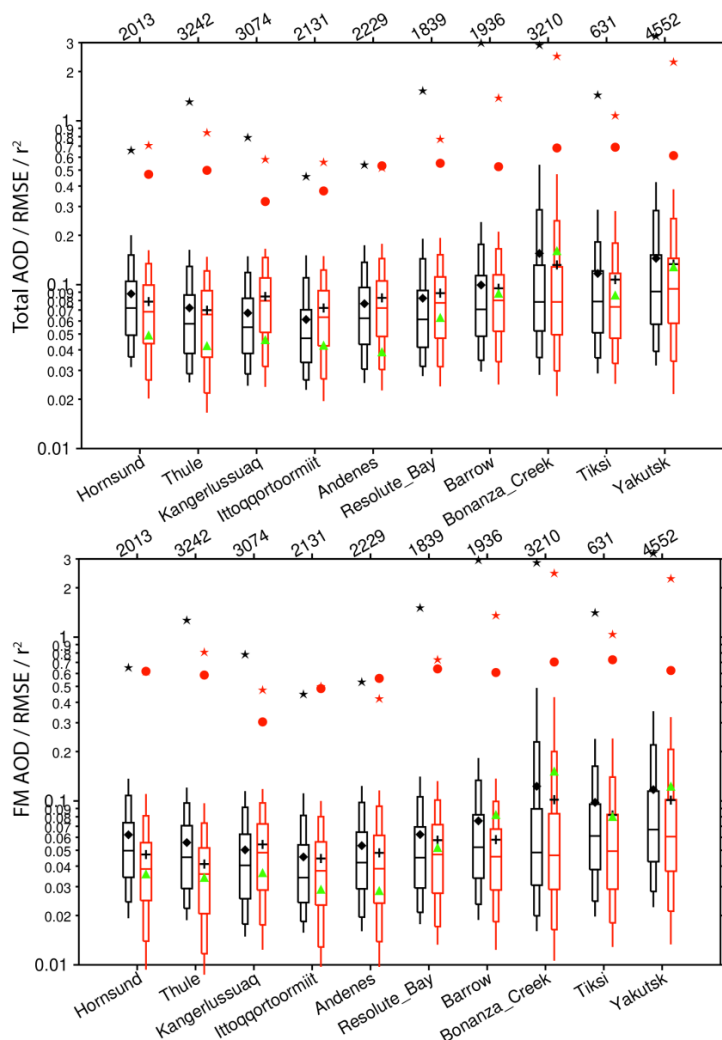
922

Figure 14 shows the site by site, total and FM AOD ranges from the 6-hrly AERONET data for all 550 nm retrievals between 2003-2019 (mostly confined to the April-August time frame). Also shown are 6-hrly, pairwise NAAPS-RA AODs that enable model skill evaluation at daily to synoptic scales (see the caption of Figure 14 for the definition of “pairwise” details and note that scatter plots of NAAPS-RA vs AERONET total, FM and CM AOD are shown in Fig. S1). NAAPS-RA verification comparisons relative to MAN data (north of 70°N) is also available as Fig. S2 and S3). NAAPS-RA arithmetic

929



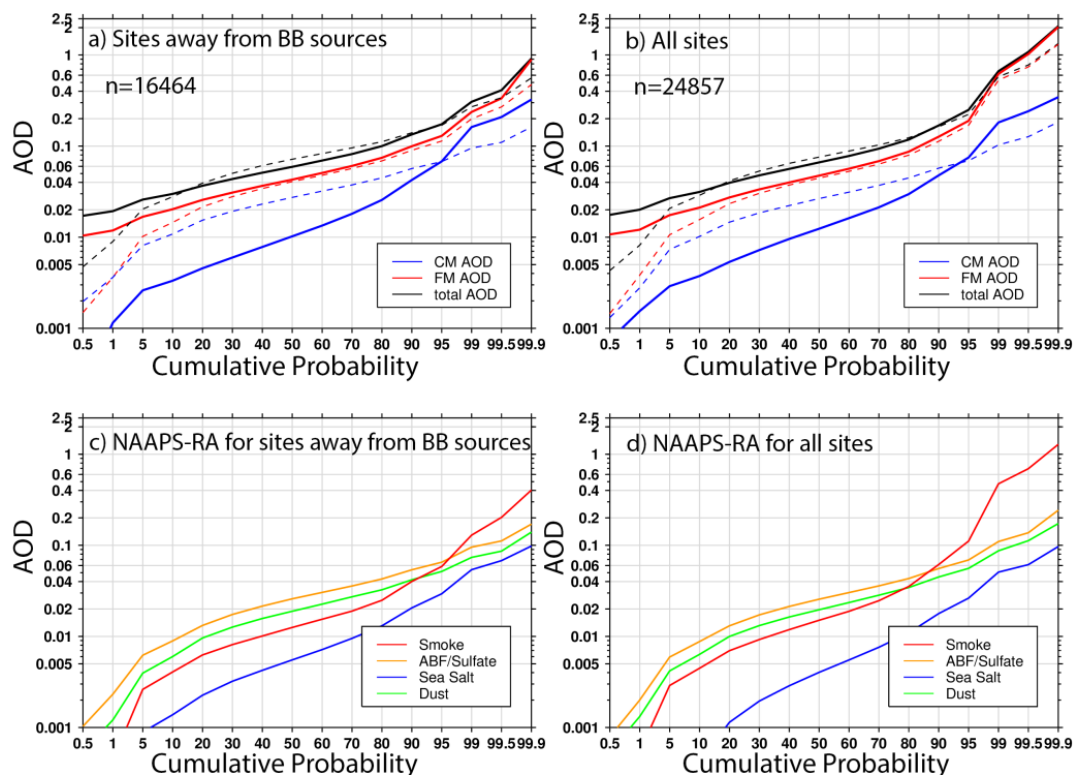
930 averages are less skillful at predicting CM AODs than FM AODs, and less skillful, on  
931 average, for the Arctic region relative to the globe (c.f. Fig. 7 in Lynch et al., 2016). In  
932 general, NAAPS-RA largely captures AERONET FM and total AOD ranges: this  
933 includes the 5%-95% percentiles of total AERONET AOD, for example ( $\sim 0.02$  to  $\sim 0.20$   
934 for most sites), and the larger  $0.02$  to  $\sim 0.4$ - $0.6$  range of sites with known strong BB  
935 smoke influence, (notably Bonanza Creek, Tiksi, and Yakutsk). Mean and median  
936 AODs are also comparable to AERONET values. The  $r^2$  values are likewise reasonable  
937 (mostly between  $0.5$ - $0.7$ , except for Hornsund, Ittoqqortoormiit, and Kangerlussuaq).  
938 The FM AOD  $r^2$  values generally exceed those of the total AOD ( $> 0.5$  for 9 sites and  $>$   
939  $0.6$  for 7 sites). The maximum AERONET FM AODs for these sites vary between  $\sim 0.4$   
940 (Andenes) to  $< 2.0$  for most sites and  $> 2.0$  for sites with strong BB smoke influence.  
941 The maximum NAAPS-RA AOD values are often biased low: this is a common  
942 challenge for global aerosol models (e.g. Sessions et al., 2015; Xian et al., 2019).  
943 RMSE values for total and FM AOD are generally large ( $\sim$  AERONET means for the  
944 sites suffering from strong smoke influence) and moderately significantly smaller for  
945 other sites.



946  
 947 **Figure 14.** Comparison of the 6-hrly (550 nm) total (top) and FM AOD (bottom) of the  
 948 NAAPS-RA (red) at 95, 90, 75, 50, 25, 10, and 5% percentiles (respective, sequential  
 949 features of the doubled spear-like symbols from the top tip to the bottom tip) with  
 950 pairwise AERONET V3L2 data (black) for the ten AERONET sites of Table 1 and Figure  
 951 1 for the 2003-2019 time period (“pairwise” refers to those NAAPS-RA AODs that  
 952 correspond to a resampled AERONET AOD whose  $\pm 3$ hr bin contains at least one  
 953 AERONET retrieval). Also shown are the site means of the NAAPS-RA and AERONET  
 954 AODs (“+” and “◆” symbols respectively) and the NAAPS-RA RMSE (“▲”), the  
 955 coefficient of determination ( $r^2$ ) between the NAAPS-RA and AERONET (“●”) and the  
 956 maximum AERONET and NAAPS-RA AODs (“★” and “★” respectively). Note that  
 957 values greater than 2.0 are not shown. The numbers of 6-hrly AERONET data points for  
 958 each site are shown just above the plot.



959



960

961

962 **Figure 15.** Upper panes (a, b): cumulative probability distributions of 6-hrly total, FM  
963 and CM AOD at 550 nm for AERONET V3L2 data (solid lines) and pair-wise NAAPS-  
964 RA (dashed line). Lower panes (c,d): cumulative probability distributions for the  
965 corresponding speciated AODs from NAAPS-RA. Left hand panes (a,c): AODs for sites  
966 that are distant from BB source regions, including Barrow, Resolute Bay,  
967 Kangerlussuaq, Thule, Andenes, Hornsund and Itoqqoortoormiit. Right-hand panes  
968 (b,d) all sites north of 60°N. “n” represents the total number of 6-hrly data points over  
969 the 2003-2019 period.

970

971 Figure 15 shows the cumulative probability distribution of 6-hrly total, FM and CM AOD  
972 at 550 nm for AERONET V3L2 data and pair-wise NAAPS-RA FM and CM AODs  
973 (Figures 15a,b) and speciated AODs (Figures 15c,d). For all sites north of 60°N, and for  
974 20%-80% cumulative probability, NAAPS-RA total AOD biases slightly positive (<0.01)  
975 due to a relatively large positive bias in CM AOD of ~ 0.01 below a cumulative  
976 probability of 95% (a positive bias that is generally evident in Table 2). The bias  
977 becomes negative (~ -0.05) above 95%. It is common for models to bias low for extreme  
978 events (e.g. Sessions et al. 2015): this negative bias at the largest values of CM AOD



979 could conceivably be associated with an underestimation of the CM AOD generated by  
 980 sea salt aerosols in the presence of strong winds. We should however, add this caveat:  
 981 despite the quality-control measures taken to filter out cloud-contaminated AERONET  
 982 data, the impact of CM residual clouds may still influence estimates of CM AOD.

983 **Table 5.** AERONET V2L3 FM, CM and Total AOD at 550nm (with additional filtering for  
 984 cloud contamination) at different percentiles for the listed Arctic sites. “N” presents total  
 985 number of 6hrly data during 2003-2019. Also listed are MAN data statistics for data  
 986 collected north of 70°N.

	Total   FM   CM AOD at 550nm								N
	Median	75%	90%	95%	99%	99.9%	maximum		
Hornsund	0.072 0.050 0.014	0.105 0.074 0.029	0.151 0.108 0.054	0.200 0.137 0.091	0.386 0.296 0.196	0.580 0.568 0.376	0.663 0.654 0.414		2013
Kangerlussuaq	0.055 0.040 0.009	0.083 0.063 0.020	0.119 0.091 0.038	0.149 0.115 0.060	0.234 0.198 0.111	0.510 0.461 0.221	0.794 0.786 0.244		3074
Resolute_Bay	0.061 0.045 0.011	0.092 0.069 0.021	0.144 0.106 0.041	0.190 0.141 0.063	0.499 0.396 0.160	1.530 1.516 0.452	1.530 1.516 0.452		1839
Barrow	0.071 0.052 0.013	0.114 0.082 0.025	0.176 0.134 0.048	0.241 0.183 0.079	0.466 0.415 0.198	2.999 2.962 0.454	2.999 2.962 0.454		1936
Thule	0.058 0.045 0.007	0.087 0.071 0.015	0.129 0.097 0.036	0.163 0.121 0.061	0.305 0.194 0.179	0.807 0.794 0.315	1.310 1.272 0.328		3242
Ittoqqortoormiit	0.047 0.034 0.006	0.070 0.054 0.015	0.110 0.082 0.033	0.151 0.111 0.058	0.278 0.215 0.161	0.456 0.446 0.329	0.459 0.450 0.342		2131
Andenes	0.062 0.042 0.014	0.096 0.064 0.027	0.137 0.098 0.050	0.174 0.123 0.075	0.277 0.210 0.154	0.451 0.432 0.249	0.541 0.534 0.258		2229
Bonanza_Creek	0.078 0.048 0.022	0.131 0.089 0.036	0.286 0.229 0.059	0.539 0.489 0.086	1.657 1.619 0.246	2.619 2.591 0.499	2.908 2.857 0.541		3210
Yakutsk	0.091 0.067 0.015	0.152 0.115 0.028	0.283 0.220 0.056	0.422 0.353 0.098	0.985 0.968 0.215	3.018 2.972 0.361	3.296 3.259 0.379		4552
Tiksi	0.079 0.061 0.011	0.121 0.096 0.021	0.182 0.163 0.040	0.286 0.239 0.060	0.936 0.915 0.123	1.442 1.413 0.238	1.442 1.413 0.238		631
MAN	0.052 0.029 0.021	0.090 0.062 0.031	0.126 0.097 0.042	0.164 0.118 0.052	0.281 0.253 0.085	0.777 0.761 0.234	0.777 0.761 0.234		520

987  
 988

989 Above the 95% percentile mark, BB smoke plays a dominant (all sites) Arctic role  
 990 compared to other aerosol species (Figure 15b,d). Even for sites distant from BB source  
 991 regions (including Resolute Bay, Kangerlussuaq, Thule, Andenes, Hornsund,  
 992 Ittoqqortoormiit, and to a mixed extent Barrow as per Eck et al., 2009), BB smoke is the  
 993 principal driver of AOD variations above the 95% percentile mark (Figure 15a,c). The  
 994 modal and total AOD values at different percentile levels for the AERONET sites and  
 995 MAN data collected north of 70°N are provided in Table 5. For the sites closer to BB  
 996 sources, including Bonanza-Creek, Yakutsk and Tiksi, the 99% percentile total AOD  
 997 and FM AOD are >~ 1.0, while for distant sites the 99% percentile total AOD varies  
 998 between 0.23-0.50. These extreme smoke cases could be caused by intense fire-  
 999 induced pyroCB events that inject smoke high in the troposphere or even well into the  
 1000 stratosphere (Fromm et al., 2010; Peterson et al., 2018). An example pyro-CB smoke  
 1001 event that occurred over British Columbia in August 2017 lead to a record-high AOD in  
 1002 the Canadian high Arctic (Ranjbar et al., 2019; Torres et al., 2020). More recently,  
 1003 Eastern Siberian fires burned during June - August 2021 facilitated more than a dozen  
 1004 cases of smoke intrusion into the high Arctic. Some smoke plumes even reached the  
 1005 North Pole and/or its vicinity. For example, on the 5<sup>th</sup> of August, operational NAAPS  
 1006 (same chemistry and physics, and same BB emission source with NAAPS-RA. NAAPS-  
 1007 RA is not available at the time of this analysis) analyzed a plume of smoke AOD value  
 1008 of 2-3 north of 80°N (Fig. 16). Smoke AOD over the source region was also 2 to >3 with  
 1009 a similar amplitude to the measured at Yakutsk. CALIOP data suggests smoke layer  
 1010 height varying between 1 to 6 km at the source region (vertical distribution of these  
 1011 smoke events is the topic for another manuscript).

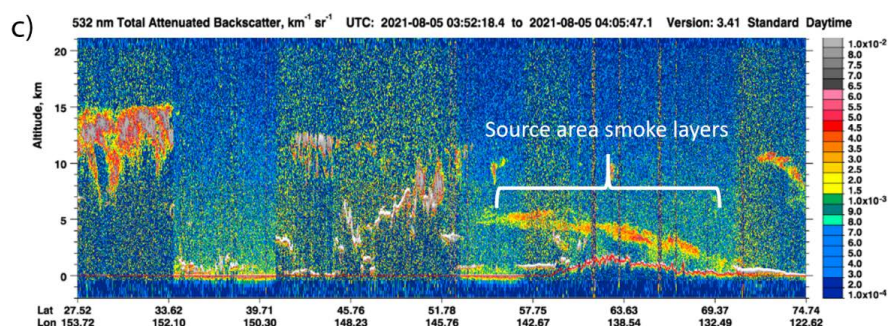
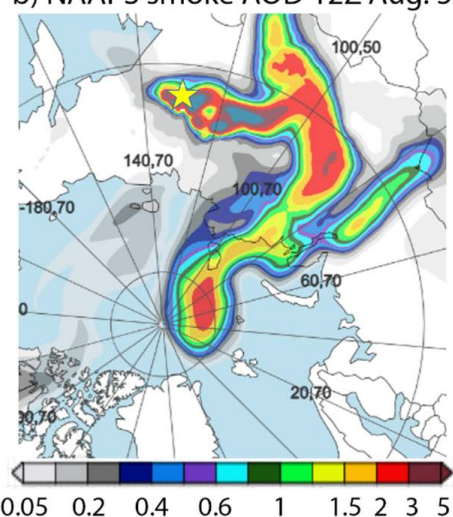


1012 For extreme BB smoke events, large particles like ash and soil components emitted  
1013 from vigorous burning (Schlosser et al., 2017; Reid et al., 2005) can likely be detected  
1014 to some degree as AERONET CM AOD (see, for example, the correlation between the  
1015 FM and “weak” CM particle size distributions for Bonanza Creek in Figure 9a of Eck et  
1016 al., 2009). For extreme AODs that are likely dominated by smoke (above the 99%  
1017 percentiles of 1.657 at Bonanza Creek, 0.985 at Yakutsk and 0.936 at Tiksi in Table 5  
1018 for example), the associated mean CM AOD values were respectively 0.048, 0.031 and  
1019 0.033. The larger CM AOD amplitudes (relative to, for example, the JJA means of Table  
1020 1) and the rough correlation suggests the presence of detectable CM smoke.  
1021

a) Terra True-color Aug. 5, 2021



b) NAAPS smoke AOD 12Z Aug. 5

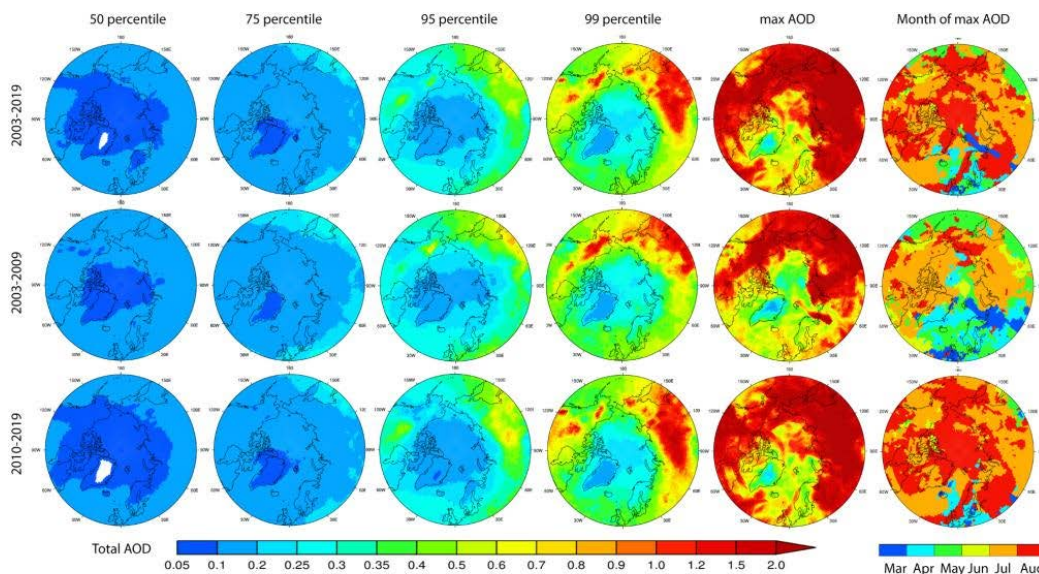


1022 **Figure 16.** An example of BB smoke intrusion into the high Arctic from fires originated in  
1023 East Siberia. a) True-color Terra satellite imagery composited on August 5, 2021. 12  
1024 September 2012. Red dots represent satellite detected fire hotspots. b) Operational  
1025 NAAPS smoke AOD analysis valid at 12Z August 5, 2021. c) CALIOP 532 nm  
1026 attenuated backscatter showing the smoke layers around the source area. The yellow  
1027 star on a) and b) represents the location of Yakutsk, which experienced a daily mean  
1028



1029 total AOD (500nm) of 2.0 (FM AOD ~1.9) and an intra-day peak around 2.5 based on  
1030 AERONET V3L1.5 data. Satellite imagery courtesy of the MODIS flying on NASA's  
1031 Terra satellite and CALIOP flying on CALIPSO satellite and available from  
1032 <https://worldview.earthdata.nasa.gov/> and <https://www-calipso.larc.nasa.gov/>.

1033  
1034 Figure 17 shows the geographical distributions of NAAPS-RA total AOD at different  
1035 percentile levels for March-August 2003-2019. The median ("50 percentile") Arctic  
1036 AODs (<~ 0.1 and specifically ~0.07 for the AERONET sites from Figure 15) are an  
1037 order of magnitude smaller than the max AODs. At the 95% percentile mark, clear BB  
1038 smoke features about the North American and Asian boreal burning regions start to  
1039 emerge. The maximum AODs are high (greater than 2.0) about those BB source  
1040 regions and relatively low over the Arctic Ocean (~ 0.3 - 1.0) and the north Atlantic (with  
1041 the lowest values over Greenland). The maximum AOD generally occurs in July and  
1042 August: this is associated with peak burning activities (except for the Norwegian Sea  
1043 area where the maximum AOD occurred in MAM; this is possibly associated with a  
1044 combined high AOD level from anthropogenic pollution and marine aerosols).



1045  
1046 **Figure 17.** Geographical distributions of NAAPS-RA daily (550 nm) total AOD at  
1047 different percentile levels for a March-August time frame and (rightmost column) month  
1048 of the occurrence of maximum AOD for sampling periods of 2003-2019 (upper row),  
1049 2003-2009 (middle row), and 2010-2019 (bottom row).

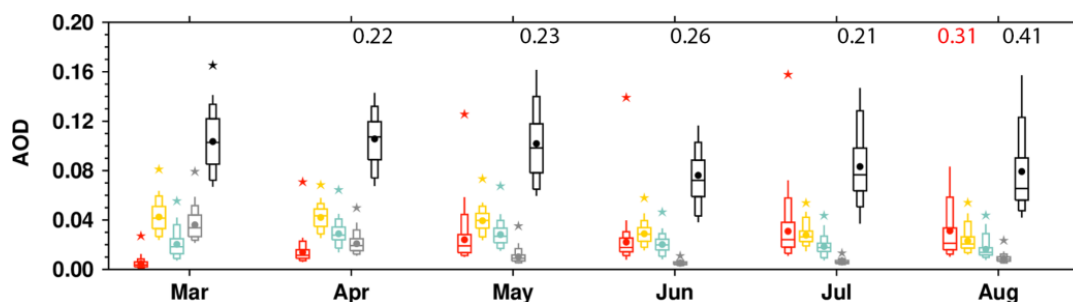
1050  
1051  
1052



#### 1053 5.4.2 Seasonality and trend of extreme events

1054 Figure 18 presents the seasonal cycle of total and speciated AOD ranges from the  
1055 NAAPS-RA based on daily and area-averaged (north of 70°N, to stay away from BB  
1056 source regions) data. The seasonal cycle of monthly mean total AOD looks similar to  
1057 that in Figure 7b for 70°N-80°N latitudinal mean with relatively higher total AOD in MAM,  
1058 and lower AOD in JJA and a minimum in June. The spread (bars and whiskers in the  
1059 plot) of ABF/sulfate AOD values is quite stable through the seasons, with a relatively  
1060 higher mean/median in MAM than JJA. Sea salt AOD and AOD spread is relatively high  
1061 in earlier months (March and April) compared to later months. Dust AOD and spread  
1062 are generally stable through the season, with a visibly higher mean/median in April and  
1063 May. Smoke AOD and spread exhibit the most prominent seasonal variations among all  
1064 species, with the lowest mean and spread in March, and increased mean and spread in  
1065 April, and much higher mean and spread in later months. July and August appear to  
1066 have the highest mean and spread, and the largest maximum smoke AOD, consistent  
1067 with Figure 17. These smoke features significantly contribute to the seasonality of  
1068 extremes in total AOD. It is also noted that for MAM, the means approximately equal the  
1069 medians, but the means are greater than the medians for JJA and especially so for  
1070 August. This is because there are more extremes in smoke AOD in the later season,  
1071 which influences the means.

1072



1073

1074 **Figure 18.** Box and whisker plot of daily and area-averaged (70°N-90°N) speciated  
1075 AOD at 550 nm from NAAPS-RA (2003-2019) for different months. Each box and  
1076 whisker column shows AOD at 95, 90, 75, 50, 25, 10, and 5% percentiles. Smoke,  
1077 ABF/Sulfate, dust, sea salt, and total AODs are presented in red, orange, green, grey,  
1078 and black colors respectively. Also shown are mean AODs in dots, and maximum AODs  
1079 in stars. For maximum AOD greater than 0.2 (beyond plotting area), AOD values are  
1080 shown in number and corresponding colors on the top.

1081

1082 As shown in Sect. 5.3 there is a slightly decreasing trend in MAM and an increasing  
1083 trend in JJA total AOD in the Arctic during 2003-2019. It is intriguing to explore the  
1084 possible trend in extreme events. We separate the whole time period into an early  
1085 (2003-2009) and a late (2010-2019) period (Figure 17, Table 6). 2009 is chosen as the



1086 separation year given the drop in ABF/sulfate emissions due to clean air acts across the  
1087 U.S. (<https://www.epa.gov/air-trends/sulfur-dioxide-trends>), Europe and China and the  
1088 decrease in ABF/sulfate AOD in these regions (Lynch et al., 2016; Zhang et al., 2017)  
1089 and in the Arctic as shown in Figure 13. Consistent with the BB emission trends in JJA  
1090 (JJA trend dominates MAM trend as JJA has much higher BB emissions), total AOD at  
1091 95% percentile in general increased over the boreal continents, except Alaska and  
1092 northeastern Siberia in 2010-2019 compared to 2003-2009.

1093 **Table 6.** Occurrence statistics of high Arctic area-mean ( $>70^{\circ}\text{N}$ ) daily BB smoke AOD  
1094 extreme event (defined as days with smoke AOD above 95% percentile, which is  $\sim 0.06$ )  
1095 based on 2003-2019 NAAPS-RA. Years without extreme smoke event is omitted.

	Extreme BB smoke days						Annual total	Mean extreme smoke AOD
	APR	MAY	JUN	JUL	AUG			
2003	9	16	0	0	0	25	0.096	
2004	0	0	0	12	0	12	0.079	
2006	0	0	0	4	0	4	0.121	
2008	4	11	0	0	0	15	0.070	
2009	0	0	0	0	5	5	0.064	
2003-2009 ave	1.9	3.9	0.0	2.3	0.7	8.7	0.086	
2010	0	0	1	0	2	3	0.074	
2012	0	0	0	3	0	3	0.072	
2014	0	0	0	1	2	3	0.065	
2015	0	0	2	17	0	19	0.079	
2016	0	4	0	0	0	4	0.072	
2017	0	0	0	0	13	13	0.098	
2019	0	0	0	7	25	32	0.117	
2010-2019 ave	0	0.4	0.3	2.8	4.2	7.7	0.083	

1096  
1097

1098 From the early period to the late period, the high Arctic ( $>70^{\circ}\text{N}$ ) 50%, 75%, 95%  
1099 percentile AODs change little, or even slightly decrease, due to decrease in  
1100 ABF/sulfate, however the maximum AOD value increased in the latter time compared to  
1101 the early time, indicating stronger extreme BB smoke influence in more recent years. It  
1102 is also noted that the maximum AOD occurred later in the season (mostly August) in  
1103 2010-2019 compared to occurring in March through August in 2003-2009 for the high  
1104 Arctic (Figure 17). This is likely attributed to the overall lower level of ABF/sulfate,  
1105 especially in MAM, a shift in extreme smoke events to later season (Table 6) and  
1106 agriculture burning control for early season (Sect. 5.3.2). The statistics of occurrence of  
1107 extreme pan-Arctic smoke events (defined as days with  $70\text{-}90^{\circ}\text{N}$  area-average daily  
1108 smoke AOD above 95% percentile) demonstrate a clear shift from all season (both  
1109 Spring and Summer) to late season, specifically July and August (Table 6). This is  
1110 consistent with the temporal shift of fire activity to a later time in Siberia over 2003-2018  
1111 (Liu et al., 2020), and the projection of emerging pan-Arctic fire regime be marked by



1112 shifts in the likelihood of extreme fires later in the growing season (McCarty et al.,  
1113 2021). An earlier fire season in the boreal region normally suggests a better-managed  
1114 forecast with fewer large and destructive fires, while a later fire season would indicate  
1115 the opposite.

1116

## 1117 **6. Discussion**

1118 The quality control processes applied on the AOD retrievals from MODIS, MISR, and  
1119 CALIOP help to generate a consistent AOD climatology and trend near the Arctic. The  
1120 cloud-clearing process on the MISR data and QA processes on the MODIS data  
1121 removed a good volume of data (about 40% for MISR and MODIS). However these QA  
1122 processes help to retain only the best-quality data, which yield a closer magnitude of  
1123 AOD for MODIS and MISR to AERONET AODs near the 70°N latitude circle (around or  
1124 less than 0.1), compared to ~0.2 using regular level 3 MODIS and MISR data in figures  
1125 20 and 23 of Tomasi et al., 2015, especially for springtime. The manual QA process on  
1126 the AERONET AOD data also reveals more frequent cloud contamination in springtime  
1127 than in summertime. The regular CALIOP AOD L3 product, with the filled values for low  
1128 AODs, yielded different spatial and seasonal patterns of AOD (not shown). After  
1129 removing the pixels with filled values, CALIOP AOD seasonal spatial AOD distributions  
1130 are similar to those from MODIS and MISR.

1131

1132 The total AOD at 550 nm from the three aerosol reanalyses are much more convergent  
1133 in spatial distribution, magnitude, and seasonality in the Arctic compared to the climate  
1134 models (e.g. AEROCOM models in Sand et al., 2017, where MAM AODs averaged over  
1135 nine Arctic AERONET sites (all included in this study) are an order of magnitude  
1136 different for the highest and lowest AOD models, and peak AOD season varies among  
1137 winter, spring and summer; CMIP5 models in Glantz et al., 2014, where spring and  
1138 summertime AODs over the Svalbard area also show an order of magnitude difference  
1139 and different seasonality for some of the models), and are similar to those from the  
1140 remote sensors near the Arctic. The possible reasons for this convergence include 1)  
1141 the hourly/daily resolved satellite-hotspot-based BB emissions used by these  
1142 reanalyses apply fine-temporal and interannual-variability-resolved emission  
1143 constraints; 2) despite that the commonly assimilated satellite AOD (e.g. MODIS AOD in  
1144 all three reanalyses) has limited coverage in the Arctic due to retrieval challenges of  
1145 dealing with bright surfaces and high cloud coverage, the observational constraint of  
1146 model fields through assimilation of AOD in the lower latitudes is effective in  
1147 constraining Arctic AOD to a good extent through transport; 3) more accurate  
1148 meteorology representations. It is reasonable that the AOD spread among the three  
1149 reanalyses increases with latitude, and into the early months (e.g., March) when  
1150 retrieval coverage for lower latitudes is less than summer months.

1151



1152 Except for the chemical processes relevant to conversion of SO<sub>2</sub> to sulfate, the aerosol  
1153 reanalysis products (or their underlying aerosol models) don't include other new particle  
1154 formation processes that may be important over the Arctic open water/leads in  
1155 Springtime or over packed ice during transitional summer to Autumn season (Abbatt et  
1156 al., 2019; Baccarini et al., 2021). High latitude dust sources, e.g. glacier dust, which are  
1157 present for some areas in the Arctic (Bullard et al., 2016), are only included in  
1158 CAMSRA, despite that Arctic dust AOD in CAMSRA is much lower than those in the  
1159 other two models (Fig. 6e).

1160

1161 To show the contribution of biomass burning on total AOD in the Arctic, we  
1162 approximated BB smoke with the sum of BC and OC/OA from MERRA-2 and CAMSRA.  
1163 This approximation is rather arguable. It is better suited for JJA than MAM, as the  
1164 climatological seasonal mean of Arctic AOD is dominated by BB smoke in JJA, which  
1165 means that BC and OC/OC are mostly from BB sources, while the contribution of BC  
1166 and OC/OA from anthropogenic sources is relatively higher in early spring (Figure 2,3).  
1167 So smoke AOD is overestimated from MERRA-2 and CAMSRA and more so for MAM.  
1168 This explains the large difference in smoke AOD (ratio to total AOD) in MAM than in  
1169 JJA between the two reanalyses and NAAPS-RA, which explicitly tracks aerosol mass  
1170 from BB sources (Figures 4, 5, 6). While NAAPS-RA includes BC and OA from  
1171 anthropogenic sources and sulfate into ABF, which is an arguably reasonable  
1172 configuration for pollution species, as observational studies show a strong correlation  
1173 between sulfate and elemental BC surface concentrations at pan-Arctic sites away from  
1174 BB sources, indicating the sources contributing to sulfate and BC are similar and that  
1175 the aerosols are internally mixed and undergo similar removal (Eckhardt et al., 2015).  
1176 BB smoke is expected to have different vertical distributions from anthropogenic  
1177 pollution if smoke is emitted above the boundary layer, which sometimes (~10%) is the  
1178 case for North American boreal fires (Val Martin et al., 2010).

1179

1180 Stratospheric aerosols from volcanic eruptions can contribute to the total AOD in the  
1181 Arctic, especially for the four years after the Mount Pinatubo eruption in 1991 (Herber  
1182 2002). For our study period (2003-2019), the eruptions of Kasatochi, Redoubt,  
1183 Sarychev, and Eyjafjallajökull in August 2008, March 2009, July 2009, and March 2010,  
1184 respectively, would have affected the stratospheric AOD and thus total column AOD.  
1185 However, these eruptions are at least one order of magnitude smaller than that of  
1186 Pinatubo. The stratospheric AOD contribution to the Arctic background AOD is  
1187 estimated to be relatively small at ~0.01 (from Figure 16 of Thomason et al., 2018; non-  
1188 Pinatubo affected years in Figure 5 of Herber 2002), despite that locally and over a  
1189 short period the AOD contribution can be large (e.g., O'Neill et al., 2012). All the  
1190 reanalyses have some sort of SO<sub>2</sub> and sulfate representation from volcanic degassing  
1191 emissions, but a full representation for explosive volcanic sources is lacking (except that



1192 MERRA-2 has time-varying explosive and degassing volcanic SO<sub>2</sub> before December  
1193 31, 2010). The volcanic influence on Arctic AOD, if detectable, would be reflected in the  
1194 ABF/sulfate AOD in the reanalyses, but its contribution would be much smaller than the  
1195 anthropogenic counterpart for our study period. It is also worth noting that volcanic  
1196 activities are not the only influence on the stratospheric aerosol budget: pyroCB-injected  
1197 BB smoke can also contribute to stratospheric AOD, as discussed earlier. Stratospheric  
1198 BB smoke was also detected over the Arctic with lidar measurements during the  
1199 MOSAiC campaign (Engelmann et al., 2021). Stratospheric injection of BB smoke  
1200 associated with pyroCB events are not represented in the reanalyses, despite that BB  
1201 emission associated with these pyroCB events are included in the emission inventories  
1202 with possible large bias in emission amount and height.

1203  
1204 Arctic shipping is often brought up as a potentially important source of BC for the Arctic  
1205 in the future. All of the reanalyses include shipping emissions, although little interannual  
1206 trend is considered especially for the late period in 2003-2019. However “Arctic shipping  
1207 is currently only a minor source of black carbon emissions overall” according to the  
1208 recent Arctic Monitoring and Assessment Programme (AMAP) report (2021).

## 1209 1210 **7. Conclusions**

1211  
1212 Using remote sensing aerosol optical depth (AOD) retrievals from the Moderate  
1213 Resolution Imaging Spectroradiometer (MODIS), the Multi-angle Imaging  
1214 SpectroRadiometer (MISR), and Cloud-Aerosol Lidar with Orthogonal Polarization  
1215 (CALIOP), and AODs from three aerosol reanalyses, including the U.S. Naval Aerosol  
1216 Analysis and Prediction System-ReAnalysis (NAAPS-RA), the NASA Modern-Era  
1217 Retrospective Analysis for Research and Applications, version 2 (MERRA-2), and the  
1218 Copernicus Atmosphere Monitoring Service ReAnalysis (CAMSR), and ground-based  
1219 Aerosol Robotic Network (AERONET) data, we have reported the Arctic/High-Arctic  
1220 (defined as 60°N-90°N/70°N-90°N) AOD climatology, trend and extreme event statistics  
1221 for spring (March-April-May, MAM) and summer (June-July-August, JJA) seasons  
1222 during 2003-2019.

1223  
1224 1) **Arctic AOD climatology.** The total AODs from space-borne remote sensing and  
1225 the aerosol reanalyses show quite consistent climatological spatial patterns and  
1226 interannual trends for both spring and summer seasons sub-Arctic (60-70°N),  
1227 where remote sensing data is available. AOD trends for the high Arctic from the  
1228 reanalyses have consistent signs too. Climatologically, fine-mode (FM) AOD  
1229 dominates coarse-mode (CM) AOD in the Arctic. Based on the reanalyses,  
1230 biomass burning (BB) smoke AOD increases from March to August associated  
1231 with seasonality of BB activities in the boreal region (>50°N);



- 1232 Sulfate/Anthropogenic and biogenic fine (ABF) AOD is slightly higher in MAM  
1233 than in JJA; sea salt AOD is highest in March and decreases with time into later  
1234 spring and summer; contribution of dust AOD to total AOD is non-negligible in  
1235 April and May. The latitudinal gradient of AOD is larger in JJA than in MAM,  
1236 consistent with observed more efficient removal in summertime (Garrett et al.,  
1237 2011). Among aerosol species, black carbon (BC) is a very efficient light  
1238 absorber, and climate forcing agent (e.g. Bond et al., 2013). We show that over  
1239 the Arctic, the contribution of BC AOD from BB source overwhelms  
1240 anthropogenic sources in both MAM and JJA, and more so in JJA during 2003-  
1241 2019.
- 1242
- 1243 2) **AOD trend:** Total AOD exhibits a general negative trend in the Arctic in MAM,  
1244 and strong positive trends in North America, Eurasia boreal regions (except  
1245 Alaska and northeast Siberia) in JJA. For the high Arctic, the total AOD trend is -  
1246 0.017/decade (-18%/decade) for MAM and 0.007/decade (8%/decade) for JJA  
1247 based on the multi-reanalysis-consensus (MRC). The total AOD trends are  
1248 driven by an overall decrease in sulfate/ABF AOD in both seasons (-  
1249 0.008/decade, or -22%/decade for MAM and -0.002/decade or -10%/decade for  
1250 JJA), and a negative trend in MAM (-0.003/decade or -10%/decade) and a strong  
1251 positive trend in JJA (0.01/decade or 22%/decade) from biomass burning smoke  
1252 AOD. The decreasing trend in sulfate in the Arctic in recent decades is in line  
1253 with other studies using surface concentration measurement (e.g., Eckhardt et  
1254 al., 2015). The smoke AOD trends are consistent with MODIS fire-hotspot-based  
1255 BB emission trends over the boreal continents.
- 1256
- 1257 3) **Impact of BB smoke on AOD interannual variability:** The interannual  
1258 variability of total AOD in the Arctic is substantial and predominantly driven by  
1259 fine-mode, and specifically BB smoke AOD in both seasons and more so in JJA  
1260 than in MAM. For AERONET sites close to BB emission sources, the difference  
1261 in monthly total AOD can be 6-fold for high versus low AOD years. For remote  
1262 regions away from BB sources, the interannual variability of total AOD can also  
1263 be explained mostly by smoke AOD.
- 1264
- 1265 4) **Extreme AOD events** during spring and summer in the Arctic, defined as AOD  
1266 greater than the 95% percentile value, are mainly attributed to BB smoke  
1267 transport events as expected. The median of 6hrly total AOD for all AERONET  
1268 sites in the Arctic during 2003-2019 is ~0.07, and the 95% percentile is ~0.22.  
1269 With the general decreasing trends in MAM and increasing trend in BB  
1270 emissions, the AOD extreme events have a tendency to occur later in the  
1271 season, ie. July and August, in the latter decade rather than spreading over



1272 March-August in the early decade during 2003-2019. Global warming is expected  
1273 to continue leading to drier conditions and increased fire activities in the high  
1274 latitudes (McCarty et al., 2021), making the Arctic more susceptible to extreme  
1275 smoke events.

1276  
1277 5) **Overall performance of the aerosol reanalyses:** The aerosol reanalyses yield  
1278 much more convergent AOD results than the climate models (e.g. AeroCOM,  
1279 Sand et al., 2017) and verify with AERONET to some good extent, which  
1280 corroborates the climatology and trend analysis. Speciated AODs appear more  
1281 diverse than the total AOD among the three reanalyses, and a little more so for  
1282 MAM than for JJA. NAAPS-RA and MERRA-2 total and FM AODs verify better in  
1283 the Arctic than CAMSRA, which tends to have a high bias in FM overall. The  
1284 reanalyses generally perform better in FM than CM. The three reanalyses exhibit  
1285 different latitudinal AOD gradients, especially in summertime, indicating different  
1286 removal efficiencies. The emerging capability of assimilating OMI Aerosol Index  
1287 (AI) to constrain absorptive aerosol amount, could potentially fill in the  
1288 observational gaps for aerosol data assimilation in reanalyses over the Arctic  
1289 (Zhang et al., 2021). With more advanced retrieval algorithms on the current  
1290 space-borne sensors for over snow/ice, new sensors on future satellites,  
1291 improvements on the underlying meteorology and aerosol representations in  
1292 models, improvements in aerosol reanalysis are expected.

1293  
1294 The results presented here provide a baseline of AOD spatiotemporal distribution,  
1295 magnitude, and speciation over the Arctic during spring and summer seasons for the  
1296 recent two decades. This will help improve aerosol model evaluations and better  
1297 constrain aerosol radiative and potentially indirect forcing calculation to evaluate aerosol  
1298 impact in the Arctic amplification. For example, the contribution of reduction in sulfate to  
1299 Arctic surface warming in recent decades (e.g., Shindell and Faluvegi, 2009; Breider et  
1300 al., 2017) could potentially be better quantified, with the caveat that speciated AOD  
1301 have larger uncertainties than total AOD in the reanalyses. It is also recommended that  
1302 climate models should take into account BB emissions besides anthropogenic climate  
1303 forcers and BB interannual variabilities in Arctic climate change studies.

1304  
1305  
1306 **Code and Data Availability:** All data supporting the conclusions of this manuscript are  
1307 available either through the links provided below or upon request.  
1308 AERONET Version 3 Level 2 data: <http://aeronet.gsfc.nasa.gov>  
1309 MAN data: [https://aeronet.gsfc.nasa.gov/new\\_web/maritime\\_aerosol\\_network.html](https://aeronet.gsfc.nasa.gov/new_web/maritime_aerosol_network.html)  
1310 MODIS DA-quality AOD: [https://nrlgodae1.nrlmry.navy.mil/cgi-](https://nrlgodae1.nrlmry.navy.mil/cgi-bin/datalist.pl?dset=nrl_modis_l3&summary=Go)  
1311 [bin/datalist.pl?dset=nrl\\_modis\\_l3&summary=Go](https://nrlgodae1.nrlmry.navy.mil/cgi-bin/datalist.pl?dset=nrl_modis_l3&summary=Go)



1312 Or <https://modaps.modaps.eosdis.nasa.gov/services/about/products/c61-nrt/MCDAODHD.html>  
1313 MISR AOD: <ftp://15ftl01.larc.nasa.gov/misrl2l3/MISR/MIL2ASAE.003/>  
1314 CALIOP from NASA Langley Research Center Atmospheric Science Data Center:  
1315 [https://doi.org/10.5067/CALIOP/CALIPSO/LID\\_L2\\_05kmAPro-Standard-V4-20](https://doi.org/10.5067/CALIOP/CALIPSO/LID_L2_05kmAPro-Standard-V4-20) for the Version  
1316 4.2 CALIPSO Level 2 5 km aerosol profile and  
1317 [https://doi.org/10.5067/CALIOP/CALIPSO/LID\\_L2\\_05kmALay-Standard-V4-20](https://doi.org/10.5067/CALIOP/CALIPSO/LID_L2_05kmALay-Standard-V4-20) for aerosol layer  
1318 products. Further QAed data are available upon request.  
1319 NAAPS RA AOD: [https://usgoda.org/cgi-](https://usgoda.org/cgi-bin/datalist.pl?dset=nrl_naaps_reanalysis&summary=Go)  
1320 [bin/datalist.pl?dset=nrl\\_naaps\\_reanalysis&summary=Go](https://usgoda.org/cgi-bin/datalist.pl?dset=nrl_naaps_reanalysis&summary=Go)  
1321 MERRA-2 AOD:  
1322 [https://disc.gsfc.nasa.gov/datasets/M2TMNXAER\\_V5.12.4/summary?keywords=%22M](https://disc.gsfc.nasa.gov/datasets/M2TMNXAER_V5.12.4/summary?keywords=%22MERRA-2%22)  
1323 [ERRA-2%22](https://disc.gsfc.nasa.gov/datasets/M2TMNXAER_V5.12.4/summary?keywords=%22MERRA-2%22)  
1324 CAMSRA AOD: <https://www.ecmwf.int/en/research/climate-reanalysis/cams-reanalysis>  
1325 FLAMBE BB smoke inventory is available upon request from U.S. NRL.  
1326

1327 **Author contributions:** P.X. and J.Z designed this study. P.X. performed most of the  
1328 data analysis and wrote the initial manuscript. All authors contributed to scientific  
1329 discussion, writing and revision of the manuscript.  
1330

1331 **Competing interests:** The authors declare that they have no conflict of interest.  
1332

### 1333 Acknowledgments

1334 We thank the NASA AERONET and MAN, and Environment and Climate change  
1335 Canada AEROCAN groups for the sun-photometer data, and NASA MODIS, MISR and  
1336 CALIOP teams for the AOD data used in the study. We acknowledge NASA GMAO,  
1337 ECMWF and U.S. ONR and NRL for making the aerosol reanalysis products available.  
1338 We acknowledge the use of imagery from the NASA Worldview application  
1339 (<https://worldview.earthdata.nasa.gov>, last access: Sept 26 2021), part of the NASA  
1340 Earth Observing System Data and Information System (EOSDIS).

### 1341 Financial support

1342 The authors acknowledge supports from NASA's Interdisciplinary Science (IDS)  
1343 program (grant no. 80HQTR20T0066), NASA's Modeling, Analysis and Prediction  
1344 (MAP) program (NNX17AG52G) and the Office of Naval Research Code 322. N.O. and  
1345 K.R's work is supported by Canadian Space Agency, SACIA-2 project, Ref. No.  
1346 21SUASACOA, ESS-DA program.  
1347

### 1348 References

1349 Abbatt, J. P. D., Leaitch, W. R., Aliabadi, A. A., Bertram, A. K., Blanchet, J.-P., Boivin-  
1350 Rioux, A., et al. (2019). Overview paper: New insights into aerosol and climate in the  
1351 Arctic. *Atmospheric Chemistry and Physics*, **19**(4), 2527– 2560.  
1352 <https://doi.org/10.5194/acp-19-2527-2019>



- 1353  
1354 AboEl-Fetouh, Y., O'Neill, N. T., Ranjbar, K., Hesarakhi, S., Abboud, I., & Sobolewski, P.  
1355 S. (2020). Climatological-scale analysis of intensive and semi-intensive aerosol  
1356 parameters derived from AERONET retrievals over the Arctic. *Journal of Geophysical*  
1357 *Research: Atmospheres*, 125, e2019JD031569. <https://doi.org/10.1029/2019JD031569>  
1358  
1359 AMAP, 2021. Impacts of Short-lived Climate Forcers on Arctic Climate, Air Quality,  
1360 and Human Health. Summary for Policy-makers. Arctic Monitoring and Assessment  
1361 Programme (AMAP), Tromsø, Norway. 20 pp  
1362  
1363 Baccarini, A., Karlsson, L., Dommen, J. *et al.* Frequent new particle formation over the  
1364 high Arctic pack ice by enhanced iodine emissions. *Nat Commun* 11, 4924 (2020).  
1365 <https://doi.org/10.1038/s41467-020-18551-0>  
1366  
1367 Balzter, H., F. F. Gerard, C. T. George, C. S. Rowland, T. E. Jupp, I. McCallum, A.  
1368 Shvidenko, S. Nilsson, A. Sukhinin, A. Onuchin, C. Schmulius, Impact of the Arctic  
1369 Oscillation pattern on interannual forest fire variability in central Siberia. *Geophys. Res.*  
1370 *Letts.* 32, L14709 (2005).  
1371  
1372 Baibakov, K., O'Neill, N. T., Ivanescu, L., Duck, T. J., Perro, C., Herber, A., Schulz,  
1373 K.-H., and Schrems, O.: Synchronous polar winter starphotometry and lidar  
1374 measurements at a High Arctic station, *AMT*, 8, 3789-3809, doi:10.5194/amt-8-3789-  
1375 2015, 2015.  
1376  
1377 Birch, C. E., Brooks, I. M., Tjernström, M., Shupe, M. D., Mauritsen, T., Sedlar, J., Lock,  
1378 A. P., Earnshaw, P., Persson, P. O. G., Milton, S. F., and Leck, C.: Modelling  
1379 atmospheric structure, cloud and their response to CCN in the central Arctic: ASCOS  
1380 case studies, *Atmos. Chem. Phys.*, 12, 3419–3435, [https://doi.org/10.5194/acp-12-](https://doi.org/10.5194/acp-12-3419-2012)  
1381 [3419-2012](https://doi.org/10.5194/acp-12-3419-2012), 2012.  
1382  
1383 Boisvert, L.N., A.A. Petty and J.C. Stroeve, 2016: The Impact of the Extreme Winter  
1384 2015/16 Arctic Cyclone on the Barents–Kara Seas. *Monthly Weather Review*, 144 (11),  
1385 4279–4287, doi:10.1175/mwr-d-16-0234.1.  
1386  
1387 Bossioli, E., Sotiropoulou, G., Methymaki, G., & Tombrou, M. (2021). Modeling extreme  
1388 warm-air advection in the Arctic during summer: The effect of mid-latitude pollution  
1389 inflow on cloud properties. *Journal of Geophysical Research: Atmospheres*, 126,  
1390 e2020JD033291. <https://doi.org/10.1029/2020JD033291>  
1391  
1392 Breider, T. J., Mickley, L. J., Jacob, D. J., Wang, Q., Fisher, J. A., Chang, R. Y. W., and  
1393 Alexander, B.: Annual distributions and sources of Arctic aerosol components, aerosol  
1394 optical depth, and aerosol absorption, *J. Geophys. Res.-Atmos.*, 119, 4107–4124,  
1395 <https://doi.org/10.1002/2013JD020996>, 2014.  
1396  
1397 Breider, T. J., Mickley, L. J., Jacob, D. J., Ge, C., Wang, J., Payer Sulprizio, M., Croft,  
1398 B., Ridley, D. A., McConnell, J. R., Sharma, S., Husain, L., Dutkiewicz, V. A.,



- 1399 Eleftheriadis, K., Skov, H., and Hopke, P. K.: Multidecadal trends in aerosol radiative  
1400 forcing over the Arctic: Contribution of changes in anthropogenic aerosol to Arctic  
1401 warming since 1980, *J. Geophys. Res.-Atmos.*, 122, 3573–3594,  
1402 <https://doi.org/10.1002/2016JD025321>, 2017.
- 1403  
1404 Bullard, J. E., et al. (2016), High-latitude dust in the Earth system, *Rev. Geophys.*, 54,  
1405 447– 485, doi:10.1002/2016RG000518
- 1406  
1407 Campbell, J. R., Tackett, J. L., Reid, J. S., Zhang, J., Curtis, C. A., Hyer, E. J., ... &  
1408 Winker, D. M. (2012). Evaluating nighttime CALIOP 0.532  $\mu\text{m}$  aerosol optical depth and  
1409 extinction coefficient retrievals. *Atmospheric Measurement Techniques*, 5(9), 2143-  
1410 2160.
- 1411  
1412 Colarco, P. R., R. A. Kahn, L. A. Remer, and R. C. Levy, 2014: Impact of satellite  
1413 viewing-swath width on global and regional aerosol optical thickness statistics and  
1414 trends. *Atmospheric Measurement Techniques*, 7, 2313-2335.
- 1415  
1416 Comiso, J. C., Large Decadal Decline of the Arctic Multiyear Ice Cover (2012). *J.*  
1417 *Climate*, Vol., 25. 1176-1193. <https://doi.org/10.1175/JCLI-D-11-00113.1>
- 1418  
1419 Coopman, Q., Garrett, T. J., Finch, D. P., & Riedi, J. (2018). High sensitivity of arctic  
1420 liquid clouds to long-range anthropogenic aerosol transport. *Geo-physical Research*  
1421 *Letters*, 45, 372–381. <https://doi.org/10.1002/2017GL075795>
- 1422  
1423 Dai, A., Luo, D., Song, M., & Liu, J. (2019). Arctic amplification is caused by sea-ice loss  
1424 under increasing CO<sub>2</sub>. *Nature Communications*, 10(1),  
1425 121. <https://doi.org/10.1038/s41467-018-07954-9>
- 1426  
1427 Dall'Osto, M., Beddows, D. C. S., Tunved, P., Krejci, R., Ström, J., Hansson, H.-C.,  
1428 et al. (2017). Arctic sea ice melt leads to atmospheric new particle formation. *Scientific*  
1429 *Reports*, 7(1), 3318. <https://doi.org/10.1038/s41598-017-03328-1>
- 1430  
1431 Dang, C., S. G. Warren, Q. Fu, S. J. Doherty, M. Sturm, and J. Su (2017),  
1432 Measurements of light-absorbing particles in snow across the Arctic, North America,  
1433 and China: Effects on surface albedo, *J. Geophys. Res. Atmos.*, 122, 10,149–10,168,  
1434 doi:10.1002/2017JD027070.
- 1435  
1436 Das, S., Colarco, P. R., Oman, L. D., Taha, G., and Torres, O.: The long-term transport  
1437 and radiative impacts of the 2017 British Columbia pyrocumulonimbus smoke aerosols  
1438 in the stratosphere, *Atmos. Chem. Phys.*, 21, 12069–12090,  
1439 <https://doi.org/10.5194/acp-21-12069-2021>, 2021.
- 1440  
1441 DeRepentigny, P., Jahn, A., Holland, M., Fasullo, J., Lamarque, J.-F., Hannay, C., Mills,  
1442 M., Bailey, D., Tilmes, S., and Barrett, A.: Impact of CMIP6 biomass burning emissions  
1443 on Arctic sea ice loss, EGU General Assembly 2021, online, 19–30 Apr 2021, EGU21-  
1444 9020, <https://doi.org/10.5194/egusphere-egu21-9020>, 2021.



- 1445  
1446 Eck, T. F., et al. (2009), Optical properties of boreal region biomass burning aerosols in  
1447 central Alaska and seasonal variation of aerosol optical depth at an Arctic coastal site,  
1448 *J. Geophys. Res.*, 114, D11201, doi:10.1029/2008JD010870.
- 1449  
1450 Eckhardt, S., A. Stohl, S. Beirle, N. Spichtinger, P. James, C. Forster, C. Junker, T.  
1451 Wagner, U. Platt, and S. G. Jennings (2003), The North Atlantic Oscillation controls air  
1452 pollution transport to the Arctic, *Atmos. Chem. Phys.*, 3(5), 1769–1778,  
1453 doi:10.5194/acp-3-1769-2003.
- 1454  
1455 Eckhardt, S., Quennehen, B., Olivié, D. J. L., Berntsen, T. K., Cherian, R., Christensen,  
1456 J. H., Collins, W., Crepinsek, S., Daskalakis, N., Flanner, M., Herber, A., Heyes, C.,  
1457 Hodnebrog, Ø., Huang, L., Kanakidou, M., Klimont, Z., Langner, J., Law, K. S., Lund, M.  
1458 T., Mahmood, R., Massling, A., Myriokefalitakis, S., Nielsen, I. E., Nøjgaard, J. K.,  
1459 Quaas, J., Quinn, P. K., Raut, J.-C., Rumbold, S. T., Schulz, M., Sharma, S., Skeie, R.  
1460 B., Skov, H., Uttal, T., von Salzen, K., and Stohl, A.: Current model capabilities for  
1461 simulating black carbon and sulfate concentrations in the Arctic atmosphere: a multi-  
1462 model evaluation using a comprehensive measurement data set, *Atmos. Chem. Phys.*,  
1463 15, 9413–9433, <https://doi.org/10.5194/acp-15-9413-2015>, 2015.
- 1464  
1465 Engelmann, R., Ansmann, A., Ohneiser, K., Griesche, H., Radenz, M., Hofer, J.,  
1466 Althausen, D., Dahlke, S., Maturilli, M., Veselovskii, I., Jimenez, C., Wiesen, R., Baars,  
1467 H., Bühl, J., Gebauer, H., Haarig, M., Seifert, P., Wandinger, U., and Macke, A.: Wildfire  
1468 smoke, Arctic haze, and aerosol effects on mixed-phase and cirrus clouds over the  
1469 North Pole region during MOSAiC: an introduction, *Atmos. Chem. Phys.*, 21, 13397–  
1470 13423, <https://doi.org/10.5194/acp-21-13397-2021>, 2021.
- 1471  
1472 Evangeliou, N., Balkanski, Y., Hao, W. M., Petkov, A., Silverstein, R. P., Corley, R.,  
1473 Nordgren, B. L., Urbanski, S. P., Eckhardt, S., Stohl, A., Tunved, P., Crepinsek, S.,  
1474 Jefferson, A., Sharma, S., Nøjgaard, J. K., and Skov, H.: Wildfires in northern Eurasia  
1475 affect the budget of black carbon in the Arctic – a 12-year retrospective synopsis (2002–  
1476 2013), *Atmos. Chem. Phys.*, 16, 7587–7604, <https://doi.org/10.5194/acp-16-7587-2016>,  
1477 2016.
- 1478  
1479 Fisher, J. A. *et al.* Sources, distribution, and acidity of sulfate-ammonium aerosol in the  
1480 Arctic in winter-spring. *Atmos Environ* **45**, 7301–7318,  
1481 <https://doi.org/10.1016/j.atmosenv.2011.08.030> (2011).
- 1482  
1483 Fisher, J. A., et al. (2010), Source attribution and interannual variability of Arctic  
1484 pollution in spring constrained by aircraft (ARCTAS, ARCPAC) and satellite (AIRS)  
1485 observations of carbon monoxide, *Atmos. Chem. Phys.*, 10(3), 977–996,  
1486 doi:10.5194/acp-10-977-2010.
- 1487  
1488 Flanner, M. G., Zender, C. S., Randerson, J. T., & Rasch, P. J. (2007). Present-day  
1489 climate forcing and response from black carbon in snow. *Journal of Geophysical*  
1490 *Research*, 112(September 2006), D11202. <https://doi.org/10.1029/2006JD008003>



- 1491  
1492 Flanner, M. G., C. S. Zender, P. G. Hess, N. M. Mahowald, T. H. Painter, V.  
1493 Ramanathan, and P. J. Rasch (2009), Springtime warming and  
1494 reduced snow cover from carbonaceous particles, *Atmos. Chem. Phys.*, 9(7), 2481–  
1495 2497, doi:10.5194/acp-9-2481-2009.
- 1496  
1497 Flannigan, M. D., and J. B. Harrington, 1988: A study of the relation of meteorological  
1498 variables to monthly provincial area burned by wildfire in Canada (1953-1980). *J. Appl.*  
1499 *Meteorol.*, **27**, 441-452.
- 1500  
1501 Gabric, A., Matrai, P., Jones, G., & Middleton, J. (2018). The nexus between sea ice  
1502 and polar emissions of marine biogenic aerosols. *Bulletin of the American*  
1503 *Meteorological Society*, **99**(1), 61– 81. <https://doi.org/10.1175/BAMS-D-16-0254.1>
- 1504  
1505 Garay, M. J., and Coauthors, 2020: Introducing the 4.4 km spatial resolution Multi-Angle  
1506 Imaging SpectroRadiometer (MISR) aerosol product. *Atmospheric Measurement*  
1507 *Techniques*, **13**, 593-628.
- 1508  
1509 Garrett, T. J., Zhao, C., and Novelli, P.: Assessing the relative contributions of transport  
1510 efficiency and scavenging to seasonal variability in Arctic aerosol, *Tellus B*, 62, 190–  
1511 196, <https://doi.org/10.1111/j.1600-0889.2010.00453.x>, 2010.
- 1512  
1513 Garrett, T. J., Brattström, S., Sharma, S., Worthy, D. E., and Novelli, P.: The role of  
1514 scavenging in the seasonal transport of black carbon carbon and sulfate to the Arctic,  
1515 *Geophys. Res. Lett.*, 38, L16805, <https://doi.org/10.1029/2011GL048221>, 2011.
- 1516  
1517 Giglio, L., Randerson, J. T., and van der Werf, G. R.: Analysis of daily, monthly, and  
1518 annual burned area using the fourth generation global fire emissions database (GFED4),  
1519 *J. Geophys. Res.-Biogeo.*, 118, 317–328, <https://doi.org/10.1002/jgrg.20042>, 2013.
- 1520  
1521 Giles, D. M., Sinyuk, A., Sorokin, M. G., Schafer, J. S., Smirnov, A., Slutsker, I., Eck, T.  
1522 F., Holben, B. N., Lewis, J. R., Campbell, J. R., Welton, E. J., Korkin, S. V., and  
1523 Lyapustin, A. I.: Advancements in the Aerosol Robotic Network (AERONET) Version 3  
1524 database – automated near-real-time quality control algorithm with improved cloud  
1525 screening for Sun photometer aerosol optical depth (AOD) measurements, *Atmos.*  
1526 *Meas. Tech.*, 12, 169–209, <https://doi.org/10.5194/amt-12-169-2019>, 2019.
- 1527  
1528 Glantz, P., Bourassa, A., Herber A., Iversen T., Karlsson J., Kirkevåg, A., Maturilli, M.,  
1529 Seland, O., Stebel, K., Struthers, H., Tesche, M., and Thomason L., (2014), Remote  
1530 sensing of aerosols in the Arctic for an evaluation of global climate model simulations, *J.*  
1531 *Geophys. Res. Atmos.*, 119, 8169–8188, doi:10.1002/2013JD021279.
- 1532  
1533 Goosse, H., Kay, J.E., Armour, K.C. *et al.* Quantifying climate feedbacks in polar  
1534 regions. *Nat Commun* **9**, 1919 (2018). <https://doi.org/10.1038/s41467-018-04173-0>
- 1535



- 1536 Graham, R.M. et al., 2017: Increasing frequency and duration of Arctic winter warming  
1537 events. *Geophysical Research Letters*, **44** (13), 6974–6983, doi:10.1002/2017gl073395.  
1538
- 1539 Groot Zwaaftink, C. D., H. Grythe, H. Skov, and A. Stohl (2016), Substantial contribution  
1540 of northern high-latitude sources to mineral dust in the Arctic, *J. Geophys. Res. Atmos.*,  
1541 **121**, 13,678–13,697, doi:10.1002/2016JD025482.  
1542
- 1543 Hall, J. V., Loboda, T. V., Giglio, L., McCarty G. W. (2016), A MODIS-based burned  
1544 area assessment for Russian croplands: Mapping requirements and challenges.  
1545 *Remote Sensing of Environment*, Vol. 184, 506-521.  
1546 <https://doi.org/10.1016/j.rse.2016.07.022>  
1547
- 1548 Hansen J. and Nazarenko, L. (2004): Soot climate forcing via snow and ice albedos.  
1549 *PNAS*, **101** (2). 423-428.  
1550
- 1551 Hansen, E., Gerland, S., Granskog, M. A., Pavlova, O., Renner, A. H. H., Haapala, J., et  
1552 al. (2013). Thinning of Arctic sea ice observed in Fram Strait: 1990–2011. *Journal of*  
1553 *Geophysical Research: Oceans*, **118**, 5202–5221. <https://doi.org/10.1002/jgrc.20393>  
1554
- 1555 Herber, A., L. W. Thomason, H. Gernandt, U. Leiterer, D. Nagel, K. Schulz, J. Kaptur, T.  
1556 Albrecht, and J. Notholt (2002), Continuous day and night aerosol optical depth  
1557 observations in the Arctic between 1991 and 1999, *J. Geophys. Res.*, **107**(D10), 4097,  
1558 doi:10.1029/2001JD000536.  
1559
- 1560 Hesarakis S, O'Neill NT, Lesins G, Saha A, Martin RV, Fioletov VE, Baibakov K, Abboud  
1561 I. Comparisons of a chemical transport model with a four-year (April to September)  
1562 analysis of fine-and coarse-mode aerosol optical depth retrievals over the Canadian  
1563 Arctic. *Atmosphere-Ocean*. 2017 Oct 20;55(4-5):213-29.  
1564
- 1565 Hyer, E. J., J. S. Reid, and J. Zhang, 2011: An over-land aerosol optical depth data set  
1566 for data assimilation by filtering, correction, and aggregation of MODIS Collection 5  
1567 optical depth retrievals. *Atmospheric Measurement Techniques*, European Geophysical  
1568 Union, 379-408.  
1569
- 1570 Inness, A., Ades, M., Agustí-Panareda, A., Barré, J., Benedictow, A., Blechschmidt, A.-  
1571 M., Dominguez, J. J., Engelen, R., Eskes, H., Flemming, J., Huijnen, V., Jones, L.,  
1572 Kipling, Z., Massart, S., Parrington, M., Peuch, V.-H., Razinger, M., Remy, S., Schulz,  
1573 M., and Suttie, M.: The CAMS reanalysis of atmospheric composition, *Atmos. Chem.*  
1574 *Phys.*, **19**, 3515–3556, <https://doi.org/10.5194/acp-19-3515-2019>, 2019.  
1575
- 1576 IPCC 2013 Chapter 8 by Myhre, G., D. Shindell, F.-M. Bréon, W. Collins, J. Fuglestedt,  
1577 J. Huang, D. Koch, J.-F. Lamarque, D. Lee, B. Mendoza, T. Nakajima, A. Robock, G.  
1578 Stephens, T. Takemura and H. Zhang, 2013: Anthropogenic and Natural Radiative  
1579 Forcing. In: *Climate Change 2013: The Physical Science Basis. Contribution of Working*  
1580 *Group I to the Fifth Assessment Report of the Intergovernmental Panel on Climate*  
1581 *Change* [Stocker, T.F., D. Qin, G.-K. Plattner, M. Tignor, S.K. Allen, J. Boschung, A.



- 1582 Nauels, Y. Xia, V. Bex and P.M. Midgley (eds.]. Cambridge University Press,  
1583 Cambridge, United Kingdom and New York, NY, USA.  
1584
- 1585 Iziomon, M. G., U. Lohmann, and P. K. Quinn (2006), Summertime pollution events in  
1586 the Arctic and potential implications, *J. Geophys. Res.*, 111, D12206,  
1587 doi:10.1029/2005JD006223.  
1588
- 1589 Jacob, D. J., J. H. Crawford, H. Maring, A. D. Clarke, J. E. Dibb, L. K. Emmons, R. A.  
1590 Ferrare, C. A. Hostetler, P. B. Russell, and H. B. Singh (2010), The arctic research of  
1591 the composition of the troposphere from aircraft and satellites (ARCTAS) mission:  
1592 Design, execution, and first results, *Atmos. Chem. Phys.*, 10(11), 5191–5212.  
1593
- 1594 Jacobson, M. Z. (2004), Climate response of fossil fuel and biofuel soot, accounting for  
1595 soot's feedback to snow and sea ice albedo and emissivity, *J. Geophys. Res.*, 109,  
1596 D21201, doi:10.1029/2004JD004945.
- 1597 Kang S., Y. Zhang, Y. Qian, and H. Wang. 2020. "A review of black carbon in snow  
1598 and ice and its impact on the cryosphere." *Earth - Science Reviews* 210. PNNL-SA-  
1599 154137. doi:10.1016/j.earscirev.2020.103346
- 1600 Kapsch, M.-L., R.G. Graversen and M. Tjernström, 2013: Springtime atmospheric  
1601 energy transport and the control of Arctic summer sea-ice extent. *Nature Climate*  
1602 *Change*, 3, 744, doi:10.1038/nclimate1884.  
1603
- 1604 Khan, A. L., S. Wagner, R. Jaffe, P. Xian, M. Williams, R. Armstrong, and D. McKnight  
1605 (2017), Dissolved black carbon in the global cryosphere: Concentrations and chemical  
1606 signatures, *Geophys. Res. Lett.*, 44, 6226–6234, doi:10.1002/2017GL073485.  
1607
- 1608 Kim, J. S., Kug, J. S., Jeong, S. J., Park, H., and Schaepman-Strub, G.: Extensive fires  
1609 in southeastern Siberian permafrost linked to preceding Arctic Oscillation, *Sci. Adv.*, 6,  
1610 eaax3308, <https://doi.org/10.1126/sciadv.aax3308>, 2020.  
1611
- 1612 Kim, M. H., and Coauthors, 2018: The CALIPSO version 4 automated aerosol  
1613 classification and lidar ratio selection algorithm. *Atmospheric Measurement Techniques*,  
1614 11, 6107-6135.  
1615
- 1616 Kleidman, R. G., N. T. O'Neill, L. A. Remer, Y. J. Kaufman, T. F. Eck, D. Tanre', O.  
1617 Dubovik, and B. N. Holben (2005), Comparison of Moderate Resolution Imaging  
1618 Spectroradiometer (MODIS) and Aerosol Robotic Network (AERONET) remote-sensing  
1619 retrievals of aerosol fine mode fraction over ocean, *J. Geophys. Res.*, 110, D22205,  
1620 doi:10.1029/2005JD005760.  
1621
- 1622 Kokhanovsky, A., and Tomasi, C. (Eds.): *Physics and Chemistry of the Arctic*  
1623 *Atmosphere*. Springer Nature Switzerland AG 2020. <https://doi.org/10.1007/978-3-030-33566-3>  
1624  
1625



- 1626 Köllner, F., Schneider, J., Willis, M. D., Schulz, H., Kunkel, D., Bozem, H., Hoor, P.,  
1627 Klimach, T., Helleis, F., Burkart, J., Leaitch, W. R., Aliabadi, A. A., Abbatt, J. P. D.,  
1628 Herber, A. B., and Borrmann, S.: Chemical composition and source attribution of sub-  
1629 micrometre aerosol particles in the summertime Arctic lower troposphere, *Atmos.*  
1630 *Chem. Phys.*, 21, 6509–6539, <https://doi.org/10.5194/acp-21-6509-2021>, 2021.
- 1631  
1632 Kondo, Y., et al. (2011), Emissions of black carbon, organic, and inorganic aerosols  
1633 from biomass burning in North America and Asia in 2008, *J. Geophys. Res.*, 116,  
1634 D08204, doi:10.1029/2010JD015152.
- 1635  
1636 Korontzi, S., J. McCarty, T. Loboda, S. Kumar, and C. Justice (2006), Global distribution  
1637 of agricultural fires in croplands from 3 years of Moderate Resolution Imaging  
1638 Spectroradiometer (MODIS) data, *Global Biogeochem. Cycles*, 20, GB2021,  
1639 doi:10.1029/2005GB002529.
- 1640  
1641 Kwok, R. and Rothrock D. A. (2009) Decline in Arctic sea ice thickness from submarine  
1642 and ICESat records: 1958-2008. *Geophys. Res. Lett.* 36 L15501.
- 1643  
1644 Law, K. S. and A. Stohl, 2007: Arctic air pollution: Origins and  
1645 impacts. *Science*, 315, 1537–1540, doi:10.1126/science.1137695.
- 1646  
1647 Lubin, D., and Vogelmann, A. M. (2006). A climatologically significant aerosol longwave  
1648 indirect effect in the Arctic. *Nature*, 439, 453–456. <https://doi.org/10.1038/nature04449>
- 1649  
1650 Lynch, P., J. S. Reid, D. L. Westphal, J. Zhang, T. Hogan, E. J. Hyer, C. A. Curtis, D.  
1651 Hegg, Y. Shi, J. R. Campbell, J. Rubin, W. Sessions, J. Turk and A. Walker: An 11-year  
1652 Global Gridded Aerosol Optical Thickness Reanalysis (v1.0) for Atmospheric and  
1653 Climate Sciences. *Geosci. Model Dev.*, 9, 1489-1522, doi:10.5194/gmd-9-1489-2016,  
1654 2016.
- 1655  
1656 Macias Fauria, M, E. A. Johnson, Large-scale climatic patterns control large lightning  
1657 fire occurrence in Canada and Alaska forest regions. *J. Geophys. Res.* 111, G04008  
1658 (2006).
- 1659  
1660 Markowicz, K. M., et al. (2016), Impact of North American intense fires on aerosol  
1661 optical properties measured over the European Arctic in July 2015, *J. Geophys. Res.*  
1662 *Atmos.*, 121, 14,487–14,512, doi:10.1002/2016JD025310.
- 1663  
1664 Mauritsen, T., Sedlar, J., Tjernström, M., Leck, C., Martin, M., Shupe, M., Sjogren, S.,  
1665 Sierau, B., Persson, P. O. G., Brooks, I. M., and Swietlicki, E.: An Arctic CCN-limited  
1666 cloud-aerosol regime, *Atmos. Chem. Phys.*, 11, 165–173, [https://doi.org/10.5194/acp-](https://doi.org/10.5194/acp-11-165-2011)  
1667 [11-165-2011](https://doi.org/10.5194/acp-11-165-2011), 2011.
- 1668  
1669 McCarty, J. L., Aalto, J., Paunu, V.-V., Arnold, S. R., Eckhardt, S., Klimont, Z., Fain, J.  
1670 J., Evangeliou, N., Venäläinen, A., Tchepakova, N. M., Parfenova, E. I., Kupiainen, K.,  
1671 Soja, A. J., Huang, L., and Wilson, S.: Reviews & Syntheses: Arctic Fire Regimes and



- 1672 Emissions in the 21st Century, Biogeosciences Discuss. [preprint],  
1673 <https://doi.org/10.5194/bg-2021-83>, in review, 2021.  
1674
- 1675 McNaughton, C. S., Clarke, A. D., Freitag, S., Kapustin, V. N., Kondo, Y., Moteki, N.,  
1676 Sahu, L., Takegawa, N., Schwarz, J. P., Spackman, J. R., Watts, L., Diskin, G.,  
1677 Podolske, J., Holloway, J. S., Wisthaler, A., Mikoviny, T., de Gouw, J., Warneke, C.,  
1678 Jimenez, J., Cubison, M., Howell, S. G., Middlebrook, A., Bahreini, R., Anderson, B. E.,  
1679 Winstead, E., Thornhill, K. L., Lack, D., Cozic, J., and Brock, C. A.: Absorbing aerosol in  
1680 the troposphere of the Western Arctic during the 2008 ARCTAS/ARCPAC airborne field  
1681 campaigns, *Atmos. Chem. Phys.*, 11, 7561–7582, [https://doi.org/10.5194/acp-11-7561-](https://doi.org/10.5194/acp-11-7561-2011)  
1682 2011, 2011.  
1683
- 1684 Meier, W. N., Hovelsrud, G. K., van Oort, B. E. H., Key, J. R., Kovacs, K. M., Michel, C.,  
1685 et al. (2014). Arctic sea ice in transformation: A review of recent observed changes and  
1686 impacts on biology and human activity. *Reviews of*  
1687 *Geophysics*, 52, 185–217. <https://doi.org/10.1002/2013RG000431>  
1688
- 1689 Morrison, A.L. et al., 2018: Isolating the Liquid Cloud Response to Recent Arctic Sea  
1690 Ice Variability Using Spaceborne Lidar Observations. *Journal of Geophysical Research:*  
1691 *Atmospheres*, 123 (1), 473–490, doi:10.1002/2017jd027248.  
1692
- 1693 Notz D. and Stroeve, J. Observed Arctic sea-ice loss directly follows anthropogenic  
1694 CO<sub>2</sub> emission (2016) *Science*. Vol. 354, Issue 6313, pp. 747-750 DOI:  
1695 10.1126/science.aag2345  
1696
- 1697 Nummelin, A., C. Li and P.J. Hezel, 2017: Connecting ocean heat transport changes  
1698 from the midlatitudes to the Arctic Ocean. *Geophysical Research Letters*, 44 (4), 1899–  
1699 1908, doi:10.1002/2016GL071333.  
1700
- 1701 O'Neill, N.T., T.F.Eck, B.N.Holben, A.Smirnov, O.Dubovik, and A.Royer (2001) Bimodal  
1702 size distribution influences on the variation of Angstrom derivatives in spectral and  
1703 optical depth space, *J. Geophys. Res.*, 106, 9787-9806.  
1704
- 1705 O'Neill, N. T., Perro, C., Saha, A., Lesins, G., Duck, T. J., Eloranta, E. W., Nott, G. J.,  
1706 Hoffman, A., Karumudi, M. L., Ritter, C., Bourassa, A., Abboud, I., Carn S., A.,  
1707 Savastiouk, V. (2012) Properties of Sarycheve Sulphate aerosols over the Arctic. *J.*  
1708 *Geophys. Res. Atmos.* Vol. 117, D04203, <https://doi.org/10.1029/2011JD016838>  
1709
- 1710 O'Neill, N. T., Eck, T. F., Smirnov, A., Holben, B. N., and Thulasiraman S. (2003)  
1711 Spectral discrimination of coarse and fine mode optical depth. *J. Geophys. Res.*, 108,  
1712 D05212, doi:10.1029/2002JD002975.  
1713
- 1714 Perovich, D. K., and C. Polashenski (2012), Albedo evolution of seasonal Arctic sea ice,  
1715 *Geophys. Res. Lett.*, 39, L08501, doi:10.1029/2012GL051432  
1716



- 1717 Prenni, A. J., Harrington, J. Y., Tjernstöm, M., DeMott, P. J., Avramov, A., Long, C. N.,  
1718 Kreidenweis, S. M., Olsson, P. Q., and Verlinde, J.: Can ice-nucleating aerosols affect  
1719 arctic seasonal climate?, *B. Am. Meteorol. Soc.*, 88, 541–550,  
1720 <https://doi.org/10.1175/BAMS-88-4-541>, 2007.
- 1721  
1722 Quinn, P. K., et al. (2008), Short-lived pollutants in the Arctic: Their climate impact and  
1723 possible mitigation strategies, *Atmos. Chem. Phys.*, 8(6), 1723–1735, doi:10.5194/acp-  
1724 8-1723-2008.
- 1725  
1726 Randles, C. A., daSilva, A. M., Buchard, V., Colarco, P. R., Darmenov, A., Govindaraju,  
1727 R., et al.: The MERRA-2 aerosol reanalysis, 1980 onward. Part I: System description  
1728 and data assimilation evaluation. *Journal of Climate*, 30(17), 6823-6850.  
1729 <https://doi.org/10.1175/JCLI-D-16-0609.1>, 2017.
- 1730  
1731 Randerson, J. T., and Coauthors, 2006: The impact of boreal forest fire on climate  
1732 warming. *Science*, 314, 1130–1132, doi:10.1126/science.1132075.
- 1733  
1734 Ranjbar, K., O'Neill, N. T., Lutsch, E., McCullough, E. M., AboEl-Fetouh, Y., Xian, P., et  
1735 al. (2019). Extreme smoke event over the high Arctic. *Atmospheric Environment*, 218,  
1736 117002. <https://doi.org/10.1016/j.atmosenv.2019.117002>
- 1737  
1738 Reid, J. S., Hyer, E. J., Prins, E. M., Westphal, D. L., Zhang, J., Wang, J., Christopher,  
1739 S. A., Curtis, C. A., Schmidt, C. C., Eleuterio, D. P., Richardson, K. A., and Hoffman, J.  
1740 P.: Global Monitoring and Forecasting of Biomass-Burning Smoke: Description of and  
1741 Lessons from the Fire Locating and Modeling of Burning Emissions (FLAMBE)  
1742 Program, *IEEE J. Sel. Top. Appl.*, 2, 144–162, JSTARS-2009-00034, 2009.
- 1743  
1744 Reid, J. S., Koppmann, R., Eck, T. F., and Eleuterio, D. P.: A review of biomass burning  
1745 emissions part II: intensive physical properties of biomass burning particles, *Atmos.*  
1746 *Chem. Phys.*, 5, 799–825, <https://doi.org/10.5194/acp-5-799-2005>, 2005.
- 1747  
1748 Rinke, A., Maturilli, M., Graham, R. M., Hatthes, H., Handorf, D., Cohen, L., Hudson, S.  
1749 R. and Moore, J. C., (2017), Extreme cyclone events in the Arctic: Wintertime variability  
1750 and trends. *Environ. Res. Lett.* **12** 094006
- 1751  
1752 Rosel, A., Itkin, P., King, J., Divine, D., Wang, C., Granskog, M. A., Krumpfen, T., and  
1753 Gerland, S. (2018). Thin sea ice, thick snow and widespread negative freeboard  
1754 observed during N-ICE2015 north of Svalbard. *J. Geophys. Res: Oceans*, 123, 1156–  
1755 1176. <https://doi.org/10.1002/2017JC012865>
- 1756  
1757 Saha, A., et al. (2010), Pan-Arctic sunphotometry during the ARCTAS-A campaign of  
1758 April 2008, *Geophys. Res. Lett.*, 37, L05803, doi:10.1029/2009GL041375.
- 1759  
1760 Sand, M., T. K. Berntsen, Ø. Seland, and J. E. Kristjánsson (2013), Arctic surface  
1761 temperature change to emissions of black carbon within Arctic or midlatitudes, *J.*  
1762 *Geophys. Res. Atmos.*, 118, 7788–7798, doi:10.1002/jgrd.50613.



- 1763  
1764 Sand, M., Berntsen, T., Von Salzen, K., Flanner, M., Langner, J., and Victor, D.:  
1765 Response of Arctic temperature to changes in emissions of short-lived climate forcers,  
1766 *Nat. Clim. Change*, 6, 286–289, <https://doi.org/10.1038/nclimate2880>, 2016.  
1767  
1768 Sand, M., Samset, B. H., Balkanski, Y., Bauer, S., Bellouin, N., Berntsen, T. K., Bian,  
1769 H., Chin, M., Diehl, T., Easter, R., Ghan, S. J., Iversen, T., Kirkevåg, A., Lamarque, J.-  
1770 F., Lin, G., Liu, X., Luo, G., Myhre, G., Noije, T. V., Penner, J. E., Schulz, M., Seland,  
1771 Ø., Skeie, R. B., Stier, P., Takemura, T., Tsigaridis, K., Yu, F., Zhang, K., and Zhang,  
1772 H.: Aerosols at the poles: an AeroCom Phase II multi-model evaluation, *Atmos. Chem.*  
1773 *Phys.*, 17, 12197–12218, <https://doi.org/10.5194/acp-17-12197-2017>, 2017.  
1774  
1775 Sayer, A. M. and Knobelspiesse, K. D.: How should we aggregate data? Methods  
1776 accounting for the numerical distributions, with an assessment of aerosol optical depth,  
1777 *Atmos. Chem. Phys.*, 19, 15023–15048, <https://doi.org/10.5194/acp-19-15023-2019>,  
1778 2019.  
1779  
1780 Serreze, M.C. and R.G. Barry, 2011: Processes and impacts of Arctic amplification: A  
1781 research synthesis. *Global and Planetary Change*, **77** (1– 2), 85–96,  
1782 doi:10.1016/j.gloplacha.2011.03.004.  
1783  
1784 Serreze, M.C., Francis, J.A. The Arctic Amplification Debate. *Climatic Change* **76**, 241–  
1785 264 (2006). <https://doi.org/10.1007/s10584-005-9017-y>  
1786  
1787 Sharma, S., M. Ishizawa, D. Chan, D. Lavoué, E. Andrews, K. Eleftheriadis, and S.  
1788 Maksyutov (2013), 16-year simulation of Arctic black carbon: Transport, source  
1789 contribution, and sensitivity analysis on deposition, *J. Geophys. Res. Atmos.*, 118, 943–  
1790 964, doi:10.1029/2012JD017774.  
1791  
1792 Shi, Y., J. Zhang, J. S. Reid, E. J. Hyer, and N. C. Hsu, 2013: Critical evaluation of the  
1793 MODIS Deep Blue aerosol optical depth product for data assimilation over North Africa.  
1794 *Atmospheric Measurement Techniques*, **6**, 949-969.  
1795  
1796 Shi, Y., J. Zhang, J. S. Reid, B. Holben, E. J. Hyer, and C. Curtis, 2011: An analysis of  
1797 the collection 5 MODIS over-ocean aerosol optical depth product for its implication in  
1798 aerosol assimilation. *Atmos. Chem. Phys.*, **11**, 557-565.  
1799  
1800 Shindell, D. and Faluvegi, G.: Climate response to regional radiative forcing during the  
1801 twentieth century, *Nat. Geosci.*, 2, 294–300, <https://doi.org/10.1038/ngeo473>, 2009.  
1802  
1803 Schlosser, J. S., R. A. Braun, T. Bradley, H. Dadashazar, A. B. MacDonald, A. A.  
1804 Aldhaif, M. A. Aghdam, A. H. Mardi, P. Xian, and A. Sorooshian (2017), Analysis of  
1805 aerosol composition data for western United States wildfires between 2005 and 2015:  
1806 Dust emissions, chloride depletion, and most enhanced aerosol constituents, *J.*  
1807 *Geophys. Res. Atmos.*, 122, 8951–8966, doi:10.1002/2017JD026547.  
1808



- 1809 Skiles S. M., Flanner, M., Cook, J. M., Dumont, M. and Painter, T. (2018) Radiative  
1810 forcing by light-absorbing particles in snow. *Nature Climate Change*, 8, 964-971.  
1811 <https://doi.org/10.1038/s41558-018-0296-5>  
1812
- 1813 Skinner, W. R., B. J. Stocks, D. L. Martell, B. Bonsal, and A. Shabbar, 1999: The  
1814 association between circulation anomalies in the mid- troposphere and area burned by  
1815 wildland fire in Canada. *Theoretical and Applied Climatology*, **63**, 89-105.  
1816
- 1817 Stohl, A., et al. (2006), Pan-Arctic enhancements of light absorbing aerosol  
1818 concentrations due to North American boreal forest fires during summer 2004, *J.*  
1819 *Geophys. Res.*, 111, D22214, doi:10.1029/2006JD007216.  
1820
- 1821 Stohl, A., et al. (2007), Arctic smoke—Record high air pollution levels in the European  
1822 Arctic due to agricultural fires in eastern Europe in spring 2006, *Atmos. Chem. Phys.*,  
1823 7(2), 511–534, doi:10.5194/acp-7-511-2007.  
1824
- 1825 Stone, R. S., G. P. Anderson, E. Andrews, E. G. Dutton, E. P. Shettle, and A. Berk  
1826 (2007), Incursions and radiative impact of Asian dust in northern Alaska, *Geophys. Res.*  
1827 *Lett.*, 34, L14815, doi:10.1029/2007GL029878.  
1828
- 1829 Taylor, P., B. Hegyi, R. Boeke and L. Boisvert, 2018: On the Increasing Importance of  
1830 Air-Sea Exchanges in a Thawing Arctic: A Review. *Atmosphere*, **9** (2),  
1831 doi:10.3390/atmos9020041.  
1832
- 1833 Tomasi, C., Kokhanovsky, A. A., Lupi, A., Ritter, C., Smirnov, A., O'Neill, N. T., Stone,  
1834 R. S., Holben, B. N., Nyeki, S., Wehrli, C., Stohl, A., Mazzola, M., Lanconelli, C., Vitale,  
1835 V., Stebel, K., Aaltonen, V., de Leeuw, G., Rodriguez, E., Herber, A. B., Radionov, V.  
1836 F., Zielinski, T., Petelski, T., Sakerin, S. M., Kabanov, D. M., Xue, Y., Mei, L., Istomina,  
1837 L., Wagener, R., McArthur, B., Sobolewski, P. S., Kivi, R., Courcoux, Y., Larouche, P.,  
1838 Broccardo, S., & Piketh, S. J. (2015). Aerosol remote sensing in polar regions. *Earth-*  
1839 *Science Reviews*, 140, 108–157. <https://doi.org/10.1016/j.earscirev.2014.11.001>.  
1840
- 1841 Tomasi, C., Vitale, V., Lupi, A., Di Carmine, C., Campanelli, M., Herber, A., Treffeisen,  
1842 R., Stone, R. S., Andrews, E., Sharma, S., Radionov, V., von Hoyningen-Huene, W.,  
1843 Stebel, K., Hansen, G. H., Myhre, C. L., Wehrli, C., Aaltonen, V., Lihavainen, H.,  
1844 Virkkula, A., Hillamo, R., Ström, J., Toledano, C., Cachorro, V. E., Ortiz, P., de Frutos,  
1845 A. M., Blindheim, S., Frioud, M., Gausa, M., Zielinski, T., Petelski, T., & Yamanouchi, T.  
1846 (2007). Aerosols in polar regions: a historical overview based on optical depth and in  
1847 situ observations. *Journal of Geophysical Research, Atmospheres*, 112, D16.  
1848 <https://doi.org/10.1029/2007JD008432>.  
1849
- 1850 Thomason, L. W., Ernest, N., Luis, M. L., Rieger, L., Bourassa, A., Vernier, J.-P.,  
1851 Manney, G., Luo, B., Arfeuille, F., & Peter, T. (2018). A global space-based  
1852 stratospheric aerosol climatology: 1979–2016. *Earth System Science Data*, 10, 469–  
1853 492. <https://doi.org/10.5194/essd-10-469-2018>.  
1854



- 1855 Torres, O., Bhartia, P. K., Taha, G., Jethva, H., Das, S., Colarco, P., Krotkov, N., Omar,  
1856 A., and Ahn, C.: Stratospheric Injection of Massive Smoke Plume From Canadian  
1857 Boreal Fires in 2017 as Seen by DSCOVR-EPIC, CALIOP, and OMPS-LP  
1858 Observations, *J. Geophys. Res.-Atmos.*, 125,  
1859 e2020JD032579, <https://doi.org/10.1029/2020JD032579>, 2020.  
1860
- 1861 Toth, T. D., Campbell, J. R., Reid, J. S., Tackett, J. L., Vaughan, M. A., Zhang, J., &  
1862 Marquis, J. W. (2018). Minimum aerosol layer detection sensitivities and their  
1863 subsequent impacts on aerosol optical thickness retrievals in CALIPSO level 2 data  
1864 products. *Atmospheric Measurement Techniques*, 11(1), 499-514.  
1865
- 1866 Toth, T. D., Zhang, J., Campbell, J. R., Reid, J. S., & Vaughan, M. A. (2016). Temporal  
1867 variability of aerosol optical thickness vertical distribution observed from  
1868 CALIOP. *Journal of Geophysical Research: Atmospheres*, 121(15), 9117-9139.  
1869
- 1870 Valkonen, E., Cassano, J., & Cassano, E. (2021). Arctic cyclones and their interactions  
1871 with the declining sea ice: A recent climatology. *Journal of Geophysical Research:*  
1872 *Atmospheres*, 126, e2020JD034366. <https://doi.org/10.1029/2020JD034366>  
1873
- 1874 van der Werf, G. R., J. T. Randerson, L. Giglio, G. J. Collatz, P. S. Kasibhatla, and A. F.  
1875 Arellano Jr., 2006: Interannual variability in global biomass burning emissions from 1997  
1876 to 2004. *Atmos. Chem. Phys.*, 6, 3423–3441, doi:[10.5194/acp-6-3423-2006](https://doi.org/10.5194/acp-6-3423-2006).  
1877
- 1878 Warneke, C., Froyd, K. D., Brioude, J., Bahreini, R., Brock, C. A., Cozic, J., et al.  
1879 (2010). An important contribution to springtime Arctic aerosol from biomass burning in  
1880 Russia. *Geophysical Research Letters*, 37, L01801.  
1881 <https://doi.org/10.1029/2009GL041816>  
1882
- 1883 Waseda, T., Nose, T., Kodaira, T., Sasmal, K and Webb, A. (2021) Climatic trends of  
1884 extreme wave events caused by Arctic cyclones in the western Arctic Ocean. *Polar*  
1885 *Science*. Vol 27, 100625, doi:10.1016/j.polar.2020.100625  
1886
- 1887 Wendisch, M., Macke, A., Ehrlich, A., Lupkes, C., Mech, M., Chechin, D., et al. (2019).  
1888 The Arctic cloud puzzle: Using ACLOUD/PASCAL multiplatform observations to unravel  
1889 the role of clouds and aerosol particles in Arctic amplification. *Bulletin of the American*  
1890 *Meteorological Society*, 100, 841–871. <https://doi.org/10.1175/BAMS-D-18-0072.1>  
1891
- 1892 Wex, H., Huang, L., Zhang, W., Hung, H., Traversi, R., Becagli, S., Sheesley, R. J.,  
1893 Moffett, C. E., Barrett, T. E., Bossi, R., Skov, H., Hünerbein, A., Lubitz, J., Löffler, M.,  
1894 Linke, O., Hartmann, M., Herenz, P., and Stratmann, F.: Annual variability of ice-  
1895 nucleating particle concentrations at different Arctic locations, *Atmos. Chem. Phys.*, 19,  
1896 5293–5311, <https://doi.org/10.5194/acp-19-5293-2019>, 2019.  
1897
- 1898 Winker, D. M., Pelon, J. R., & McCormick, M. P. (2003, March). CALIPSO mission:  
1899 spaceborne lidar for observation of aerosols and clouds. In *Lidar Remote Sensing for*



- 1900 *Industry and Environment Monitoring III* (Vol. 4893, pp. 1-11). International Society for  
1901 Optics and Photonics.  
1902  
1903 Woods, C., & Caballero, R. (2016). The role of moist intrusions in Winter Arctic warming  
1904 and sea ice decline. *Journal of Climate*, 29, 4473–4485. [https://doi.org/10.1175/JCLI-D-](https://doi.org/10.1175/JCLI-D-15-0773.1)  
1905 [15-0773.1](https://doi.org/10.1175/JCLI-D-15-0773.1)  
1906  
1907 Xian, P., Klotzbach, P. J., Dunion, J. P., Janiga, M. A., Reid, J. S., Colarco, P. R., and  
1908 Kipling, Z.: Revisiting the relationship between Atlantic dust and tropical cyclone activity  
1909 using aerosol optical depth reanalyses: 2003–2018, *Atmos. Chem. Phys.*, 20, 15357–  
1910 15378, <https://doi.org/10.5194/acp-20-15357-2020>, 2020.  
1911  
1912 Xian, P., Reid J. S., Hyer, E., Sampson, C.R., Rubin, J., Ades M., et. al., Current state of  
1913 the global operational aerosol multi-model ensemble: an update from the International  
1914 Cooperative for Aerosol Prediction (ICAP), 2019, *Quarterly J. of the Royal Met. Soc.*  
1915 <https://doi.org/10.1002/qj.3497>  
1916  
1917 Xian, P., J. S. Reid, J. F. Turk, E. J. Hyer and D. L. Westphal: Impact of models versus  
1918 satellite measured tropical precipitation on regional smoke optical thickness in an  
1919 aerosol transport model, *Geophys. Res. Lett.*, 36, L16805, doi:10.1029/2009GL038823,  
1920 2009.  
1921  
1922 Yang, Y., Wang, H., Smith, S. J., Easter, R. C., and Rasch, P. J.: Sulfate Aerosol in the  
1923 Arctic: Source Attribution and Radiative Forcing, *J. Geophys. Res.-Atmos.*, 123, 1899–  
1924 1918, <https://doi.org/10.1002/2017JD027298>, 2018.  
1925  
1926 Zamora, L. M., Kahn, R. A., Cubison, M. J., Diskin, G. S., Jimenez, J. L., Kondo, Y.,  
1927 McFarquhar, G. M., Nenes, A., Thornhill, K. L., Wisthaler, A., Zelenyuk, A., and Ziemba,  
1928 L. D.: Aircraftmeasured indirect cloud effects from biomass burning smoke in the Arctic  
1929 and subarctic, *Atmos. Chem. Phys.*, 16, 715–738, [https://doi.org/10.5194/acp-16-715-](https://doi.org/10.5194/acp-16-715-2016)  
1930 [2016](https://doi.org/10.5194/acp-16-715-2016), 2016.  
1931  
1932 Zhang, J. L., and J. S. Reid, 2006: MODIS aerosol product analysis for data  
1933 assimilation: Assessment of over-ocean level 2 aerosol optical thickness retrievals. *J.*  
1934 *Geophys. Res.-Atmos.*, **111**.  
1935  
1936 Zhang, J. L., and J. S. Reid, D. L. Westphal, N. L. Baker, and E. J. Hyer, 2008: A  
1937 system for operational aerosol optical depth data assimilation over global oceans. *J.*  
1938 *Geophys. Res.*, 113, D10208, doi:[10.1029/2007JD009065](https://doi.org/10.1029/2007JD009065).  
1939  
1940 Zhang, J. and Reid, J. S.: A decadal regional and global trend analysis of the aerosol  
1941 optical depth using a data-assimilation grade over-water MODIS and Level 2 MISR  
1942 aerosol products, *Atmos. Chem. Phys.*, 10, 18879-18917, doi:10.5194/acpd-10-18879-  
1943 2010, 2010.  
1944



- 1945 Zhang J., Reid, J. S., Alfaro-Contreras, R., Xian P., Has China been exporting less  
1946 particulate air pollution over the past decade?, *Geophysical Research Letters*,  
1947 10.1002/2017GL072617, 2017.  
1948  
1949 Zhang, J., Spurr, R. J. D., Reid, J. S., Xian, P., Colarco, P. R., Campbell, J. R., Hyer, E.  
1950 J., and Baker, N. L.: Development of an Ozone Monitoring Instrument (OMI) aerosol  
1951 index (AI) data assimilation scheme for aerosol modeling over bright surfaces – a step  
1952 toward direct radiance assimilation in the UV spectrum, *Geosci. Model Dev.*, 14, 27–42,  
1953 <https://doi.org/10.5194/gmd-14-27-2021>, 2021.  
1954  
1955 Zhao, C., & Garrett, T. J. (2015). Effects of Arctic haze on surface cloud radiative  
1956 forcing. *Geophysical Research Letters*, 42, 557–564.  
1957 <https://doi.org/10.1002/2014GL062015>  
1958